Virgo Laboratory Group

Data Analysis on Simulated Gravitational Chirps

Authors: Clemente Smarra, Alessio Zicoschi

June 7, 2020

SAPIENZA
UNIVERSITÀ DI ROMA

Contents

Abstract

A well-studied and repeatedly detected class of gravitational signals is that of gravitational chirps, produced by astronomical binary coalescing systems. One of the most challenging aspects in this field is parameters estimation, since signals are highly embedded in interferometers and ambient noises. Therefore, the retrieval of the exact waveform hidden in the noise is particularly demanding. The aim of this report is to present the result of parameters assessment on simulated gravitational chirps detections through the exploitation of different methods. The matched filtering technique is applied in order to detect simulated signals, using different algorithms to choose filters characteristics. The main goal is to evaluate the masses of the two objects generating the signals. However, gravitational waveforms do not directly depend on the two masses, but only on particular combinations of them. Therefore, it is shown that the most efficient and precise way to recover the actual waveform is to perform analysis in different parameter spaces. In particular, a change of space parameter coordinates is shown to be a critical pillar of the whole procedure. Further on, the development of fine-tuning procedures enables to achieve a higher degree of accuracy on parameters evaluation. In the end, the applicability of outlined procedures to real interferometers data is discussed, in order to legitimate the validity of developed techniques.

Introduction

In 1916, Albert Einstein published the General Theory of Relativity, revolutionizing the old concepts of space and time. In this framework, he predicted the existence of *gravitational waves* as propagating perturbations of the space-time manifold. After almost one century, on the 14th of September 2015, gravitational waves were detected for the first time[1]. Although several types of gravitational waves exist, depending on the mechanism of production, this work is concerned with the analysis of gravitational chirps emitted by two circularly orbiting and gravitationally bound compact bodies[2].
In the so called *Newtonian approximation*, exhaustively pointed out in Appendix A, the generated waveforms depend on a single variable, the *chirp mass* $\mathcal{M}$ of the system. Appendix D entirely deals with the detection of a signal embedded in white noise in the Newtonian picture[3].
However, in proximity the *merger*[4], the Newtonian approximation yields wrong predictions, requiring Post-Newtonian corrections to be implemented[5]. In the Post-Newtonian picture, the emitted waveforms do depend on the separate masses of the bodies. Therefore, the analysis should be carefully carried out taking this difference into account.
The core of this report is to develop a new procedure, which leads to better estimation in a computationally feasible way and overcomes the limits of the proposed matched filtering technique. In the following, this new method will be referred to as the "*Grid* ($\mathcal{M}$-ν) *approach*". The starting point is to notice that the previous analysis has been conducted in non-optimal coordinates. In fact, being a correction of the Newtonian picture, the Post-Newtonian expansion firstly aims at reproducing the source's *chirp mass*. Therefore, masses arbitrarily different from the true ones may give rise to high *Signal to Noise Ratios*[6], as long as they provide a sufficiently good estimation of the *chirp mass*.
However, looking closely at the formulae in E.1, the Post-Newtonian terms can be written also as an expansion involving the *symmetric mass ratio* ν. Thus, all the previous analysis can be performed in the ($\mathcal{M}$-ν) plane, showing a better convergence to the source values. Then, through the change of coordinates described in E.2, it is possible to go back to the initial (m_1-m_2) plane to calculate the resulting

[1] Although indirect proofs already were provided.

[2] Terms arising from spin-orbit coupling will not be taken into account.

[3] The implemented mathematical and computational tools are thoroughly reported in Appendices B and C.

[4] Phase immediately before the coalescence, between the *inspiral* and the *ringdown*.

[5] As a matter of fact, only the *early inspiral*, which is often too small to be revealed, can be satisfactorily described in the Newtonian landscape. The Post-Newtonian picture accurately describes even the *late inspiral*, but not the actual *merger*.

[6] Denoted as SNR in the following.

estimate on the masses.
In Section 1 the outcomes of the Newtonian and the Post-Newtonian pictures are contrasted. As for the time of detection, an interesting comparison is made, showing that treating a Post-Newtonian chirp signal with a Newtonian approach brings inaccurate results[7], as expected. In the end, an example of a network of detectors [8] is illustrated, leading to the ultimate estimate of the couple of masses. It will be remarked that these achievements strongly depend on the characteristics of the selected range of masses. In conclusion, the final error on the masses is underestimated by a factor of 2 circa[9].
In particular, Section 2 sets the conceptual basis of the "*Grid* ($\mathcal{M}$-ν) *approach*" and should be understood as the first level of a multilayered analysis. Analogously to what done beforehand, the procedure's intrinsic limit is displayed and the compatibility between the time of detection and the time of arrival is checked up. Having done these preliminary tests, a sensible first estimate of the precision of the two masses can be provided. It must be noticed that, in contrast to the (m_1-m_2) picture, the error does not depend on the range of masses chosen, since the analysis is performed in the ($\mathcal{M}$-ν) plane. The error associated to the gauged masses selects a region in the ($\mathcal{M}$-ν) space.
Moving from this achievement, Section 3 develops a further analysis. The main idea is to examine the above-mentioned region evaluating the SNR for tenths of thousands number of internal points. Simulating a network of separate detectors, fictitiously all parallel, characterised by white noise and organized so as to be completely equivalent, a proper assessment of the final error on the masses can be furnished. Remarkably, the ultimate error is strongly reduced with respect to the previous procedure.
Finally, Section 4 briefly targets the study of a signal embedded in real noise. In particular, data coming from the LIGO "GW150914" event are taken into account and fully examined. The approach is carefully outlined and involves the *"Spectral whitening"* of the initial data. As expected, it is shown that, once the input is whitened, the situation in real noise tends to the white noise case. Therefore, dealing with Gaussian white noise represents a meaningful approximation.

[7]It must be specified that spinning and angular parameters, as well as precise waveforms modelled from numerical integration simulations will not be considered in this report.

[8]With same orientation, sensitivity and characterised by white noise.

[9]Notice that, in principle, one could overcome this issue enlarging the range of masses or using a finer grid, whose structure is fully exploited in Appendix C. However, this is incredibly demanding from a computational point of view.

1 Gravitational Chirp Simulations

In this section, the actual simulation of gravitational waves detection[10] is outlined. Detections are performed using the matched filtering method (see Appendix B for a detailed explanation and implementation). Different parameters for filters are tested on data using the "Grid of Masses" technique (see Appendix C). The purpose is to simulate the detection of a chirp signal in the Newtonian approximation, evaluating its chirp mass and arrival time. Noise in detectors is modeled as white (i.e. flat power spectrum). The core idea of the whole work is to use a network of detectors that carry out independent measures. At the end the whole structure produces an overall estimate. Considerations on the accuracy of this results are discussed in paragraph 1.2. The workflow could be summarized as follows:

1. **Parameters Setting:** Ranges in which the analysis is carried out are fixed. Then, amplitude of noise, number of detectors etc. are chosen.
2. **Signal and Noise Generation:** A signal from a randomly chosen couple of masses is generated. At the same time, different white noise is produced in every sensor.
3. **Injection:** Starting from a randomly chosen time, signal is injected into noise in every detector.
4. **Detection:** Using the above-described technique, SNR is computed in every detector for the set grid of masses.
5. **Selection:** Maximum of SNR is chosen in every simulated sensor. Also the couple of masses that maximizes SNR over all the detectors is determined.
6. **Time Measurements:** Matched filtering technique automatically provides the time at which the signal is detected in every sensor: this measure is compared to its injection time.
7. **Results:** Obtained results are plotted by exploiting an easy-to-read structure.

Combined Measures An estimation of parameters from the whole network can be given in the following way: SNR is evaluated over the whole grid for every detector. Then, the obtained values corresponding to every couple of masses are averaged over all detectors. In this way, the average SNR grid is obtained. The maximum over this new grid usually gives a better estimate of the parameters than single-detector measurements, since noise is "averaged" over all detectors.

[10] Refer to codes `Newtonian_Detectors.mlx` (explained in appendix D.3 and fully reported in appendix D.5) and `PN_Simple_Detectors.mlx`

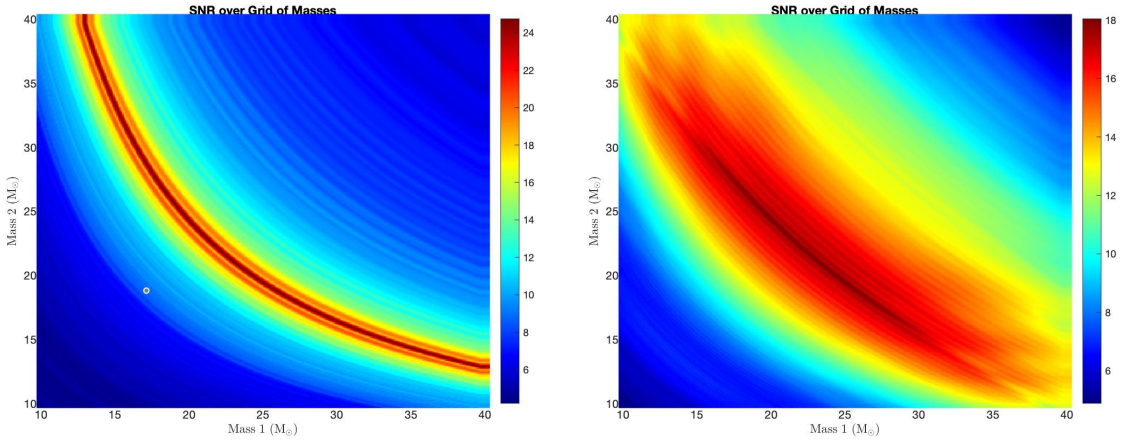

Figure 1: Average SNR over all the detectors from a run simulating a signal with $m_1 = 25\,\mathrm{M}_\odot$ and $m_2 = 20\,\mathrm{M}_\odot$ in the Newtonian (left) and in the post-Newtonian (rigth) case. A grid step of $0.1\,\mathrm{M}_\odot$ is used. This plot confirms that the Newtonian signal depends only on the parameter $\mathcal{M}$, since all the couples of masses on the curves with $\mathcal{M} = const.$ return the same SNR value. In the post-Newtonian case, instead, small differences allow single masses identification: bands having same value of SNR are much smaller.

1.1 Example Runs

In order to have a better understanding of the simulation performed, it is useful to take a look at the results both in the Newtonian and the post-Newtonian cases. It is important to keep in mind that in the former case only the chirp mass is evaluated, while in the latter one an estimation of both masses can be provided. All the hereafter presented results have been produced by simulating 4 detectors and choosing noise RMS equal to 3 times the signal mean absolute value, a grid step of $0.2\,\mathrm{M}_\odot$ and fixing the masses values to $m_1 = 25\,\mathrm{M}_\odot$ and $m_2 = 20\,\mathrm{M}_\odot$ ($\mathcal{M} = 19.44\,\mathrm{M}_\odot$). Examples of the pattern of the mean SNR over the 4 detectors are presented in Figure 1, where the application of grid technique to data in both Newtonian and post-Newtonian cases is explicitly shown.

It is evident that, in both cases, the parameter that mostly influences the outcome of the application of matched filtering is the chirp mass: same-color curves represent combinations of masses having the same value of $\mathcal{M}$. It is also interesting to report the displayed outputs, which are presented in a user-friendly table. Examples of such tables, reported in Figure 2, are presented for the same runs used for Figure 1. The main difference between the Newtonian is in the columns dedicated to errors: whereas in the former case it was only meaningful to study the error on the measured $\mathcal{M}$, in the latter it is important to evaluate the precision of the estimation provided for both masses. It must be remarked that the names

Newtonian Case

	SNR	Mass 1	Mass 2	Chirp Mass	Rel. Error	Delay (s)	Delay (smpl)
1 Virgo	24.5430	16.5000	30.8000	19.4379	2.0936e-04	1.6373e-04	0
2 LIGO 1	26.0176	14.3000	36.3000	19.4230	9.7583e-04	1.6373e-04	0
3 LIGO 2	24.6893	17.1000	29.6000	19.4406	6.9497e-05	1.6373e-04	0
4 Kagra	23.7663	13.8000	38.0000	19.4505	4.4256e-04	1.6373e-04	0
5 Best Comb.	24.7321	15.1000	34.1000	19.4377	2.1579e-04	1.6373e-04	0

Post-Newtonian Case

	SNR	Mass 1	Mass 2	Chirp Mass	Rel. Error 1	Rel. Error 2	Delay (s)	Delay (smpl)
1 Virgo	18.5120	18.9000	26.3000	19.3563	0.0520	0.0550	-0.0040	-17.0000
2 LIGO 1	16.4665	19.4000	25.7000	19.4002	0.0280	0.0300	-0.0018	-8.0000
3 LIGO 2	18.7020	22.2000	22.7000	19.5424	0.0920	0.1100	0.0053	21.0000
4 Kagra	18.7452	20.5000	24.4000	19.4553	0.0240	0.0250	0.0009	3.0000
5 Best Comb.	18.0382	19.9000	25.1000	19.4300	0.0040	0.0050	-0.0002	-1.7500

Figure 2: Screenshots of the displayed results over 4 detectors for runs with $m_1 = 25\,\mathrm{M}_\odot$, $m_2 = 20\,\mathrm{M}_\odot$ ($\mathcal{M} = 19.44\,\mathrm{M}_\odot$), grid step of $0.2\,\mathrm{M}_\odot$, and noise RMS equal to 5 times the signal mean absolute value are reported in both Newtonian (upper) and post-Newtonian (lower) cases. The last lines of each table reports results for the combination having the best overall SNR. Detectors names are fictitious, being all exactly equivalent (same orientation and same characteristics). In the Newtonian case, the masses are not well evaluated, but the estimated chirp mass is very close to its true value, as one expects. In the post-Newtonian case, instead, a better measure of the two masses is also provided, even if it is not always highly accurate.

of detectors in the tables are not linked to real detectors characteristics: they have only been used to identify different simulated sensors, all being exactly equivalent.

1.2 Behaviour of Precision

The most interesting results obtained from many iterations of these simulations are presented in this section. A complete catalogue of the results obtained from these simulations is reported in Appendix D.4 for the Newtonian case and in Appendix F.4 for the post-Newtonian case. In all simulations, the post-Newtonian corrections were considered up to order 2.5 (see Appendix F.4.1).

Dependance on Noise RMS `A`. 50 experiments were performed for every choice of `A` for 4 detectors: this means that measurements for single detectors

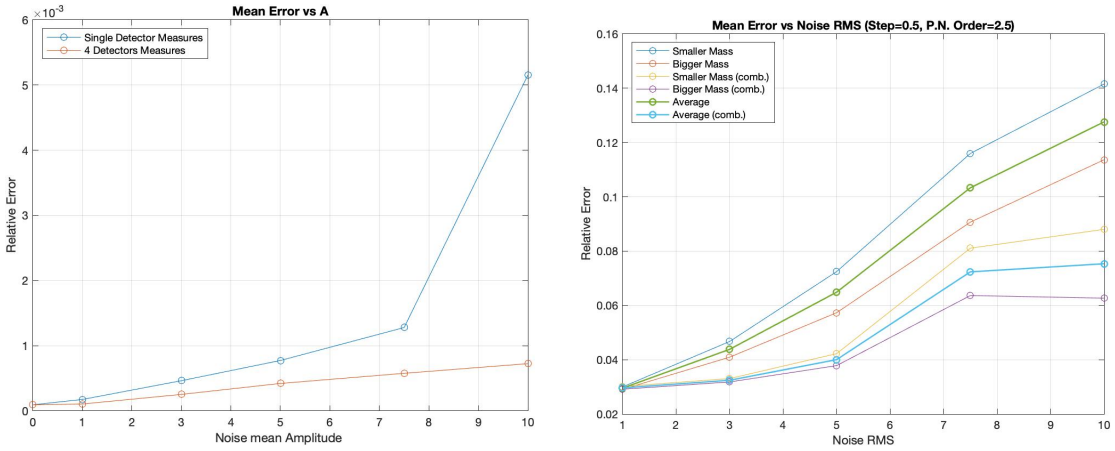

Figure 3: The behavior of the mean error on parameters identification with respect to the ratio between noise RMS and signal mean absolute amplitude `A` is presented. In the Newtonian case (left) the error on the chirp mass $\mathcal{M}$ is studied, while in the post-Newtonian case (right) the error on the masses is reported. In both cases, errors increase almost linearly with `A` for small values.

are averaged over 50x4=200 values, while combined measures are averaged simply over 50 values. In Figure 3, the results are presented. `A` is defined as the ratio between noise RMS and signal mean absolute amplitude[11].

It has been observed that the error increases almost linearly with the noise RMS for small values. Furthermore, it is evident that combined measures give a much more precise estimate in particular for high noises: this happens because the noise is "averaged" an all detectors.

1.2.1 Dependence on Grid Steps

To investigate the dependance of the error on the step of the grid, the noise RMS `A` was fixed equal to 1 for the Newtonian case and equal to 3 in the post-Newtonian case. The two cases are reported in Figure 4.

Even if these results seem to legitimate the grid technique as a good one to perform such evaluations, it has been observed (see Appendix F.4.3) that this behavior is not valid when using smaller grid steps in the post-Newtonian case. A signal of this behavior could be identified in the fact that combined measures do not increase in precision going from a step of $0.25\,\mathrm{M}_\odot$ to $0.1\,\mathrm{M}_\odot$. This implies that it is not possible to reduce the error on masses evaluation by using denser grids. An example of this behavior is reported in Figure 5. It must be remarked that, in this

[11]Sometimes `A` will be referred to as 'noise RMS", assuming the normalisation by the signal mean absolute value.

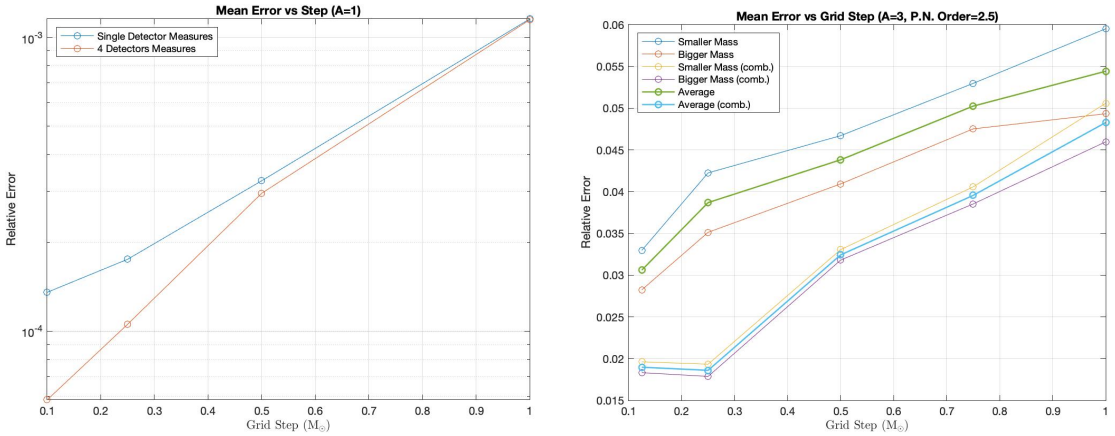

Figure 4: The left figure shows that the errors in the Newtonian case (left) decrease logarithmically with diminishing grid step for a low value of noise. In post-Newtonian case (right), instead, the error on the masses decreases almost linearly with the grid step. Thus, it is much more difficult to achieve better precisions.

case, errors on masses are pretty low. This happens only because the selected range is $[30\,M_\odot, 33\,M_\odot]$: masses having ratio close to 1 (as in this case), are always pretty well estimated (see Appendix F.2), but the considerations on the non-decreasing trend are still valid. Therefore, in order to achieve better measurements (especially for "unbalanced" couples of masses), the methods presented in Sections 2 and 3 have been developed.

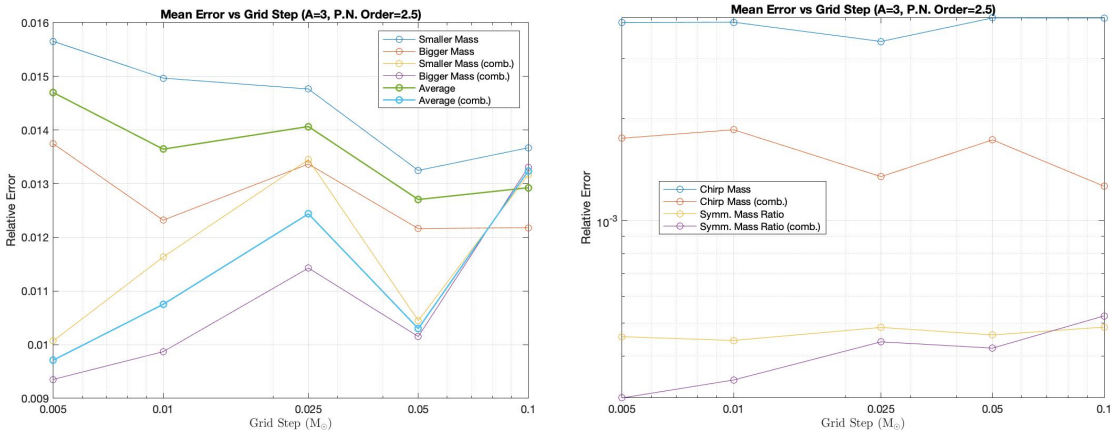

Figure 5: The mean errors on the masses (left) and on $\mathcal{M}$ and ν (right) are reported as a function of the grid step. Smaller values (in order to use denser grids) are used. It is clear that precision does not significantly increase using smaller steps.

2 Grid ($\mathcal{M} - \nu$) : a New Approach

The grid of masses approach, outlined in Appendix C and fully exploited in Appendices D and F, has proved to be extremely powerful for the analysis of chirp signals. However, as explained in detail in F.4.3, the strongest limitation is that the error on the estimate of the source masses does not seem to undergo a significant reduction decreasing the grid step (see Figure 76).

While, at first glance, this behavior might appear indicative of an error, it should be remarked that the Post-Newtonian approximation, being a correction of the Newtonian approach, firstly aims at seeking the combination which best reproduces the *chirp mass* of the injected signal. Secondly, coupling the equation for the *chirp mass* $\mathcal{M}$ with the estimate of the *symmetric mass ratio* ν, the values of the two masses are calculated. Therefore, grid pairs having a different *chirp mass* and *symmetric mass ratio* (defined later on in 1) from the initial binary system produce a low SNR. As a consequence, they will not be classified as the best couple, no matter how close they are to the original masses in the (m_1-m_2) plane. In a certain sense, all the previous analysis has been carried out in a non-optimal basis, in which there is not convergence to the true values of the masses, even if the step becomes smaller.
According to [1], the Post-Newtonian terms (as for power radiated in GWs, signal amplitude etc.) can be written as an expansion in the dimensionless variable x, depending from the *source orbital frequency*. Looking at the complete expressions (reported in Appendix E.1), it is evident that both x and the *orbital phase* $\phi(t)$ are explicitly dependent from the *symmetric mass ratio*, defined as:

$$\nu \equiv \frac{m_1 m_2}{(m_1 + m_2)^2}, \tag{1}$$

This remark suggests that the Post-Newtonian approximation does not depend on the two separate masses, but rather on their combinations, like the *total mass* or the *symmetric mass ratio*. Since the ultimate purpose of the analysis is the estimate of the single masses constituting a binary gravitating system, there will be need only for two coupled formulae in the unknowns m_1 and m_2. Looking at the previous statements (and considering that the Post-Newtonian approach slightly corrects the Newtonian behavior), a system can be defined in the simplest way by its *chirp mass* $\mathcal{M}$ and its *symmetric mass ratio* ν. As a consequence, this "natural basis" is better represented in the ($\mathcal{M}$-ν) plane, where the following analysis will be performed. In the subsequent work, it will be clear that in these coordinates the high-SNR region is confined in a spot-like area centered approximately on the true values. Besides, the SNR decreases almost monotonically considering an outgoing radial path centered on the right masses; so, the algorithm appears to be more "convergent" than the previously described grid of masses. This Section's

purpose is to give a first estimate of the involved quantities, delegating a more refined analysis to Section 3.

2.1 Discretisation Limit

Analogously to the results obtained in F.1, the following discussion aims at evaluating the errors coming from the discreteness of the grid, thus establishing the intrinsic limit of the procedure. Even though the subsequent results might seem comparable or just slightly improved with respect to the grid of masses case, some advancements should be taken into account: firstly, the computational time required decreases significantly achieving the same outcomes; secondly, the algorithm is more "robust" with respect to masses estimation. As for the second statement, while in the grid of masses case the initial range considered may well influence the results, excluding potential points having suitable values of the *chirp mass*, the new approach, exploiting the analysis directly in the $(\mathcal{M} - \nu)$ plane, circumvents this issue. Moreover, the current method manifests a better and faster convergence than the (m_1-m_2) one, since the more distant the new grid points are from the ($\mathcal{M}_{sr}$-ν_{sr}) source couple, the lesser the filter they produce matches with the actual incoming signal.
In order to produce meaningful results, the analysis will be carried out fixing one of the two parameter steps and letting the other vary. From the following graphs, it will be understood that both the steps need to be decreased simultaneously if a more refined analysis is desired. All these results are obtained averaging over 36 different simulations, where the *chirp mass* and the *symmetric mass ratio* are generated randomly in $[20\,\mathrm{M}_\odot,\ 25\,\mathrm{M}_\odot]$ and $[0.20,\ 0.25]$, respectively.

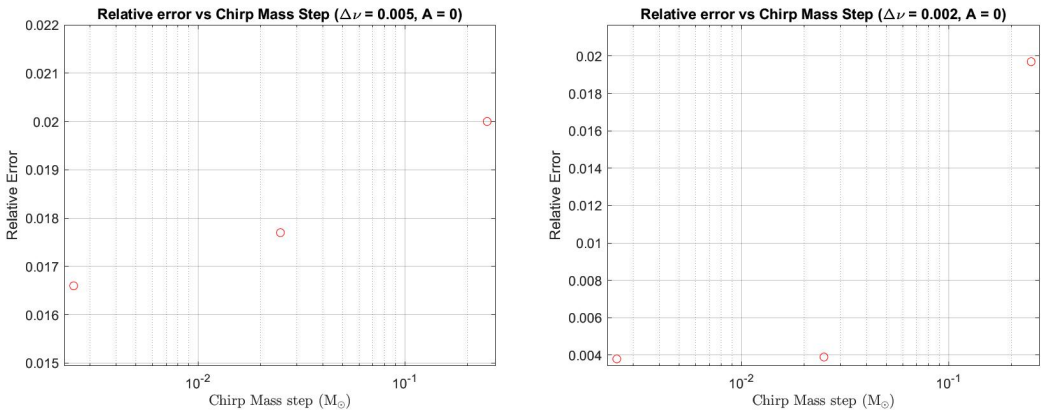

Figure 6: Relative error on the estimation of the masses as a function of the *chirp mass* step in the absence of noise. Left: $\Delta\nu = 0.005$. Right: $\Delta\nu = 0.005$.

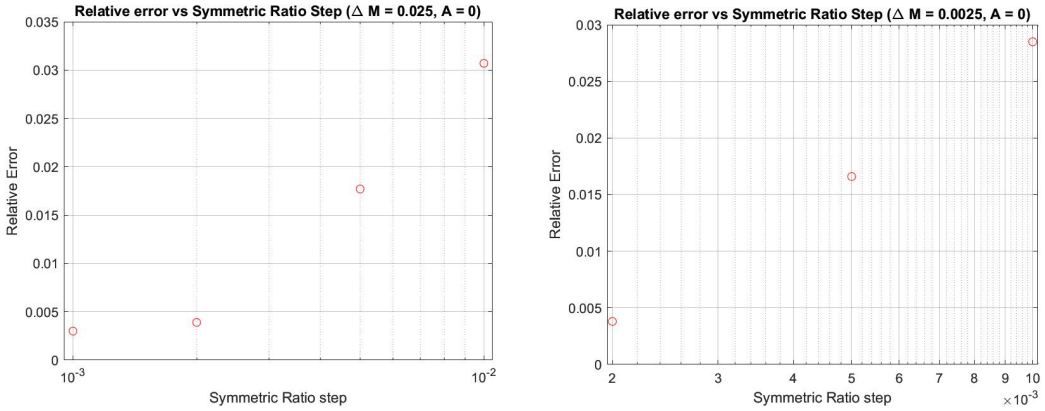

Figure 7: Relative error on the estimation of the masses as a function of the *symmetric mass ratio* step in the absence of noise. Left: $\Delta\mathcal{M} = 0.025\,\mathrm{M}_\odot$. Right: $\Delta\mathcal{M} = 0.0025\,\mathrm{M}_\odot$.

As previously anticipated, these plots show that the grid spacing needs to be scaled in both the axis in order to claim a sensible result. This appears evident looking at Figures 6 and 7 , where the precision on the estimate of the masses saturates to a constant after a certain step, no matter how much the step on the *chirp mass* or on the *symmetric mass ratio* is decreased. In this case the spacing in one of the two dimensions dominates the error on the final outcome, leading to a higher uncertainty on the gauging of the masses[12]. The comparison between the two cases in Figure 7[13] provides further confirmation, informing that analysing with a smaller *chirp mass* step does not produce any benefit[14], as long as the spacing in the *symmetric mass ratio* dimension is too high (and vice-versa). Finally, some meaningful plots are presented. In this picture, it should be recalled that the *z-axis* is shown in arbitrary units.

[12] Just think about the propagation of errors...

[13] Notice that in the rightmost figure smaller steps have not been considered, being too computationally demanding. However, being the analysis performed in an unphysical `A`=0, it is not particularly necessary to furnish any further details.

[14] However, it must be stressed that the reached limit is quite good, as far as the errors coming from the discretisation of the grid is concerned.

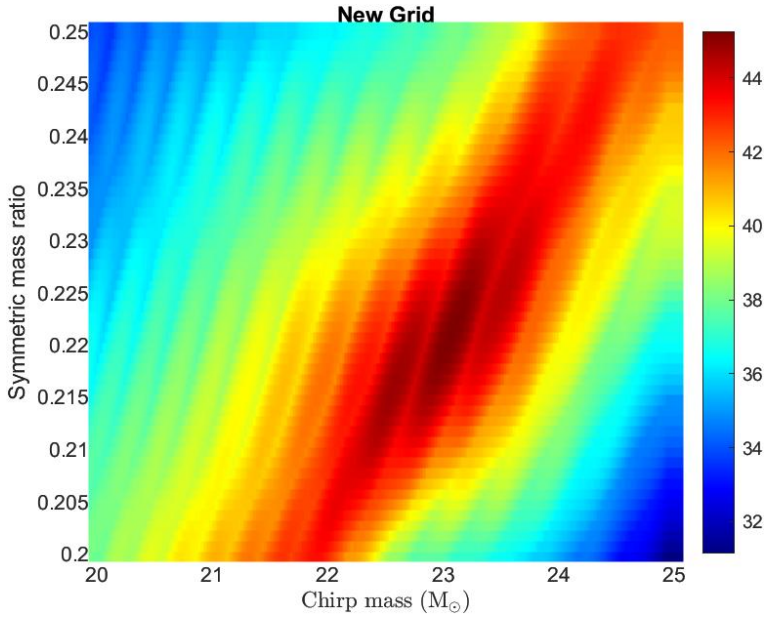

Figure 8: Identification of the couple having the correct *chirp mass* and *symmetric mass ratio* in the new ($\mathcal{M}$-ν) grid, in the absence of noise. $\Delta\mathcal{M} = 0.025\,\mathrm{M}_\odot$ and $\Delta\nu = 0.001$.

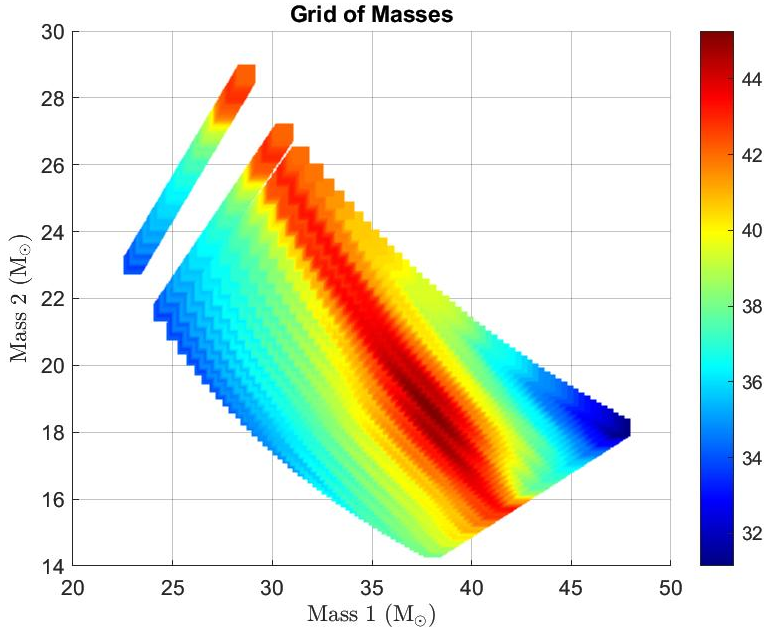

Figure 9: Figure 8 converted in the (m_1-m_2) plane.

These figures illustrate why the new algorithm is more "convergent": there

are no bright curve or distant but equally bright regions. The true masses always reside in the most shining area in both of the coordinates, and the z-values decrease (though not monotonically) moving on an outgoing radial path. In conclusion, the final error will be smaller than the one obtained in the (m_1-m_2) grid approach, once having carefully chosen the grid parameters.

2.2 Signal Embedded in White Noise

Having established the limit due to the discretization of parameters, the focus shall be shifted to the analysis of a signal buried in Gaussian white noise. The final results of this section shall be compared with the grid of masses case (Appendix F) and will bring further insight on the"convergence" of the method. The plots below will follow the same line of reasoning outlined in the previous paragraph, so there will be no need for additional explanation.

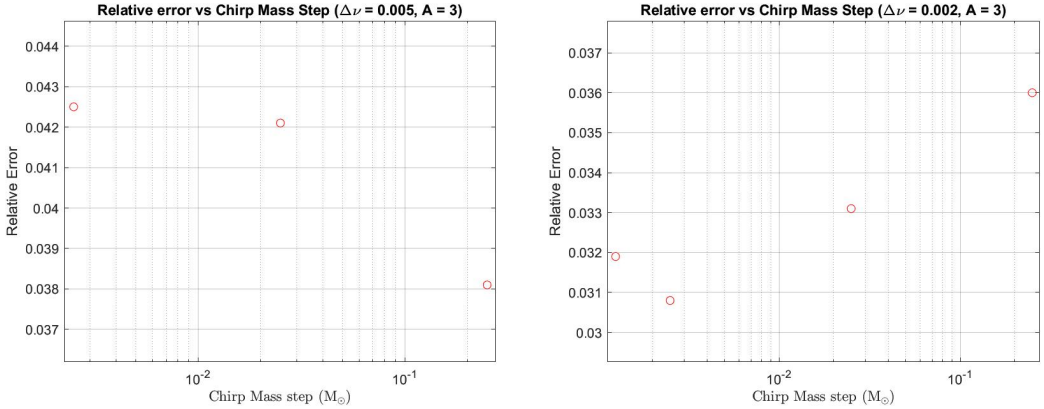

Figure 10: Relative error on the estimate of the masses as a function of the *chirp mass* step, with A = 3. Left: $\Delta\nu = 0.005$. Right: $\Delta\nu = 0.002$.

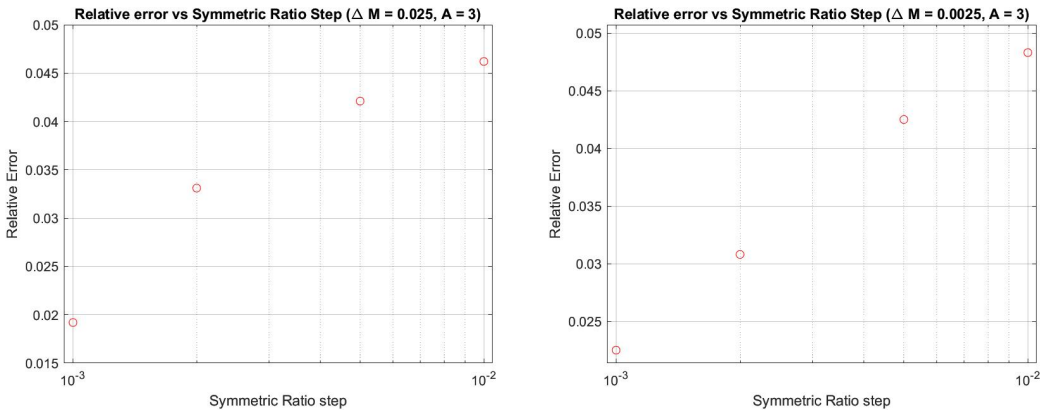

Figure 11: Relative error on the estimate of the masses as a function of the *symmetric mass ratio* step, with A = 3. Left: $\Delta\mathcal{M} = 0.025\,\mathrm{M}_\odot$. Right: $\Delta\mathcal{M} = 0.0025\,\mathrm{M}_\odot$.

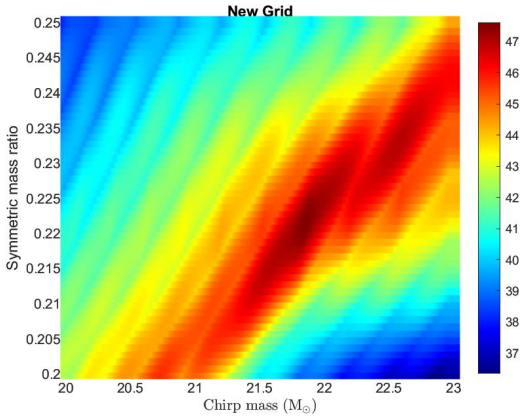

Figure 12: Identification of the couple having the correct *chirp mass* and *symmetric mass ratio* in the new ($\mathcal{M}$-ν) grid. $\Delta\mathcal{M} = 0.025\,\mathrm{M}_\odot$, $\Delta\nu = 0.001$ and A=3.

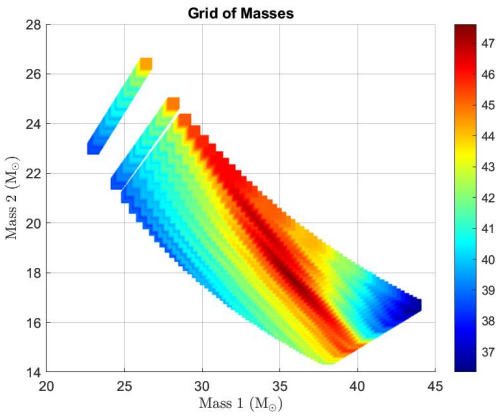

Figure 13: Figure 12 converted in the (m_1-m_2) plane. A=3.

It is also interesting to study the behaviour of the error on the masses as a function of the noise *r.m.s* `A`, keeping the steps fixed:

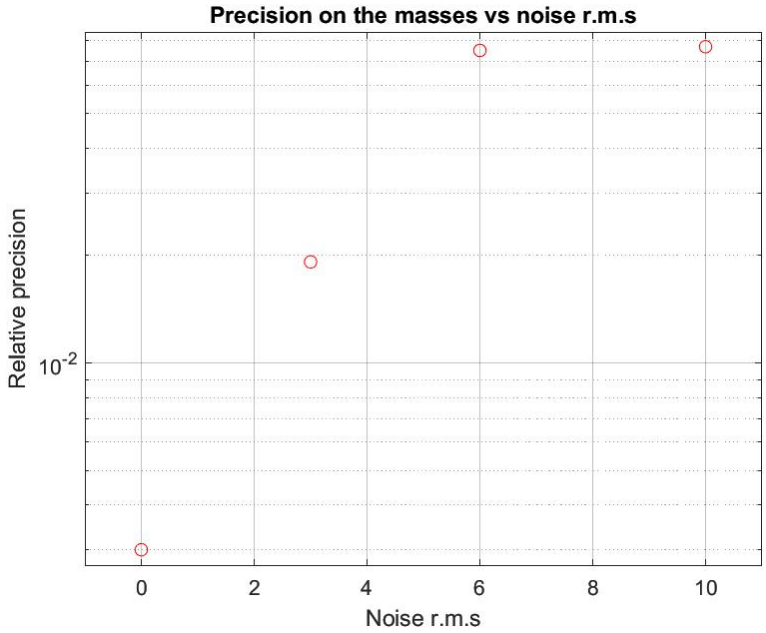

Figure 14: Precision on the masses as a function of noise $r.m.s$, averaged on 36 random simulations. $\Delta\mathcal{M} = 0.01\,\mathrm{M}_{\odot}$, $\Delta\nu = 0.001$.

It might be argued that these results do not constitute an improvement, since, sometimes, the error estimated with this procedure turns out to be higher than the corresponding one found in the grid of masses picture. However, it should be recalled that, in the old method, the analysis was carried out in an initially chosen range, which could possibly eliminate some suitable couples of masses. In this case, instead, the algorithm has been developed in the ($\mathcal{M}$-ν) plane; so, all the pairs having proper values of the *chirp mass* and of the *symmetric mass ratio* are taken into account[15]. Therefore, the current method is not linked to the specific domain of the parameters involved. Moreover, it has been decided to carry out these simulations considering *high mass-ratio* pairs, for which the errors have been previously estimated to be higher than the ones obtained looking for similar masses (as discussed in Section F.2). In this way, it is possible to furnish an upper evaluation of the uncertainty that needs to be associated to the final measurement. In conclusion, an independent-from-the-domain error can be assigned, leading to a more "robust" result. Finally, the outcome of the ($\mathcal{M}$-ν) grid will be refined applying the techniques in Section 3, which will provide the ultimate achievement of the entire procedure.

[15]Of course, the concept of "proper values" is closely related to the spacing of the new grid.

2.3 Time of detection

The estimation of the time of arrival represents one of the principal issues in the detection of a chirp signal. Therefore, when developing a new method (such as the ($\mathcal{M}$-ν) analysis), it should always be checked whether the time of arrival is correctly found or not. In this approach, in line with all the expectations, the standard deviation of the difference between the time of detection and the time of arrival (i.e, the *delay*) behaves in the following way:

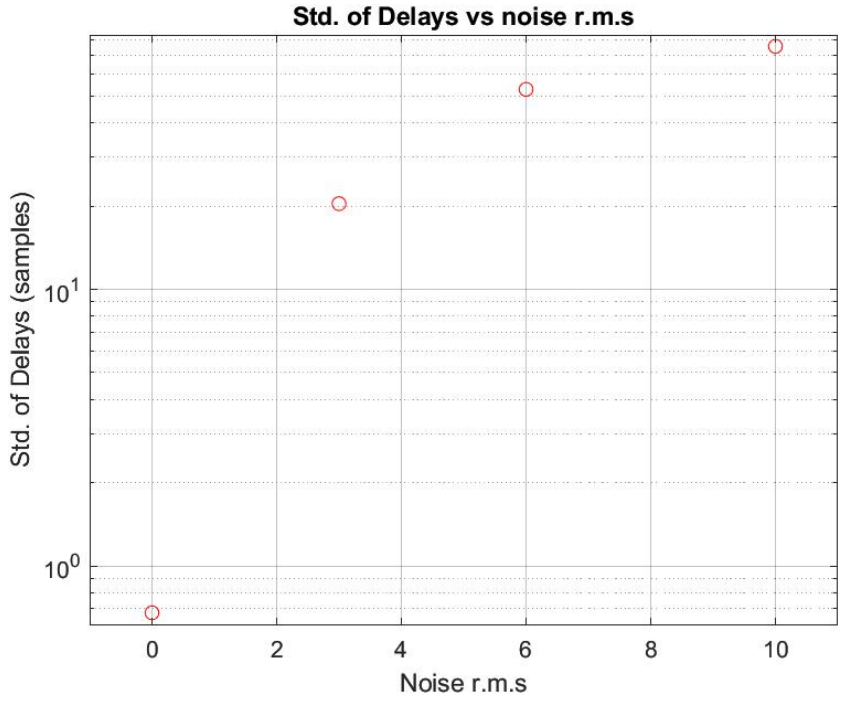

Figure 15: Standard deviation of delays as a function of noise r.m.s, averaged on 36 random simulations. $\Delta\mathcal{M} = 0.01\,\mathrm{M}_\odot$, $\Delta\nu = 0.001$.

Only the *correct detections* have been plotted[16]. In particular, when `A` $= 10$, the *false detection rate* amounts to a significant 13%; so, it would have been meaningless to graph higher noise *r.m.s*.
Comparing Figures 60 and 15, there appears not to have been a significant improvement. However, it must be recalled that this section deals with a first approximate estimate of the involved physical quantities, delegating a more accurate approach to Section 3.

[16]See D.2 for a definition of *correct detections* and *false detection rate*.

2.4 Chunk method

In order to perform more precise simulations, it could be useful to implement the *chunk method* [17] (discussed clearly in C.1), adapted to deal with the ($\mathcal{M}$ - ν) coordinates. However, the approach and the operations remain exactly the same even in the new grid; so, there will be no further description of the procedure. It must be noticed that, as already specified, this method brings, on average, a slight improvement on the masses, but at great cost: the executions is several times slower. Therefore, since this part of the work aims at giving just a first estimate, the *chunk method* has never been taken into account in the previous results. On the other hand, it might be interesting to provide some plots, like Figures 16, 17, 18 and 19.

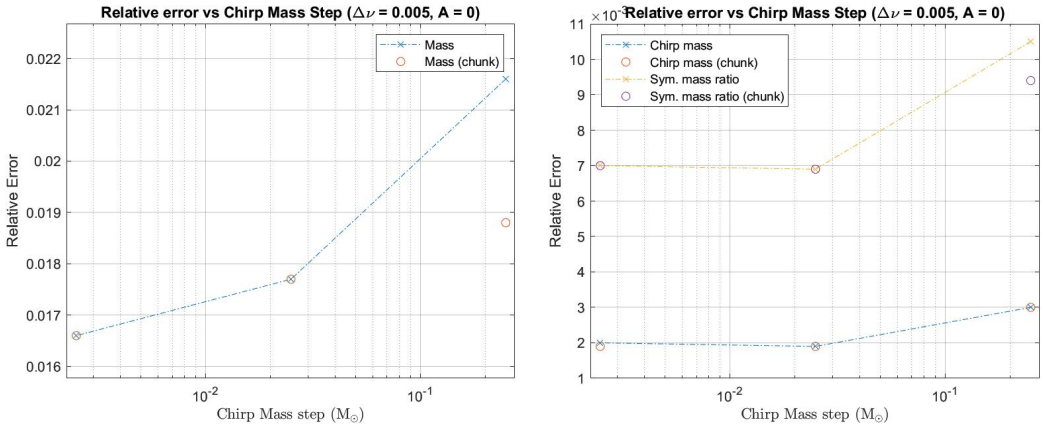

Figure 16: Left: relative error on the masses as a function of chirp mass step. Right: relative error of *chirp mass* and *symmetric mass ratio* as a function of chirp mass step. Average on 36 random simulations, $\Delta\nu = 0.005$ and A=0.

[17] The filter is divided in various pieces (i.e. *chunks*), each one filtering the data independently.

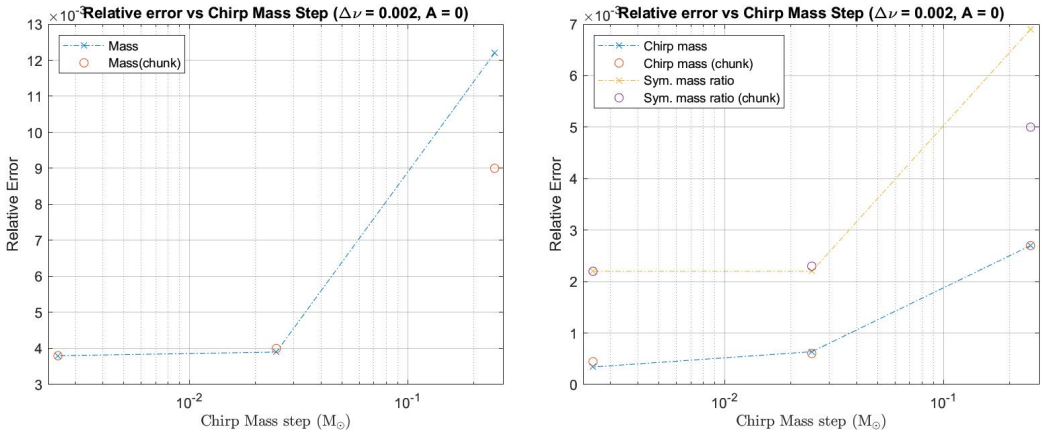

Figure 17: Left: relative error on the masses as a function of chirp mass step. Right: relative error of *chirp mass* and *symmetric mass ratio* as a function of chirp mass step. Average on 36 random simulations, $\Delta\nu = 0.002$ and A=0.

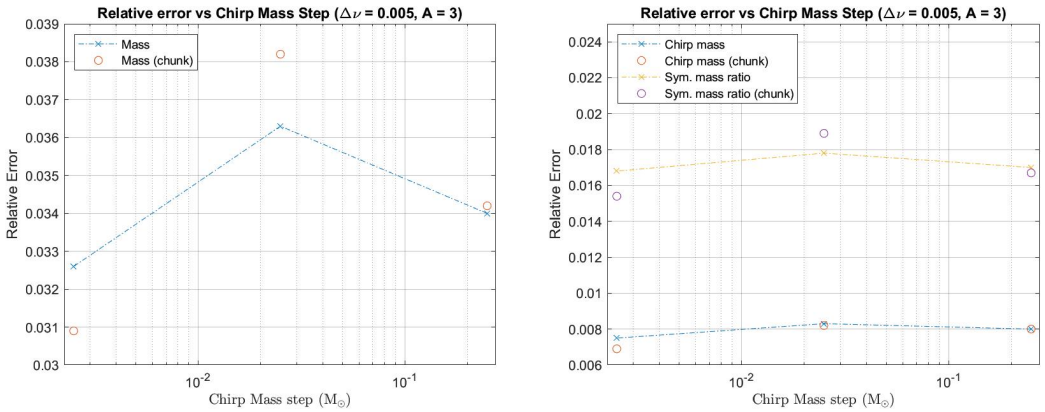

Figure 18: Left: relative error on the masses as a function of chirp mass step. Right: relative error of *chirp mass* and *symmetric mass ratio* as a function of chirp mass step. Average on 36 random simulations, $\Delta\nu = 0.005$ and A=3.

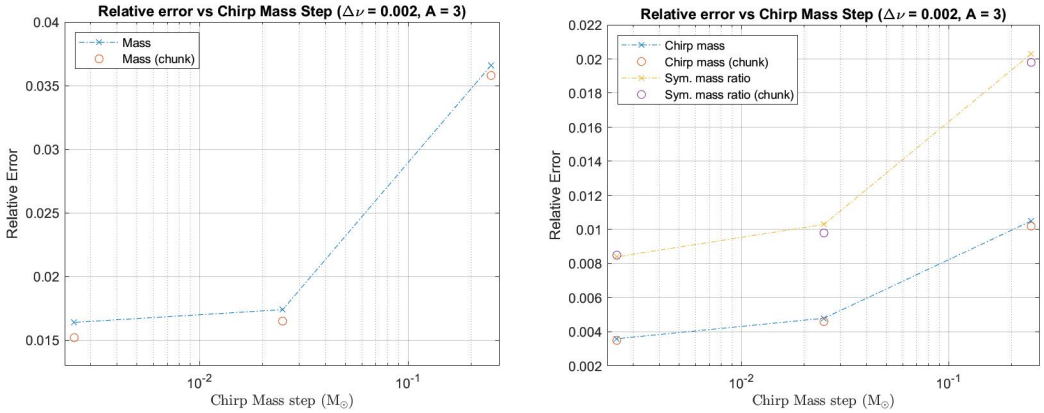

Figure 19: Left: relative error on the masses as a function of chirp mass step. Right: relative error of *chirp mass* and *symmetric mass ratio* as a function of chirp mass step. Average on 36 random simulations, $\Delta\nu = 0.002$ and A=3.

Figures 16 and 17 show an advancement on the estimate of the intrinsic limit of the procedure when dealing with higher values of the *chirp mass* step. Although this achievement turns out to be useful when trying to give a rough estimate of the discretisation limit (see paragraph 2.1), the *chunk* approach gives almost the same results for small grid spacing. However, it must be noticed that, in the limit $\mathtt{A} = 0$, the absence of noise makes only suitable points assume a high value of SNR; so, as for a refined grid, there is no room for ambiguity. Therefore, the focus shall be moved to the case $\mathtt{A} = 3$. While the case $\Delta\nu = 0.005$ does not display any improvement when performing the *chunk* analysis, Figure 19 shows modestly lower errors both on the masses and on the descriptive quantites (*chirp mass* and *symmetric mass ratio*) involved. This confirms what stated at the beginning of Section 2: a "too large" step in one dimensions prevents the procedure from furnishing better results, since it dominates the final errors. For this reason, the *chunk* method will be effective only defining the grid properly, as done in Figure 19. In conclusion, according to the previous discussion, the *chunk* method reveals to be helpful; however, in the majority of cases, it's not worth the hassle.
Starting from the results here stated, a more refined analysis will be the purpose of the following section.

3 A Deeper Analisys: "Rand_CMR"

In this section, the "**Rand**om **C**hirp **M**ass-**R**atio" method will be presented, which allows to sensibly reduce errors on parameters estimation. In the grid methods described in the previous sections, three main issues occur when one wants to get a refined estimate of the parameters of the signal:

1. Matched filtering is applied to several grid points with very low SNR (this can be clearly seen from Figures 1 and 8).

2. The error on estimated parameters strongly depends on the grid step: this characteristic is intrinsic of the grid method.

3. The "grid of masses" technique works perfectly only if the masses to detect are *exactly* a grid point, which is an unphysical situation. A step toward the resolution of this problem was taken by developing the approach presented in Section 2.

The underlying ideas to solve this problem are the following:

1. **Focus:** only interesting areas of parameters spaces are deeply analyzed (this means that a previous raw analysis to identify these areas is needed).

2. **Random:** using random numbers, it is possible to eliminate the dependence of the error from the step of the grid.

The developed technique consists in the generation of random numbers (the choice of the used distribution will be soon discussed) around a central value. Then, matched filtering is applied with filters using parameters corresponding to all this points, in order to identify the one with the highest SNR. It is important to remark that this method needs a previous grid analysis, even if not highly accurate. The advantage of this technique can be easily understood recalling Figure 8: it is meaningful to analyze very dense points only on the yellow spot-like area, that contains all the points with high SNRs. Due to the considerations outlined in the previous sections, the points are selected firstly in the $\mathcal{M} - \nu$ plane and are later translated in terms of the two masses.

3.1 Random Distributions

Random points can be selected using different distributions: the choice of the best one for different purposes will be the topic of this paragraph. Two different cases have been studied, which are the most intuitive ones:

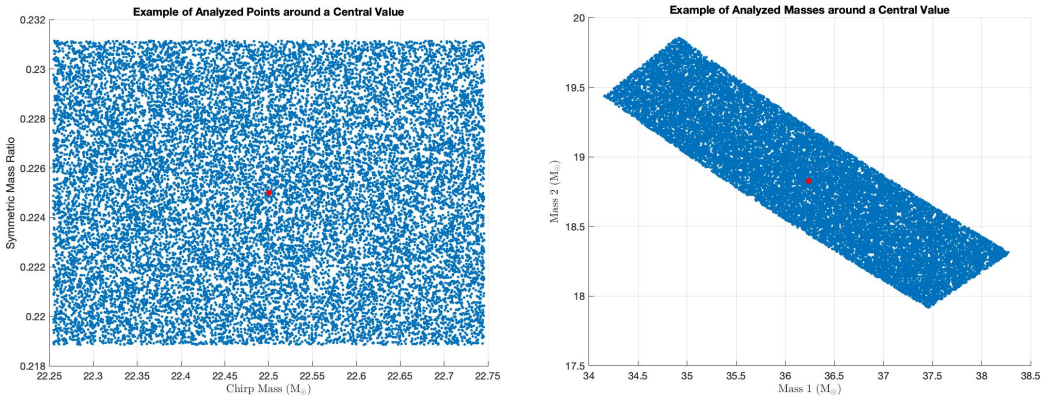

Figure 20: Left: $2 * 10^4$ random uniform points in the $\mathcal{M} - \nu$ plane. Right: corresponding points in the two masses plane.Widths: $0.25\,\mathrm{M}_\odot$ for $\mathcal{M}$, 0.005 for ν. Red point: estimate furnished by Section 2.

Uniform Distribution Random points are generated around a previously estimated value in the $\mathcal{M} - \nu$ plane using a flat distribution. The width should be adjusted taking into account the confidence on the previous estimate (see paragraph 3.4). An example is reported in Figure 20.

Normal distribution If the 2-D function describing SNR was exactly monotonous in all directions, it would be more meaningful to use a uniform distribution centered on the previously estimated value. An example of this case is presented in Figure 21.

Updating Central Value Algorithm An algorithm was build in order to try to approximate the best value using a step-by-step procedure: a normal distribution is used, but its central value is updated every time that a better value if SNR is identified. The idea behind this procedure is to construct a basic optimization algorithm that gradually converges to the highest value of the SNR.

3.2 Comparison of Results

In order to decide the best distribution to use to estimate parameters, the comparison outlined in this paragraph was performed[18]. A dataset consisting of 100 simulations was generated. $\mathcal{M}$ and ν on these simulations were estimated using the grid technique and they presented a mean relative error of 0.004 on the chirp mass and 0.010 on the symmetric mass ratio. Then, the above-described procedure

[18]Refer to code `Error_Eval_CM.m`

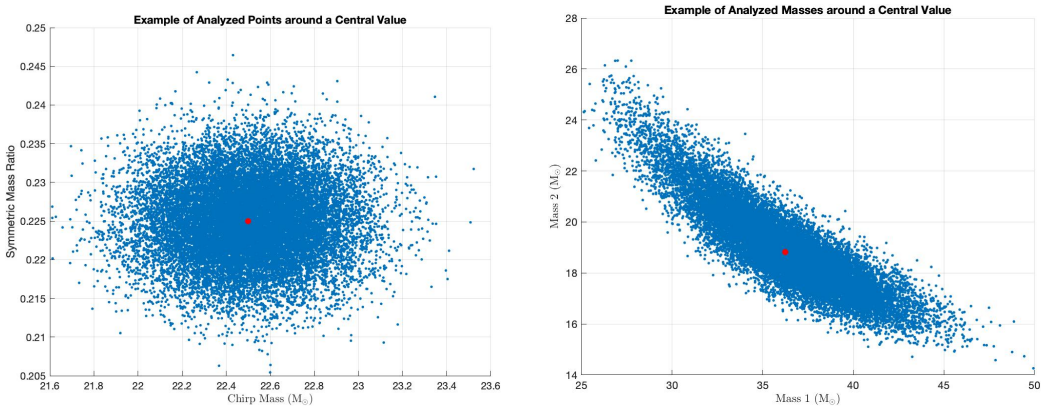

Figure 21: Left: $2 * 10^4$ Gaussian distributed points in the $\mathcal{M} - \nu$ plane. Right: corresponding points in the two masses plane. $\sigma_{\mathcal{M}} = 0.25$, $\sigma_\nu = 0.005$. Red point: estimate furnished by Section 2.

was applied to this dataset. The average error on estimated masses is reported in Figure 22 for all the three cases before mentioned.

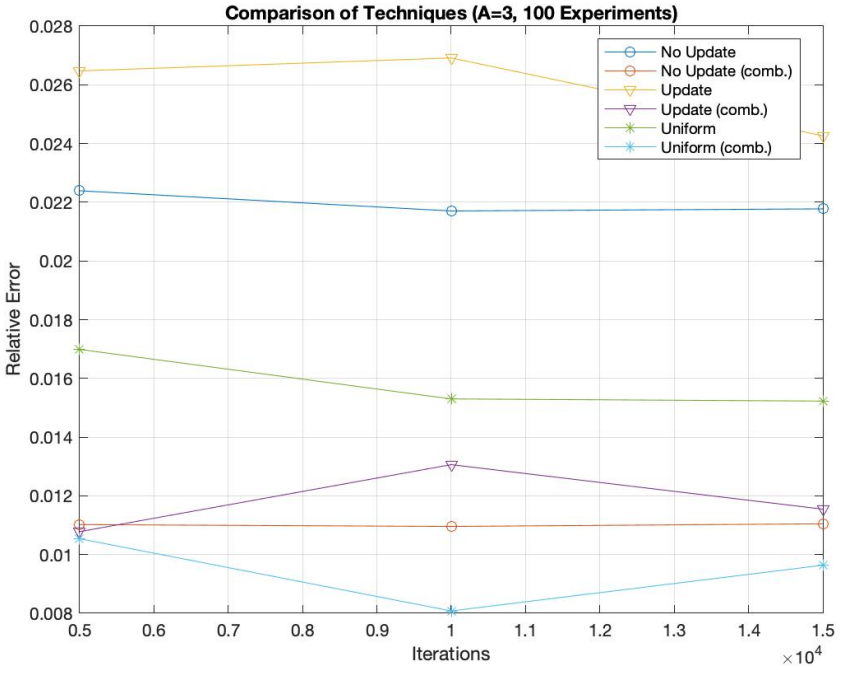

Figure 22: Comparison of average error on masses for different methods.

It can be seen that the uniform distribution gives the most accurate estimation of the parameters: this happens because the normal distribution strongly relies

on the previous estimation, which is not always precise. The updating algorithm, instead, even if more refined, produces results even worse than the simple normal case.
This result may appear not intuitive, but a simple explanation of the failure of the updating algorithm can be given: it relies on monotony of the SNR function, which is only globally respected (higher values are concentrated in the yellow spot-like area), but not locally (inside the spot there not monotony). The conclusion that can be drawn is that this algorithm can be used as an efficient way to quickly individuate the area in the parameter space that produces high values of SNR, but it cannot be used to perform a fine estimation of parameters. Thus, it could be used as a smarter replacement of the grid method for the initial estimate, but the final refined search should be still done using the uniform distribution, which has a less important dependence on the starting point.
Since the aim of this chapter was to find a method to perform a refined analysis of the parameters, it has been shown that only the uniform distribution fulfills this requirements. Therefore, only this one will be used in the following analysis.

3.3 Precision as a Function of the Iteration

Intuitively, it can be guessed that the precision of the measure will increase when increasing the number of points. This behavior is generally observed, as in reported in the followed graphs, obtained from 30 experiments with a previous estimation of parameters having a mean relative error of 0.004 on the chirp mass and 0.01 on the symmetric mass ratio, as in the previous case.

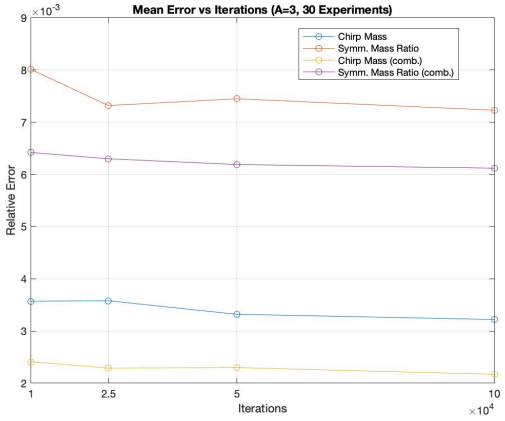

Figure 23: Relative error on chirp mass and on symmetric mass ratio as a function of tried points using the uniform distribution.

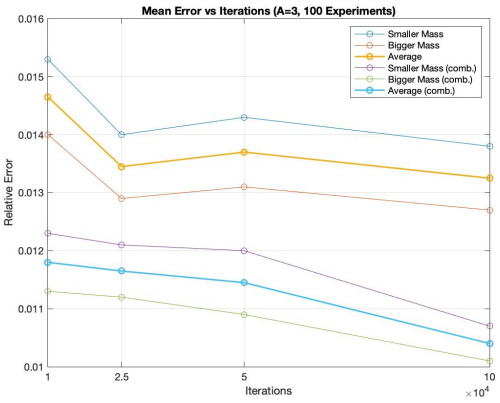

Figure 24: Relative error on masses as a function of tried points using the uniform distribution.

It can be seen that after $2.5 * 10^4$ iterations, the convergence becomes very slow. However, it is important to underline that the precision on these measure is already very high.

3.4 Precision as a Function of the Previous Estimate

It is very interesting to study how the mean relative error depends on the previous estimate of the parameters, once the number of iterations is fixed. It is important to remark that the precision of the previous estimation fixes the width of the analyzed region in parameters space, and consequently the density of the points. The width of the distribution was always chosen in order to be equal to two times the mean error coming from the previous estimate. Datasets of 30 experiments each having the following couples of mean error on parameter where studied. They are presented in order of increasing precision in Table 1.

Rel. Error	$\mathcal{M}$	ν	m_1	m_2
Couple 1	0.0103	0.019	0.0358	0.0331
Couple 2	0.0079	0.015	0.0288	0.0266
Couple 3	0.0062	0.011	0.0211	0.0194
Couple 4	0.0035	0.008	0.0153	0.0140

Table 1: Relative error on chirp mass and on symmetric mass ratio from different sets of measures after using the standard grid method.

The precision on estimated parameters after the application of this technique using $5 * 10^4$ iterations is presented in Figures 25 and 26. The precision increase is also reported in Figures 27 and 28.

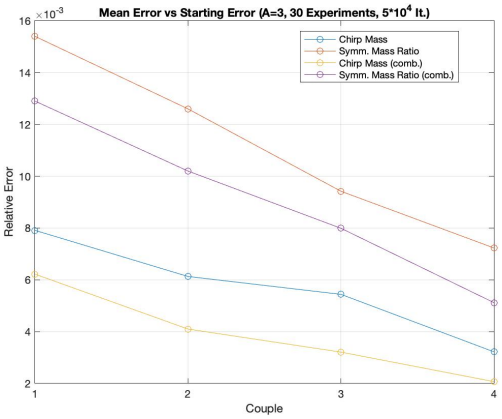

Figure 25: Relative error on chirp mass and on symmetric mass ratio as a function of previous precision using the uniform distribution with $5 * 10^4$ points.

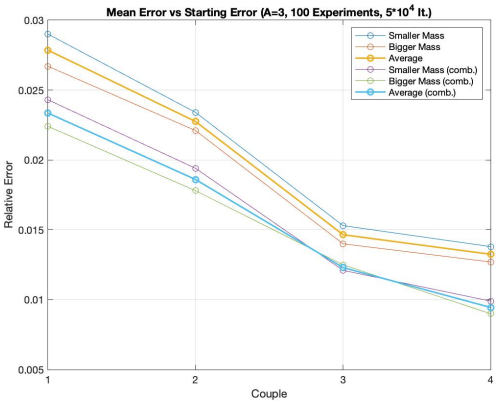

Figure 26: Relative error on masses as a function of previous precision using the uniform distribution with $5 * 10^4$ points.

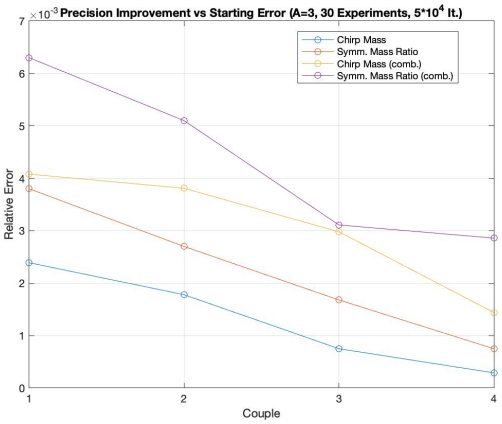

Figure 27: Improvement of relative error on chirp mass and on symmetric mass ratio with respect to the previous estimation.

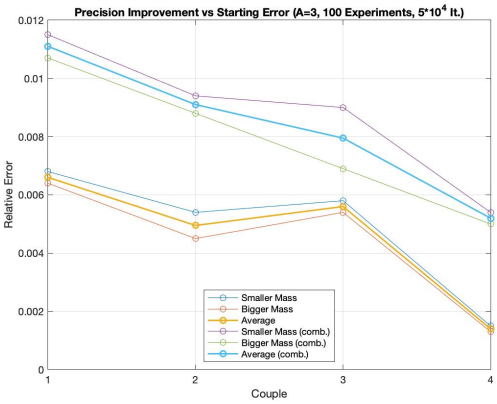

Figure 28: Improvement of relative error on masses with respect to the previous estimation.

It can be seen that errors are significantly reduced on measures that were not accurate at the beginning, but they do not reach the same precision. This happens because the density of the points is different: higher ranges must be selected when dealing with less accurate estimations. It is important to highlight that in the latter case, the mean relative error on the masses was reduced below 1.4% even for single detector measures (below 1% for combined measures): this result should

give an idea of the power of this method, even considering that probably it could be even reduced using higher computational power, if the trend in Figures 24 and 26 are respected.
In cases with a lower number of iterations, it was also verified that the same precision can be achieved even if starting from different values of the initial mean error on the parameters. Indeed, the starting mean error depends only on the parameters (i.e. the grid steps) chosen for the first analysis, but all the simulated situations are exactly equivalent in terms of noise (`A=3` in all cases).

4 Real Noise

In real interferometers, data is not white (see [2] and [3]): different frequency bands show different behavior of noise, and there are several non-stationary and non-gaussian disturbances that may occur. The aim of this paragraph is to show that it is possible to "whiten" noise, in order to recover the situation used for the simulations performed in the previous sections. In particular, data chunks[19] from the LIGO interferometers containing the"GW150914" event (see [4]) will be studied, since the embedded signal has a very high SNR (it is very easy to detect). Examples of these chunks (lasting 32 seconds) are reported in Figure 29.

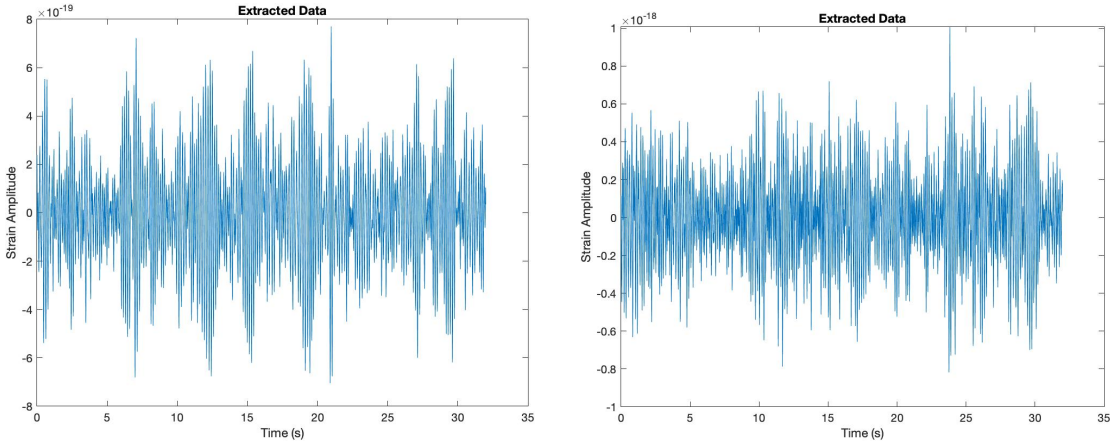

Figure 29: Data measured from LIGO Hanford (right) and Livingston (left) interferometers.

The estimated waveform is reported in Figure 30, along with the corresponding one including simply Post-Newtonian corrections, but not the merger and the ringdown parts (for more details, see Appendix A.2.3). It should be noticed that in this case the noise amplitude is 2-3 orders of magnitude larger than the signal. It will be shown that also this issue is solved using the procedure outlined in the following section.

4.1 Spectral Whitening

The spectral whitening procedure (readapted from [5]) is both powerful and intuitive: the way it was implemented[20] can be summed up as in the following steps:

[19] take

[20] Refer to code `Det_Real_DATA.mlx`

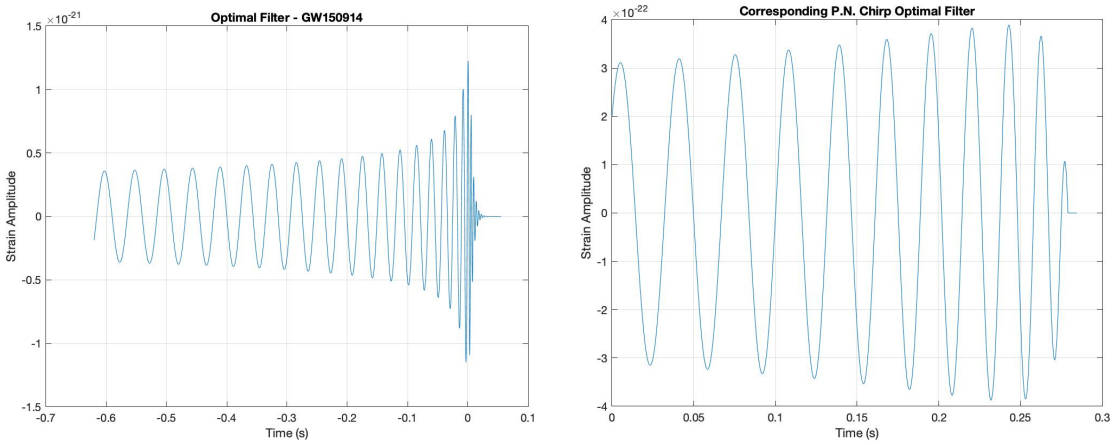

Figure 30: The templates describing the "GW150914" event are reported. The left figure shows the template including also the "merger" and the "ringdown" parts, while the right one is the corresponding truncated waveform up to post-Newtonian correction of order 2.5. Masses of $29\,M_\odot$ and $36\,M_\odot$ (errors are not reported) were evaluated from the LIGO-Virgo collaboration (see [4]). These are the values used for the generation of the left waveform.

1. **Spectral Analysis:** The power spectrum of the data is in a range sufficiently small to approximate the noise as stationary.

2. **Smoothing:** The square root of the power spectrum is smoothed, in order to identify the general trend. A more detailed description of the smoothing process is reported further on.

3. **Effective Whitening:** The square root of the power spectrum of data is divided by its smoothed version. In this way, an almost flat spectrum should be obtained.

4. **Return to Time Domain:** The real part of inverse Fourier Transform of the smoothed spectrum should be taken, in order to get back to time domain.

The power spectrum of data processed with this algorithm become almost flat. A particular emphasis should be given to the two technical procedures described hereafter:

Windowing The Fourier Transform operation is a key factor in this algorithm. Since data and signals have limited lengths, it is important to apply windowing, in order to mitigate finite-size effects. A valid choice of the used window is the "Flat-Top Cosine-Edge", which is characterized by flatness of the central half, reduced side lobs, and good peak gain (see [6]).

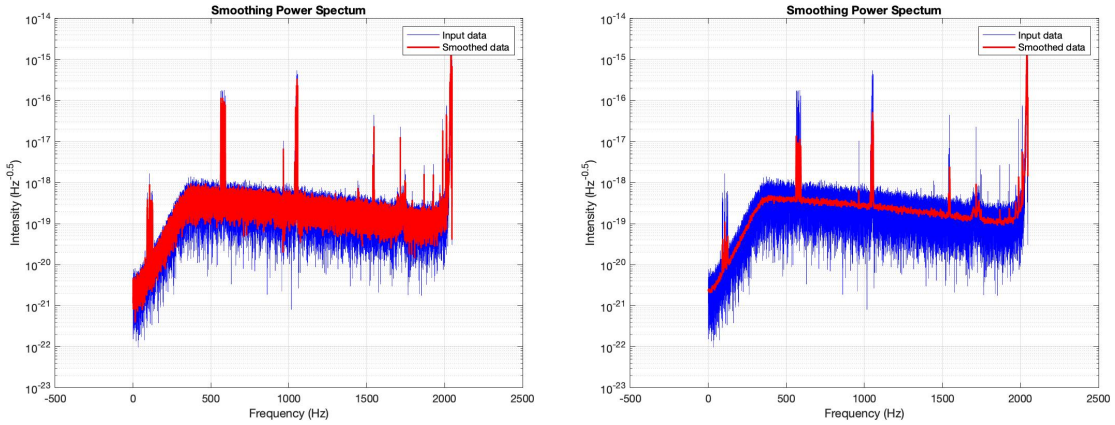

Figure 31: Original and smoothed power spectra of data measured from LIGO Hanford interferometer. Smoothing factors (numbers which determine the accuracy of the smoothing) of 0.01 (left) and 0.3 (right) are used in MATLAB moving average algorithms. A flat-top cosine-edge window is used

Smoothing Power spectrum of data is smoothed using MATLAB built-in functions relying on moving average algorithms. Smoothing can be done to different accuracies: it is important to select the best tradeoff in order to obtain a white power spectrum, but not to distort the signal too much. Smoothing accuracy is determined by a number called *smoothing factor*. Examples of the smoothing process with different accuracies is reported in Figure 31: The smoothed spectrum is the one from LIGO Hanford data in Figure 29 (left). Using a greater accuracy allows to get a whiter spectrum, but it may alter very much the characteristic of the signal and invalidate the matched filtering procedure. Thus, it is important to choose the smoothing factor coherently with the characteristics of the signals to detect. The whitened spectrum in both cases is reported in Figure 32. It can be seen that the first case returns a flatter spectrum, as one would expect.

An important remark that should be made is the following: spectral whitening affects also the signal embedded in the noise, which will be distorted. Thus, the filter used for matched filtering should be distorted appropriately: its spectrum must be divided for the smoothed spectrum of data evaluated at the second point of the procedure. Then, this distorted version has to be taken back to time domain, in order to perform matched filtering. More efficient algorithms performing spectral whitening and matched filtering in Fourier space all at once might be developed, but it was not the purpose of this work.

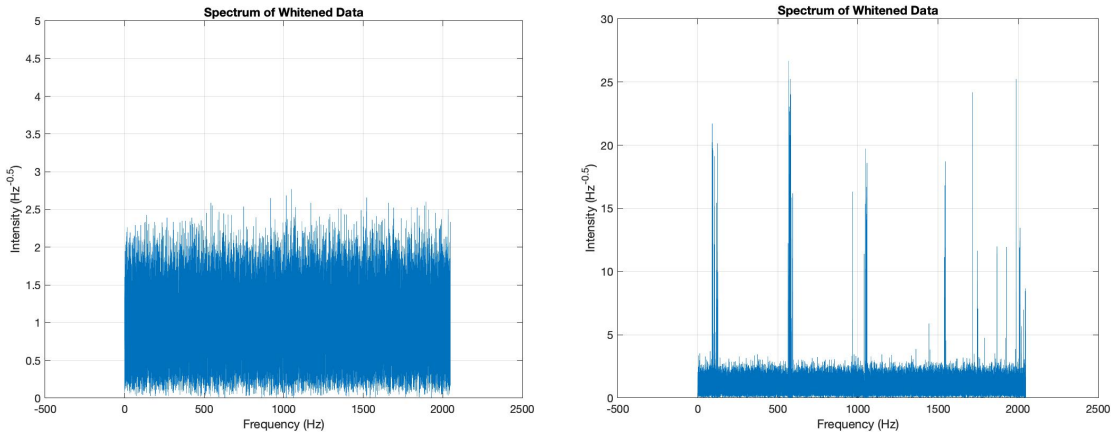

Figure 32: The power spectrum of whitened data using smoothing factors of 0.01 (left) and 0.3 (right) is reported. A flat-top cosine-edge window is used

Especially when highly whitened noises (for example Figures 31 and 32 left), it is evident that to deal with whitened data is equivalent to deal with simulated white noise (as done in all other sections.). The only difference is that the sought signal is distorted, as previously explained. The outputs of matched filtering using the GW150914 waveforms (Figure 30) are reported in Figure 4.1. The signal is detected in both cases, but with a much higher SNR (17.71) using the refined waveform with respect to the simple post-Newtonian case (10.05).

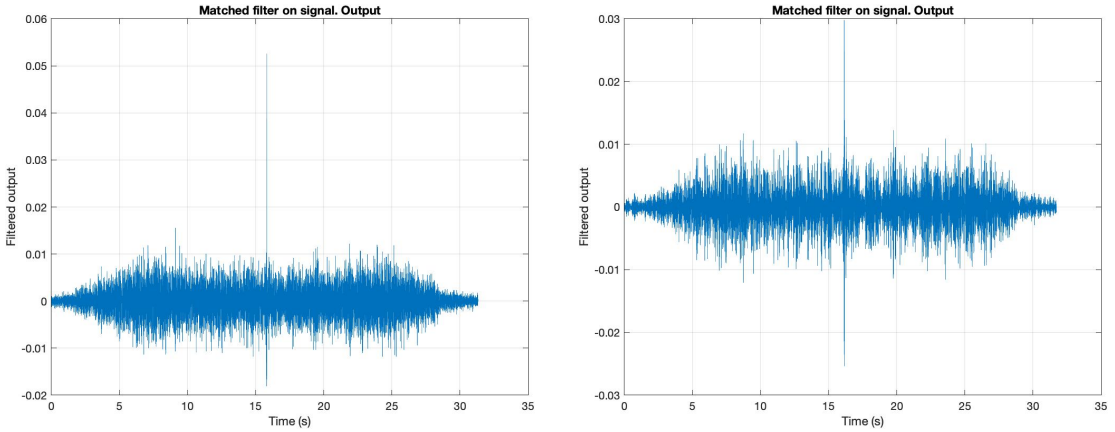

Figure 33: Outputs of matched filtering using the GW150914 waveforms from Figure 30 are presented. The signal is detected with a SNR of 17.71 using the complete waveform ad a SNR of 10.05 using only the post-Newtonian waveform. Thus, the importance of the accuracy of the waveforms is evident: the significance of the first detection is much higher.

It must be stressed that matched filtering can be performed on whitened data exactly as in the case of simulated white noise. Furthermore, the ratio between the whitened signal mean absolute amplitude and the whitened noise RMS (corresponding to `A` in previous sections) is always in a range between 2 and 10 for different waveforms, windows and values of smoothing accuracy.
These considerations legitimate all the analysis outlined in the other paragraphs and show that the results obtained can be linearly extended to the treatment signals embedded in real interferometers noise.

5 Conclusions

Many results were obtained and reported in the previous sections. The most important ones are highlighted here, along with the key steps that addressed the whole work. In the end, some possible future prospects are introduced.
The main goal of this paper is to present techniques to regularly apply matched filtering to data containing gravitational chirps. In particular, one typically uses filters built with different parameters in order to finally estimate the couple of masses which better resembles the signal embedded in noise. Thus, the aim justifies the initial intuitive choice of using the **"Grid of Masses" technique**. In fact, it seems reasonable to let the two masses regularly vary in order to find the couple whose corresponding template mostly resembles the signal. It has been reported that this procedure works significantly well, but it does not allow to obtain fine estimates of the parent masses: the mean relative error, using a single detector, usually fluctuates around 3% for masses in a range between $10\,\mathrm{M}_\odot$and $40\,\mathrm{M}_\odot$.
Consequently, it was discovered that a more accurate analysis can be carried out translating the masses in terms of the new variables **Chirp Mass** $\mathcal{M}$ and **Symmetric Mass Ratio** ν. By letting the tested filters' parameter vary in this new space, it was possible to achieve interesting results, taking advantage of a more robust procedure. The better solidity can be easily checked by verifying the presence of a clusterization of higher values of the *Signal to Noise Ratio* in this new space of parameters, which is absent in the m_1-m_2 case. In this situation, finding a clusterization hints that a step toward a "diagonalization" of the problem was taken. Furthermore, it is important to stress that this parameters provide a physically more accurate description: the two masses are the two most intuitive parameters one can think of, but the actual waveforms are theoretically modeled as depending by $\mathcal{M}$ and ν. An important remark about this point is that these considerations are valid when working with waveforms shaped including exclusively the first post-Newtonian corrections. Waveforms modeling also the *merger* and the *ringdown* phases of the coalescence will depend on many more parameters, but the underlying ideas can be generalized to this case too.
An original contribution was also brought from the development of the **"Chunks Technique"**. Although this method is computationally demanding, it is meaningful to develop techniques which allow to better refine parameters estimation in a field such as GW detections, where the measurable events are not very frequent. Indeed, the procedure is designed only to fine-tune already pre-estimated values, but not for a systematical use. Further on, a different approach was investigated with the **"rand_CMR" method**. The shift from a regular search to a randomized and more focused one allowed to deeper investigate the areas of interest, returning very precise estimates. In particular, a significant result was achieved from the evaluation of the two masses up to a mean relative error around 1.35% (below 1%

for measures combined from different simulated detectors).
In addition, the section involving the analysis of signals in real interferometers' noise assumes a key role: it would be pointless to perform analysis in white noise (as conspicuously done) without an adequate whitening procedure for measured data. Thus, the depicted proof that real data can be whitened in order to reproduce an experimental situation equivalent to the simulated one is conceptually fundamental.
Last but not least, it might be worth indicating that an important technical upgrade was represented by the use of MATLAB built-in functions to perform convolution, which is the key operation in matched filtering. Even if intuitively it might seem advantageous to perform convolution in Fourier's domain, MATLAB's optimized algorithms allow to obtain quicker and more precise results by working directly in time domain. Matched filtering is the core of all presented techniques and the operation of convolution is the most iterated one over the whole work, thus, it is necessary to find the most efficient way to perform it.

5.1 Future Prospects

A few potential outlooks for further works are suggested in this paragraph. There are two possible direct continuations for the presented workflow:

- The first one could be to perform signal injection in real interferometers' noise. The observed behaviors should be respected in principle due to the reported considerations about the spectral whitening technique. However, new problems may arise due to disturbances at particular frequencies.

- The second possible follow-on might be to perform analysis using more refined waveforms. In this case, a larger number of parameters would be involved, thus, every step pointing to an increasing diagonalization of the problem would be particularly significant.

Furthermore, it is important to remark that monotony of the SNR has been achieved only globally, but the local behavior still presents local maxima. In addition, some mild geometrical patterns can be observed in the SNR trend (see, for example, Figures 8 and 12). These clues indicate that diagonalization may not have been completely achieved (even if a significant level was reached). Therefore, it might be possible to find parameters accomplishing this aim.
In the end, as already mentioned in Section 3, it might be worth developing a smarter replacement of the "Grid of Masses" technique. A first idea might be given from the "Updating Central Value" algorithm. In fact, optimization procedures (such as the primitive developed one) might be used to quickly evaluate regions in the parameters space, in order to focus the most refined analysis on the interesting points.

A Gravitational Waves

According to the predictions of the General Theory of Relativity, the variation of mass-energy distribution in space-time produces gravitational waves in a process similar to electromagnetic waves generation due to accelerated charges. While EM waves propagate as perturbations of the EM field, gravitational waves are "metric waves", in the sense that they alter the metric tensor $g_{\mu\nu}$ (which describes space-time properties) at their passage.
Although any non-spherical time-changing mass-energy distribution can produce gravitational waves, those generated by the acceleration of non-relativistic astronomical objects (such as terrestrial objects or planets) are too weak to be detectable by any conceivable technology due to the smallness of the coupling constant G of gravitational force. Anyway, some astronomical phenomena can produce gravitational waves that are detectable using the current cutting-edge technology. These include violent astrophysical events such as the coalescence of a black-hole (or neutron star) binary system, rapidly rotating neutron stars, the gravitational collapse of massive stars, and various energetic processes that might have happened in the early Universe.
Gravitational waves analysis allows to extract important features related to the various sources. Therefore, it is used to complement electromagnetic astronomy to bring new information about our Universe. For this reason, it is fair to say that these last years have represented the dawn of "multi-messenger" astronomy, which is based on the matching of EM and gravitational observations.

A.1 Gravitational Waves Detection

The key to gravitational waves detection is to measure the "strain" h of space-time geometry. The most precise method for measuring small deformations is provided by laser interferometry. Gravitational waves interferometers follow the same principle underlying Michelson and Morley's device: a coherent laser beam is split by a beam splitter and sent in two orthogonal directions. These beams are reflected by two mirrors and eventually they are recombined to produce an interference pattern. A change δL of the length L of every arm of the interferometer produces a change in the interference pattern. The output is recorded in terms of the strain $h = \delta L/L$, which is an adimensional quantity. During the first (Sept. 12th, 2015 to Jan. 19th, 2016) and second observing run (Nov. 30th, 2016 to Aug. 25th, 2017), measured strains ranged between 10^{-21} and 10^{-24} [7].

Compact Binary Mergers Observations All presented results are reported from the catalogue [7]. Gravitational waves measurements are carried out using interferometers with km-length arms as detectors. At the moment, the three most

sensitive active detectors, operated by the LIGO-Virgo collaboration, are situated in Livingston (USA, state of Louisiana), Hanford (USA, state of Washington), and Cascina (Italy, province of Pisa). The sensitive frequency band ranges from 10 Hz to a few kHz: detectable signals in this domain include the coalescence of binary neutron stars systems or stellar-mass black-hole binaries, galactic supernovae, rapidly spinning neutron stars. During the first and second observation runs, 10 binary black-holes and one binary neutron star coalescences were measured using the above-described detectors.

A.2 Gravitational Chirps

Gravitational waves emitted by coalescing binary systems of compact objects constitute the simplest case to be theoretically studied and experimentally detected. In particular, current detectors are sensible to neutron stars and stellar-mass black holes coalescences. These events produce the characteristic "chirp" signals: their amplitude increase with frequency, resembling sound-waves from birds chirping. This paragraph aims to shortly derive the signal emitted by a compact coalescing binary system (for a more complete discussion, see [1]).

A.2.1 Rigidly-Rotating Binary System

We start by considering a system composed of two compact objects circularly orbiting around their centre of mass. By assuming that their orbit is much larger than their curvature radius, it is possible to use the weak field and the slow motion approximations. Thus, motion laws can be derived from Newtonian physics. Furthermore, space-time metric tensor can be written as the flat space-time metric $\eta_{\mu\nu}$ perturbed by a small strain $h_{\mu\nu}$ (with $|h_{\mu\nu}| << 1$):

$$g_{\mu\nu} = \eta_{\mu\nu} + h_{\mu\nu}. \tag{2}$$

Note that we use Einstein's convention for tensorial indices. Emitted gravitational waves can be computed using the quadrupole formula:

$$h_{ij}^{TT}(t, \bar{x}) = \frac{2G}{rc^4} \frac{d^2}{dt^2} Q_{ij}^{TT}\left(t - \frac{r}{c}\right), \tag{3}$$

where Q^{TT} is the quadrupole momentum of the mass-energy distribution and $r = |\bar{x}|$. The apices TT indicate that the whole calculation is performed in the Transverse-Traceless gauge. By computing the quadrupole moment, one gets:

$$q_{ij}(t) = \frac{1}{c^2} \int_V T^{00}(t, \bar{x}) x^i x^j d^3x = \frac{\mu L_0^2}{2} A_{ij}(t) + const. \tag{4}$$

where μ is the reduced mass of the system, L_0 is the orbital radius, and

$$A_{ij}(t) = \begin{pmatrix} cos(2\omega t) & sin(2\omega t) & 0 \\ sin(2\omega t) & -cos(2\omega t) & 0 \\ 0 & 0 & 0 \end{pmatrix},$$

where ω is the orbital frequency. This result should be projected in the TT gauge, but this transformation only changes the constant term. By plugging the TT projection of 4 into 3, one gets the emitted signal:

$$h_{ij}^{TT}(t, \bar{x}) = -\frac{4G^2}{rc^4}\frac{\mu M}{L_0}A_{ij}^{TT}\left(t - \frac{r}{c}\right). \tag{5}$$

Note that the characteristic frequency of the signal is equal to the double of the orbital frequency $\nu_{orb} = \frac{\omega}{2\pi}$.

A.2.2 Inspiraling Binary System

The study of an inspiraling system in its first phases (far from coalescence) can be done using the adiabatic approximation, supposing that the energy does not vary much during every orbit. Intuitively, referring to Formula 5, the orbital radius L_0 and the orbital frequency ω will vary in time during the inspiraling phase. The adiabatic approximation leads to neglect the variation of these parameter over a single orbit: significant changes are appreciable only after many orbital periods. It is useful to recall the definition of gravitational luminosity L_{GW}, that characterizes energy loss due to gravitational waves:

$$L_{GW} = \frac{G}{5c^5}\langle \sum_{r,s=1}^{3} \dddot{Q}_{rs}\left(t - \frac{r}{c}\right)\dddot{Q}_{rs}\left(t - \frac{r}{c}\right)\rangle, \tag{6}$$

where the $\langle\cdot\rangle$ symbol indicates the Brill-Hartle mean over many orbital periods. Plugging the reduced quadrupole momentum $Q_{rs}(t)$ (easily obtained from Equation 4) into Equation 6, one finds:

$$L_{GW} = \frac{32G^4\mu^2M^3}{5c^5}\langle\frac{1}{L_0^5}\rangle. \tag{7}$$

The orbital energy of the system can be obtained from the laws of Newtonian physics and depends on $L_0(t)$:

$$E_{orb}(t) = -\frac{1}{2}\frac{GM\mu}{L_0(t)}. \tag{8}$$

Supposing that the energy lost by the system is all converted into emitted gravitational waves, the law of conservation of energy linking the two quantities becomes:

$$\frac{dE_{orb}}{dt} + L_{GW} = 0. \tag{9}$$

Plugging the expressions 7 and 8 into 9, it is possible to evaluate the behavior of L_0 in time starting from an initial value L_0^{IN}:

$$L_0 = L_0^{IN}\left(1 - \frac{t}{t_c}\right)^{\frac{1}{4}}, \qquad t_c = \frac{5c^5}{256G^3}\frac{(L_0^{IN})^4}{\mu M^2}. \tag{10}$$

When the time t approaches the critical time t_c, the merger between the two objects begins: in this regime, the approximations made are no longer valid. According to the expression 10, by means of the second Kepler's law, the behavior of the gravitational frequency (twice the orbital frequency) can be written as

$$\nu_{GW}(t) = 2\nu_{orb} = \frac{1}{\pi}\sqrt{\frac{GM}{L_0^3(t)}} = \nu_{GW}^{IN}\left[1 - \frac{t}{t_c}\right]^{-\frac{3}{8}}. \tag{11}$$

A characteristic plot of the gravitational frequency for this kind of signals is shown below:

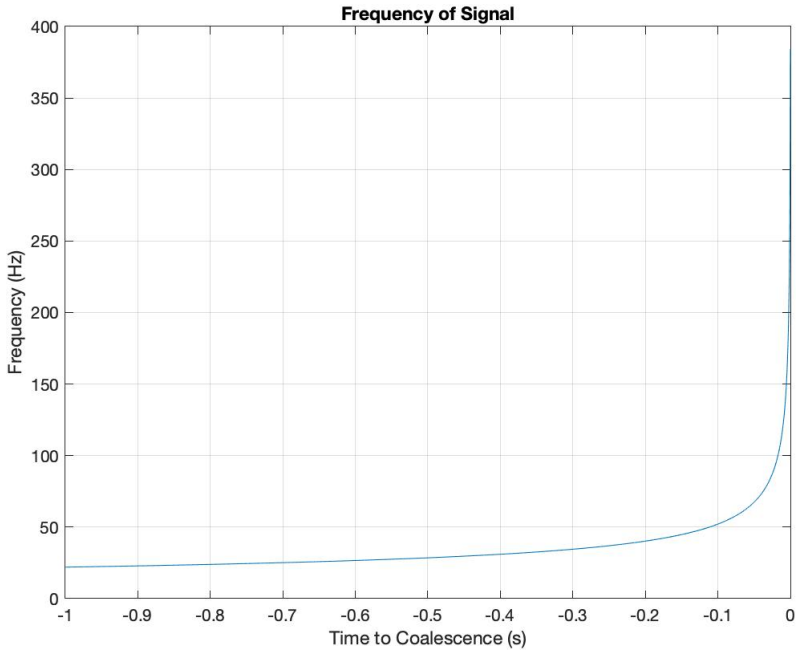

Figure 34: Behavior of the frequency for a chirp signal emitted by two coalescing black-holes using the Newtonian model.

From equation 11, it is possible to write the following expression, which will

be used later on:

$$\frac{1}{L_0} = \frac{(\pi \nu_{GW})^{\frac{2}{3}}}{(GM)^{\frac{1}{3}}}. \tag{12}$$

It is also possible to write the expression of the strain as:

$$h_{ij}^{TT}(t, \bar{x}) = -h_0(t) \cdot A_{ij}^{TT}\left(t - \frac{r}{c}\right). \tag{13}$$

Let's focus on the expression of the strain amplitude $h_0(t)$, the other term only giving the oscillating contribution. The strain amplitude is usually expressed in terms of the orbital frequency ν_{GW} and can be obtained simply by substituting equation 12 into the expression for static systems 5:

$$h_0(t) = \frac{4\pi^{\frac{2}{3}} G^{\frac{5}{3}}}{rc^4} \mathcal{M}^{\frac{5}{3}} \nu_{GW}^{\frac{2}{3}}(t) \tag{14}$$

From this formula, it is clear that the amplitude increases with frequency. The *chirp mass* $\mathcal{M}$ is a particular combination of the reduced mass μ and the total mass M defined as:

$$\mathcal{M} \equiv \mu^{\frac{3}{5}} M^{\frac{2}{5}} = \frac{(m_1 m_2)^{\frac{3}{5}}}{M^{\frac{1}{5}}} \tag{15}$$

It is important to notice that the strain amplitude depends only on this particular combination of the two masses: this implies that, analyzing this kind of signals, it is never possible to reconstruct the masses of the two objects that generated the signal, but only their chirp mass. The following image represents a plot of the strain amplitude:

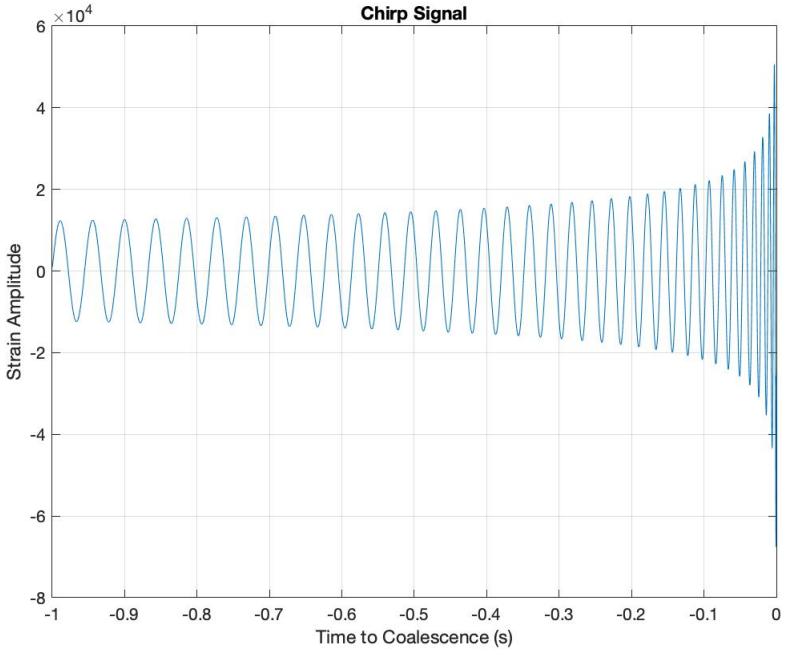

Figure 35: Template describing a chirp signal emitted by two coalescing black-holes of $30\,M_{\odot}$ using the Newtonian model.

A.2.3 Signal Analysis

As already mentioned before, the gravitational signal derived from the above calculation does not depend separately on the two masses of the compact objects, but only on their chirp mass. So, the analysis does not furnish the actual masses of the sources. It is fair to say that there is a degeneracy: the signal depends only apparently on the two masses, but it actually relies on a single parameter: the chirp mass $\mathcal{M}$. To split this degeneracy and obtain information on the single masses, it is necessary to include post-Newtonian corrections to the previous expressions. It is not significant how to obtain these corrections analytically, but it is necessary to point out that one should implement post-Newtonian corrections in the modeling of the problem to extract interesting results. An example of a waveform including post-Newtonian corrections is reported below:

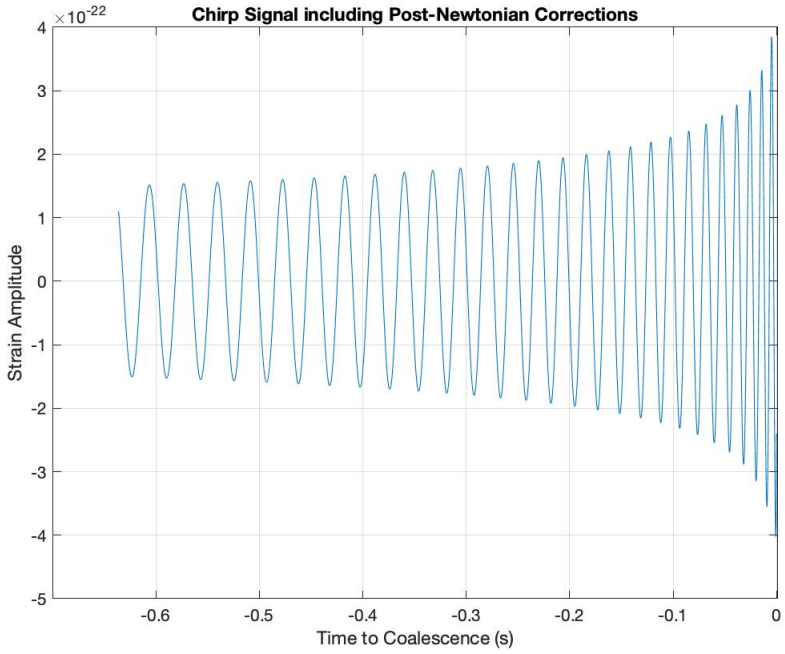

Figure 36: Template describing a chirp signal emitted by two coalescing black-holes of $30\,M_\odot$using the post-Newtonian model up to second order corrections. The difference with the previous case is not evident, but comes out during data analysis.

Furthermore, it is important to remark that all the above calculation is done using three approximations:

1. Slow-Motion approximation
2. Weak-Field approximation
3. Adiabatic approximation

When the two objects come close, none of the three is valid anymore. In these cases, Einstein's equations are not linear anymore and there are no analytical solutions. For these reasons, it is necessary to compute the actual waveforms using Numerical Relativity. The analysis of real signals is done using these much more sophisticated waveforms, which accurately describe also the phases of merger (the highest peaks of the signal) and ringdown (the last part) of the coalescence. In the following plot, it is reported the real waveform used to detect the event "GW150914", which has been used in the codes to perform real data analysis:

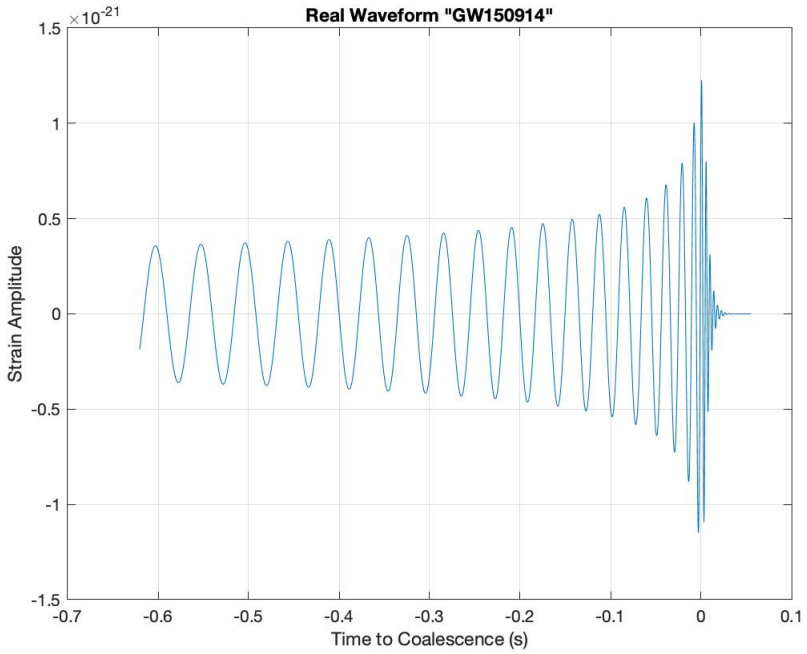

Figure 37: Best evaluated template for the event "GW150914" detected by LIGO interferometers. The main difference with the previous cases lies in the last parts, which here include the merger and the ringdown phases.

B Matched Filtering

In real experiments, any measurement is accompanied by an uncertainty, which reflects our understanding of the underlying phenomena. When it comes to the analysis of gravitational chirps, it might seem nearly impossible to provide a result within a reasonable confidence interval. In fact, gravitational signals' amplitudes are even smaller than 10^{-21}, while the detectors' noise amounts to 10^{-18} circa. However, there exists a technique, called *matched filtering*, employed to study waveforms deeply buried in noise (like in this case), allowing for the extraction of sensible information.
The following discussion deals with the theoretical basis underlying the above-mentioned method and its implementation in MATLAB scripts.

B.1 Theoretical Remarks

Let's consider raw measured data of the form:

$$r(t) = h(t) + n(t),$$

where $h(t)$ represents the signal and $n(t)$ stands for the noise [5]. According to the *matched filtering* technique, the optimal filter $f(t)$ that maximizes the *Signal to Noise Ratio (SNR)* needs to be found. By performing the operation of convolution between $r(t)$ and the filter $f(t)$, it can be written that

$$c(t) = r(t) * f(t) = h(t) * f(t) + n(t) * f(t) = y(t) + w(t),$$

where $y(t)$ and $w(t)$ are defined as a result of the convolution. Then, using the Convolution Theorem, the SNR can be expressed as:

$$SNR = \frac{|y(\tau)|^2}{E[|n(\tau)|^2]} = \frac{|\int_{-\infty}^{+\infty} H(f) \cdot F(f) e^{j2\pi f\tau} df|^2}{\int_{-\infty}^{+\infty} W(f) \cdot |F(f)|^2 df} \tag{16}$$

where $H(f)$, $F(f)$ and $W(f)$ are the Fourier transform of $h(t)$, $f(t)$ and $w(t)$, respectively. The value of τ, instead, is chosen as the one that maximizes the SNR. Through computation, it is possible to show that the optimal filter is obtained conjugating and time-reversing the original signal $h(t)$. Before proceeding, it is useful to point out that:

- the signal $h(t)$ is real, so it can be just time-reversed to find $f(t)$;
- in a real scenario, data and signals are discretized, so this analysis has to be carefully substituted with a discrete version. However, since the meaning and the results are not affected, it has been preferred to carry on a simpler continuous calculation for simplicity.

B.2 MATLAB Implementation

The results of the *matched filtering* procedure have been extensively used in MATLAB scripts as a means to detect and examine gravitational waveforms. In the following paragraphs, the Fourier domain and the time domain approaches are described in detail.

B.2.1 Fourier Domain Approach

In this first method, the calculation of SNR is performed in the Fourier domain. As previously explained, a convolution in time domain behaves like a product in the frequency domain. The logical thread is thus the following [21]:

1. Divide the input vector `data` (containing the signal embedded in noise) in chunks long as much as the injected signal;
2. Apply the Fourier Transform to each chunk and multiply by the Fourier Transform of the filter;
3. Compute the Inverse Fourier Transform and save the output in a vector `out_f`;
4. Repeat 1, 2, 3 for each chunk.

However, the steps outlined cannot account for adequate accuracy, since it will rarely happen that the real signal is located exactly at the very beginning of a data chunk. Therefore, a precision parameter `prec` is accepted as input. While in the previous case the process was carried out once for each chunk, `prec` allows for the analysis of each chunk `prec` times, moving the starting point by `Nsamp_sig/prec` after any iteration. Overlaps can be avoided saving only the appropriate outcome. This procedure is useful and fast as long as the precision parameter is not too high, i.e. 100. Otherwise, the time domain approach provides better results and performances.

B.2.2 Time Domain Approach

Being based on the MATLAB built-in function `conv`, this procedure is highly optimized and fast. Therefore, the user should switch to this method whenever the parameter `prec` of the previous case becomes too high. Some lines of the relative code [22] are here reported.

[21] Refer to `apply_MF3.m`.
[22] Refer to `apply_MF_conv.m`. See also `conv_apply_MF3.m`.

```
%reversed signal
filter_t=signal(end:-1:1);
...
%Convolution between data and Impulse Response
out = conv(data, filter_t, "valid");
```

The option `"valid"` returns an output having the length of `data` minus the length of `signal`, including only the part of the convolution computed without the zero-padded edges. In this way, it is avoided to look for signals which end outside the data. This option will be also useful to determine correctly the time of detection of a Gravitational Wave, bypassing the rescaling of the `time` vector. For clarity's sake, some plots showing datas and filtering are presented below. These results are valid under the hypothesis of Gaussian white noise, whose amplitude is still comparable with the signal (a factor of 1.5 higher than the signal's maximum).

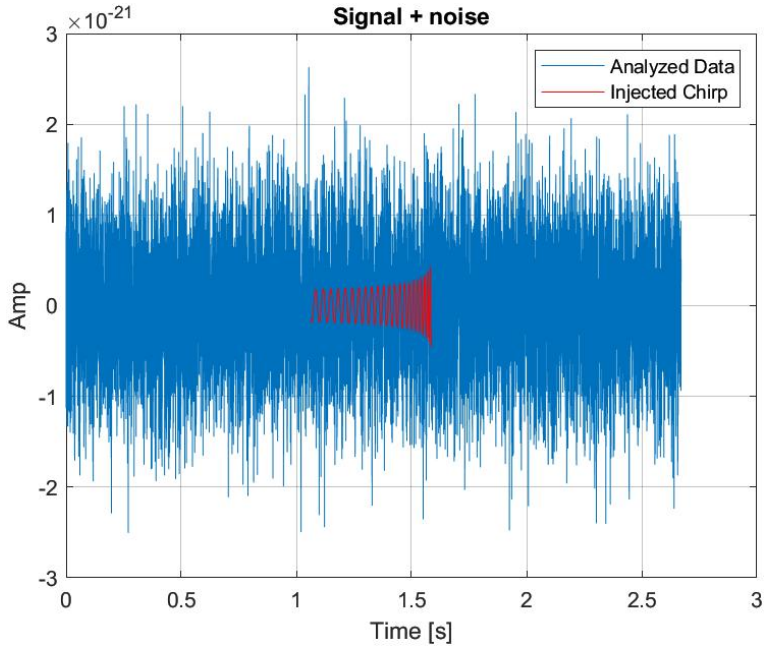

Figure 38: Blue: example of data obtained by a detector in white noise. Red: highlighted signal embedded in noise.

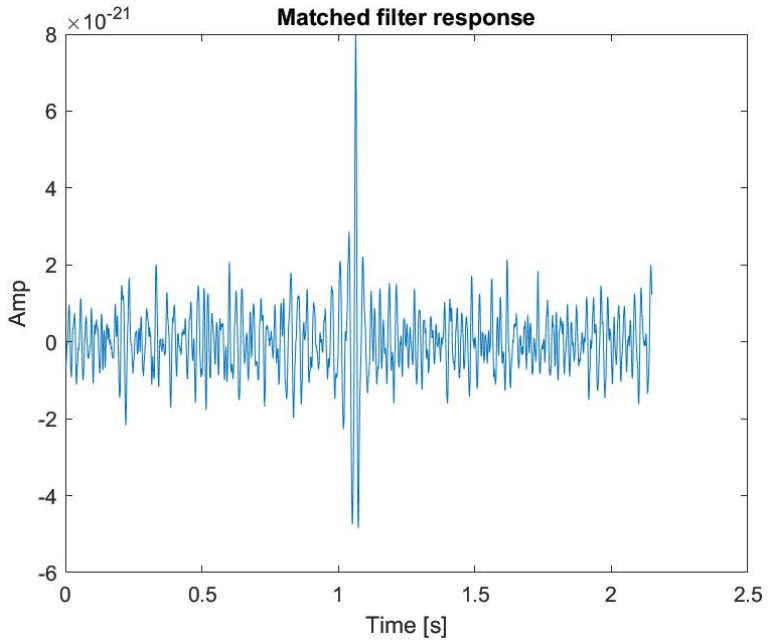

Figure 39: Output of optimal matched filter when applied to Figure 38. The peak corresponds to the time of detection of the waveform.

C Grid of Masses Technique

As already stated at the beginning of the work, chirp signals' parameters can be deduced in several ways. This section outlines a well-known and efficient method, based on the actual construction of a grid of masses, i. e. a lattice in the plane M1-M2. More specifically, the grating should be built having at least a bare idea of the sought masses. As an example, a neutron star could never be detected within a range going from $10\,M_\odot$ to $40\,M_\odot$, while a more appropriate interval might be $[0.2\,M_\odot; 2\,M_\odot]$. Then, the grid must be constituted by equally spaced values of the masses in the chosen domain. The distance between two neighbors, the so called *step*, is a crucial variable, highly influencing the result of the procedure.
For simplicity, only square meshes will be worked out: in this case, for the analysis to be effective, it is sufficient to consider only half of the grid, due to symmetry considerations. The case of of a general rectangular grid has been implemented in codes, but it is not convenient to perform analysis. Once the structure has been built, each grid point (labelled by two masses) will be used to generate a chirp signal. This waveform, in turn, will act as a filter on the injected signal, which plays the role of the propagating wave coming from a given astrophysical two-body source. By now, it should be clear that the underlying theoretical justification is related to the matched filtering technique, discussed in detail in Section B. On these basis, a detection will be claimed for the point which generate a filter such that the SNR (Equation 16) peaks at its maximum value. Thus, the general aim of the procedure is to find the couple of masses that best reproduces the experimental data.
The following results, however, are derived in a Newtonian landscape, according to which the entire process of gravitational waves emission is solely determined by a particular combination of the masses of the two orbiting bodies, the *chirp mass* $\mathcal{M}$ (Equation 15). Therefore, individual masses have no meaning at all in this picture, as long as the estimated *chirp mass* is coherent with the real one.

C.1 MATLAB Implementation

The relative MATLAB function[23] implements a grid of masses, allowing the user to insert a vector `data` to be filtered and to choose between the Newtonian and the Post-Newtonian landscape (examined in detail in Section F). Once taking into account the proper signal generation, however, the core remains the same: signals built from each grid pair filter the input vector `data`, returning an array containing the SNR and the relative couple of masses. This output allows for the estimate

[23]Refer to `apply_conv_grid.m`. See also `apply_par_grid.m` for a useful parallel implementation, as discussed in Section I.

of the pair which maximizes SNR, which must be performed in the main script. Taking a close look to the code, as for the Newtonian case:

```
%double cycle over masses
    for i = start1:step1:end1
        for j = start2:step2:end2
            ...
            %generating filter
            ch=Newt_Chirp(i,j, signal_parameters{:});
            %applying filter
            out = apply_MF_conv(ch, data, dt);
            ...
            %calculating SNR
            SNR(:, ii) = [ max(abs(out)), i, j];
            ...
        end
    end
```

As already mentioned, in the Post-Newtonian approach `Newt_Chirp` must be replaced by `chirp_signal`. Other codes[24] provide even instruments for further analysis, based on what will be called from now on *chunk* method. The main idea behind this approach can be outlined as follows:

1. Having previously applied the grid of masses, the maximum of the SNR is stored in the variable `maximum` and a parameter `tresh` is defined[25];

2. All the grid points whose relative SNR is higher than `tresh*maximum` are selected for a deeper analysis.

3. Each chosen point generates a filter, which is in turn divided in `NumCh` *chunks*. The initial data is filtered with all those different pieces and the single outputs finally add up to the final SNR, properly rescaled so that each *chunk* has the same statistical weight.

In this way, the problem of noise mimicking signal is partly avoided. In fact, the algorithm runs with `NumCh` different filters; so, if the masses are sufficiently close to the true ones, the convolution with the underlying signal will always result in a high SNR for each of the *chunks*, while the fluctuations caused by noise will be averaged to a lower value.

[24] Refer to `chunk_mm.m`.

[25] Commonly, `tresh` is assigned to a value between 0.9 and 0.95. The actual meaning will be clear in the next point.

In the following treatment, this approach will rarely be used, since it reduces the speed of execution without providing significant improvements.

D Newtonian Chirp

The purpose of this section is to combine the theoretical aspects presented in A.2 with the experimental methods explained in Sections B and C, in order to estimate the parameters of gravitational chirps in the Newtonian approximation. The guideline of the following discussion is that the *chirp mass* is the only parameter that shapes this kind of waveforms (Figure A.2.2) $\mathcal{M}$, as one can explicitly see from Formula 14.

D.1 Discretisation Limit

It may be worthwhile to provide a result in a totally ideal scenario, neglecting the contribution of noise. The outcome will then set an upper limit on the maximum achievable overall precision. The relative MATLAB code [26] establishes a discretisation limit on the precision of the masses attainable by the grid technique in the Newtonian approach. Choosing the values of the two initial masses, the script injects a chirp signal in white noise as if it was generated by an astronomical source. Then, applying a grid of masses with fixed step, the chirp mass can be estimated and compared with its real value. The analysis is conducted dividing repetitively the grid step, showing an interesting scaling law between the relative precision and the step chosen.
Let's now take a closer look at the code. Firstly, a couple of masses representing the gravitating bodies is fixed:

```
m1 = 20.53526 %solar masses
m2 = 32.33224 %solar masses
```

It might be objected that such a high precision is undoubtedly unphysical, but it should be borne in mind that the Newtonian algorithm pursues the best estimate of the *chirp mass*, without caring about the original bodies. Choosing the two original masses in this way ensures that the *chirp mass* shall have many (possibly infinitely many) decimal digits, a useful feature in further considerations. Then, the initial chirp is injected: the purpose of the analysis will be recovering the original *chirp mass* $\mathcal{M}$ through the aforementioned technique.
Secondly, a square grid of masses is constructed, choosing an appropriate range:

```
%initial values
start1 = 0;
start2 = 0;
finish1 = 40;
```

[26] Refer to `theoretical_limit.mlx`.

```
finish2 = 40;
...
%construction of the grid
M12 = [start1:step:finish1; start2:step:finish2] ;
```

Setting the grid, it becomes easy to produce a waveform for each couple of masses, which will consequently filter the original injected signal. A matrix `SNR` stores the pairs and the relative $SNRs$. Here the main `for` cycle is reported:

```
for i = 1:length(M12(1,:))
    for j = 1:i
        %chirp for each couple of masses
        [ch,chirp_freq]=CHIRP_fromparameters(M12(1,i),M12(2,j),TMAX_a,dt);
        %output of the filter
        [out, time] = conv_apply_MF3(ch'/max(ch), chTrue'/max(chTrue), dt);
        %extract SNR, then store it in a matrix.
        SNR = [SNR; max(out), M12(1,i), M12(2,j)];
    end
end
```

After this, the script proceeds as follows:

1. It finds the maximum SNR and the corresponding masses;
2. It focuses the analysis around this point, updating the limits of the grid and reducing the step by a factor 10;
3. It repeats the points 1, 2 and computes $\frac{\delta\mathcal{M}}{\mathcal{M}} = |\frac{\mathcal{M}_{meas}-\mathcal{M}_{true}}{\mathcal{M}_{true}}|$ for 4 times.

A plot illustrating the variation of $\frac{\delta\mathcal{M}}{\mathcal{M}}$ as a function of the iteration parameter is finally shown.

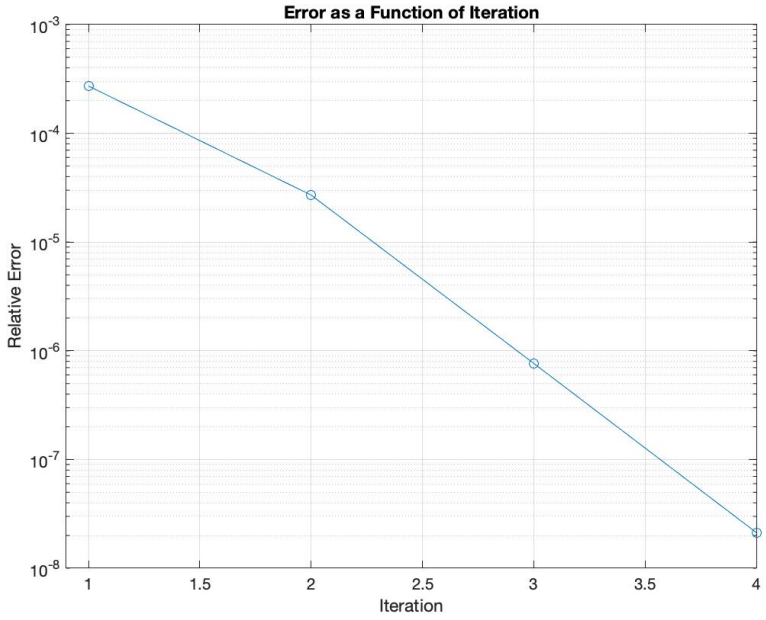

Figure 40: Relative error as a function of the iteration. Log-scale is used for the y axis.

Without going into detail, it can be seen that the relative error diminishes approximately resembling a power law. The base's value is related to the factor by which the step is reduced at each iteration (in this case 10). In conclusion, the discretisation limit confirms the expected behavior of the grid of masses technique: the smaller the step, the higher the precision. Moreover, it also gives some quantitative results, as displayed in Figure 40. Again, it should be remarked that the previously obtained scaling law is meaningful only in the ideal case.

D.2 Time of Detection

One of the main tasks to be accomplished while detecting a signal is providing a precise estimate of its time of arrival. Usually, in fact, a chunk of data is given, hopefully containing a chirp embedded in noise. Then, they should be able to characterize both the masses of the sources and the position in time of the hidden signal. The former goal has been carefully described previously; so, the following discussion regards the latter one. In the relative MATLAB script[27], a known chirp signal is injected in gaussian white noise. Subsequently, filtering this waveform with its time reversed version (i.e., the *optimal filter*, Section B), a proper estimate of the delay between the arrival of the signal and its time of detection can be given. The entire process is repeated `N_exp` times, always inserting the known waveform

[27]Refer to `CMF_Delay.mlx`.

randomly in a newly generated white noise configuration.
Let's examine the code in detail. In order to be able to furnish coherent results, the source masses are kept fixed and the simulation is repeated 1000 times (`N_exp` = 1000). The initial parameters are thus set:

```
N_exp=1000 %Number of experiments
dt=1/4096 % sampling time. The max frequency is 2048 Hz in this case.
          %Check with generated chirp
...
m1 = 24.1146 %solar masses
m2 = 28.5472 %solar masses
...
T_MAX=0.5+rand %Duration of signal in seconds
T_tot=T_MAX*(10+rand)  % Duration of background noise
A_max=1 %noise rms
...
%creation of the signal
[signal, signal_freq]=CHIRP_fromparameters(m1,m2,T_MAX,dt, 0);
```

Then, applying the matched filtering procedure, the SNR can be calculated. For each of the experiments, looking at the time corresponding to the maximum of the SNR, a possible delay between the arrival of the hidden signal and its detection can be brought to light.

```
%looking exactly for the right signal: optimal filter
[out,time]=apply_MF_conv(signal,data,dt); %Filtering

%getting detection sample as max of SNR
[~,S_det]=max(abs(out./std(data)));

%detection time
Det_time=time(S_det);

%storing into array of Delays
Delays(i)=(Det_time-TSTART)/dt; %in units of dt
```

Lastly, some plots are produced, in order to clearly understand which are the limits of this procedure. Notice that all the results are given in terms of `dt`, which stands for the *sampling time*. A typical signal coming from the selected masses lasts for about $0.5s$, which corresponds to 2048 `dt`. The histograms will be always

normalized by the number of experiments `N_exp`. The noise *r.m.s* `A_max` must be understood as a factor that, once multiplied by the chirp maximum value, gives back the real noise root mean square amplitude.

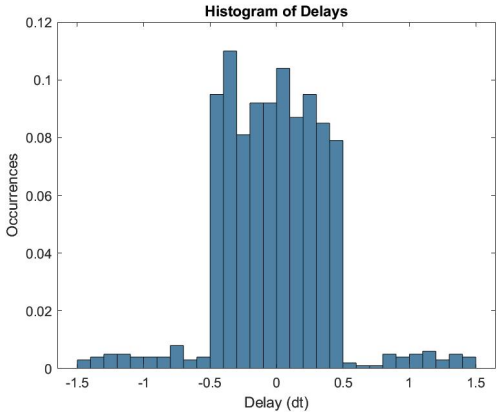

Figure 41: Normalized histogram of delays, expressed in sampling time units. Noise *r.m.s* `A_max = 0.5`, bin width 0.1`dt`.

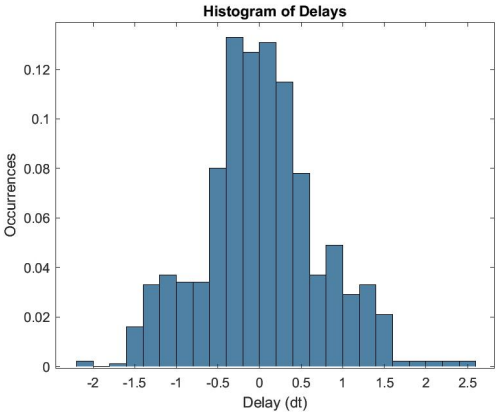

Figure 42: Normalized histogram of delays, expressed in sampling time units. Noise *r.m.s* `A_max = 1`, bin width 0.2`dt`.

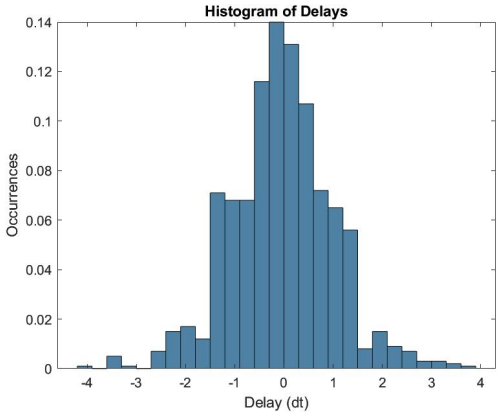

Figure 43: Normalized histogram of delays, expressed in sampling time units. Noise *r.m.s* `A_max = 1.5`, bin width 0.3`dt`.

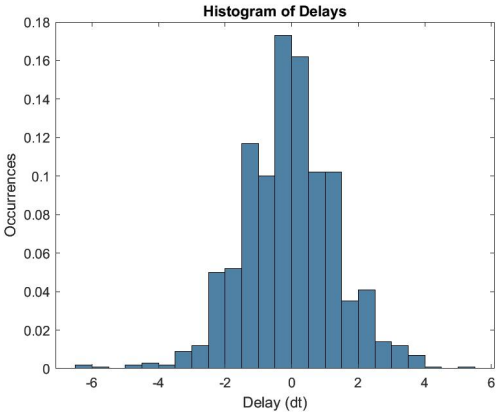

Figure 44: Normalized histogram of delays, expressed in sampling time units. Noise *r.m.s* `A_max = 2`, bin width 0.5`dt`.

Claiming a *false detection* whenever the time of detection misses the arrival by half the duration of the signal itself, the analysis can be performed in a more

accurate fashion, plotting only the standard deviations of the correct detections. In fact, as expected, the mean value is almost zero in any case.

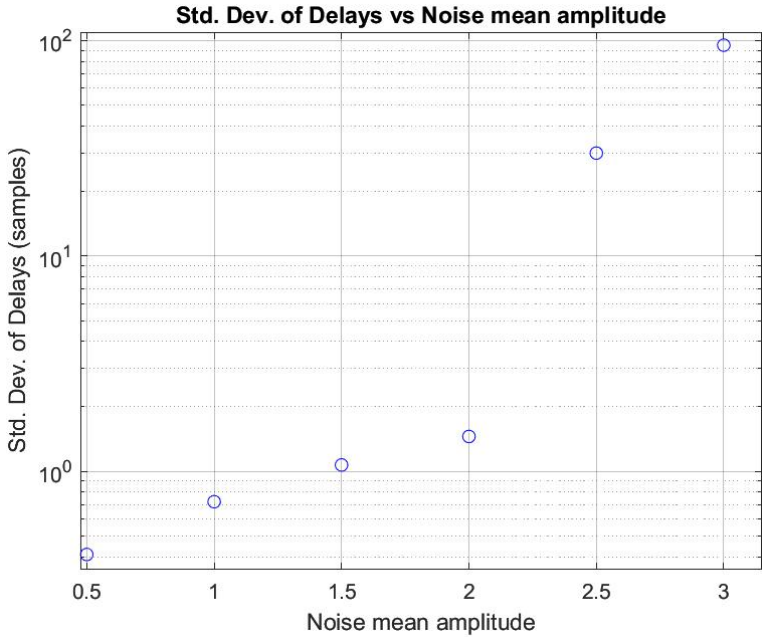

Figure 45: Standard deviation of correct detections, expressed in sampling time units, as a function of the noise r.m.s.

As for the *false detection rate*, it ranges from 0.5% to 3% of the total number of detections when `A_max` = 2.5, while it goes from 7% to 15% for `A_max` = 3. As a result, the time of detection is in perfect agreement with the actual time of arrival of the injected signal as long as the noise $r.m.s$ `A_max` is less than twice the chirp peak value. In the following, if not otherwise stated, it will be tacitly assumed that this restriction holds.

D.3 Detailed Code Explanation

In this paragraph, an exhaustive description of the code simulating the detection of a chirp signal in the newtonian case is performed, focusing on key passages. Lines will be referred to as reported in Appendix D.5. The following explanation recovers the structure of the paragraph 1:

1. The first lines (10-28) are dedicated to fixing the parameters of the simulation. A maximum of 4 detectors can be used to perform a simulation. The code works also with more than 4 detectors, but this limit has been chosen in order to resemble realistic situations. The parameter `A` fixes the

ratio between noise $r.m.s$ and signal mean absolute amplitude. Then, grid parameters are chosen: a realistic range of masses for simulating signals from stellar-mass black holes could be $[10\,M_\odot; 40\,M_\odot]$. The choice of the step is a crucial point and should be gauged carefully: its value highly influences obtained precision and execution time. A good cost-effective compromised could be to fix it to $0.5\,M_\odot$, in order to get significant results without needing excessive computational power. A more detailed discussion on this topic will be carried out in section D.4. Then, all the parameters shaping the signal are determined: the masses are randomly chosen in the grid range, while signal duration and sampling time are fixed.

2. In lines 31 to 38, signal and noise are generated. The function `Newt_Chirp` produces an array of values shaped according to Formula 14 (actually, Figure A.2.2 is obtained using this function). Notice that the signal is normalized to its maximum amplitude. White noise is generated using random normally distributed numbers for a duration equal to 4 times the extent of the signal.

3. The task of injection is performed in lines 41 to 51. Injection time is chosen in order for the signal to be placed neither at the very beginning nor outside data, so that it could be correctly detected. Notice that the injection time is the same for every detector: the implicit assumption is that the signal arrives on all the detectors at the same time. The function `signal_noise_plot` produces a plot of the signal injected in data in the first detector (an example is Figure 38).

4. The `parfor` loop in lines 63 to 75 is the main body of the program. By taking advantage of parallel computing (different detectors are executed in parallel on different CPUs), the grid of masses technique is applied to data in every detector using `apply_conv_grid`. This cycle produces two important variables: `M_list` and `SNR`. Both are storage variables: the former contains the best combinations of masses in every detector and the associated SNR, while the latter is a multi-folded structure that holds all the measured values of SNR over all the points of the grid. Every sheet of this variable corresponds to a different detector.

5. Selection of best combination of masses in every detector is obtained using the function `max_SNR` in line 73, which returns the couple that maximizes SNR for every sheet of the variable `SNR`. Lines 78 to 81 pick the pair `M1-M2` that maximizes the average SNR over the different detectors. Notice that this combination could be different from all the ones previously found.

6. Time measurements are performed in two `parfor` cycles from line 94 to 134. In the first one, filtering is done on all detectors using the optimal

combination of masses `M1-M2`. Results, in this case, are not stored singularly: their value is averaged. In the second one, instead, matched filtering is performed on every detector's best combination. It is important to always keep in mind that the purpose of the code is to produce a single measurement for every detector and a measurement from the overall network.

7. In last lines (146-153), obtained results are assembled in the handy `Res_Table` structure (an example is shown in Figure 2). In particular, it is a MATLAB container of type "Table".

D.4 Analysis of Results

In this section, some results obtained from many iterations of the code discussed in the previous paragraphs are presented. To obtain these results, it has been fundamental to use computational methods and resources reported in Appendix I. It is important to keep in mind that the aim of the code is to give an estimate of the chirp mass of the injected signal and of the arrival time: in this section, the precision of this estimate will be discussed. Two factors mainly contribute to errors on chirp mass identification: the amplitude of the noise and the step of the used grid. Reported results are obtained averaging the results of 50 runs of the previously explained code (which means that single detector errors are estimated from 200 measures, since 4 detectors were simulated in every run).

Dependence on Noise RMS `A`. In order to obtain the dependance of the error on chirp mass identification, all the parameters were fixed to some chosen values and only the noise $r.m.s$ was changed. 50 experiments were performed for every choice of `A` for 4 detectors: this means that measurements for single detectors are averaged over 50x4=200 values, while combined measures are averaged simply over 50 values. In the following graphs, the obtained results are presented. The reader should keep in mind that `A` is the ratio between noise $r.m.s$ and signal mean absolute amplitude.

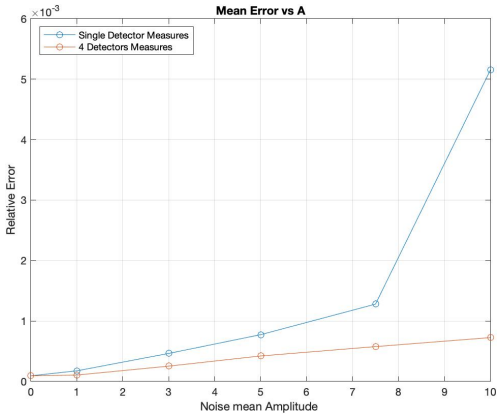

Figure 46: The behaviour of the error with respect to noise $r.m.s$ `A` is almost linear for reasonably small values.

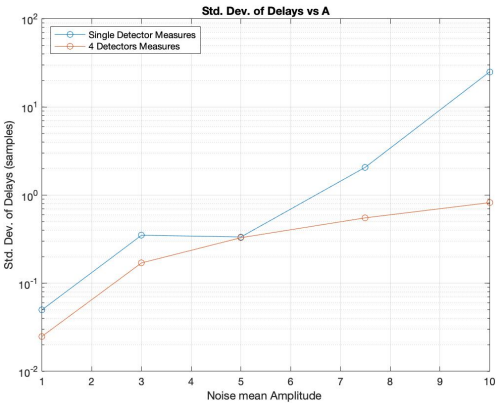

Figure 47: Standard deviation of the delay in time detection also increases almost linearly with noise $r.m.s$ `A`.

It is interesting to notice that using more than on detector gives a significantly better result especially for high noises. This happens because errors on independent measures strongly depends on the peculiar characteristics of the noise in every detector, which could distort the signal and make it more similar to a similar one having different parameters. Combined measures "average" the noise on different detectors, so, they usually give a more accurate result.

Dependance on Grid Step. In realistic situations, if the noise is stationary, its mean value can be estimated. Thus, the main parameter that influences the step of the grid one uses to perform the analysis. The following graphs show some characteristic behaviors of the errors for two different situations of noise:

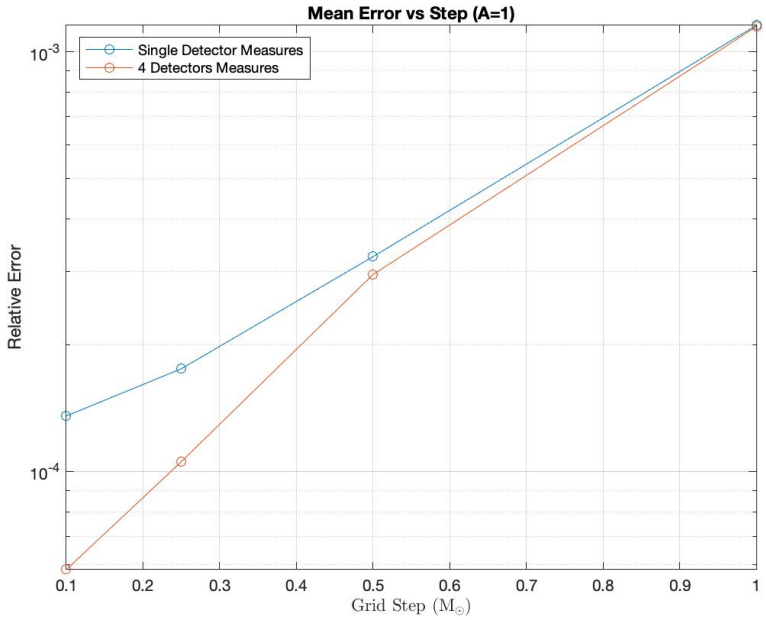

Figure 48: For low noises, the result is similar to the one obtained without noise: precision increases linearly in a logarithmic scale.

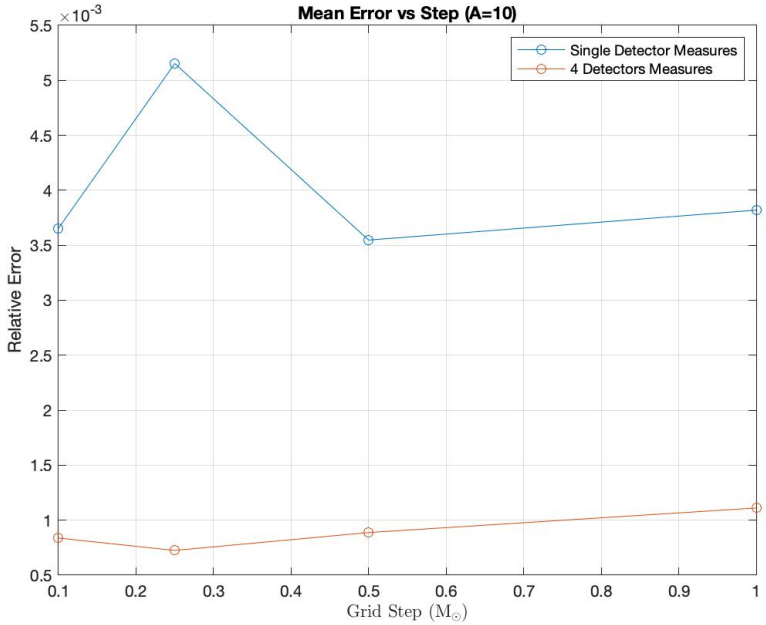

Figure 49: For high noises, the grid step does not influence much the behavior error: better estimations cannot be performed by using denser grids.

A similar behavior has been noticed for the errors on time measurements. It is

reported in the following graphs:

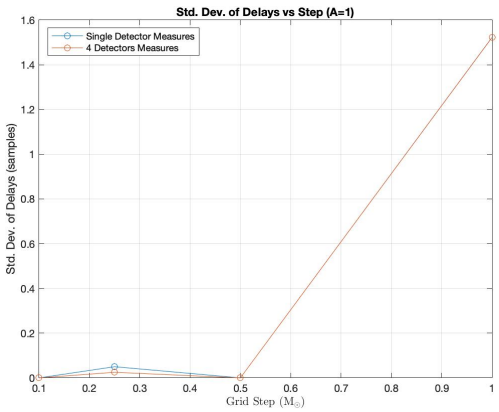

Figure 50: For low noises, time measurements become quickly very precise.

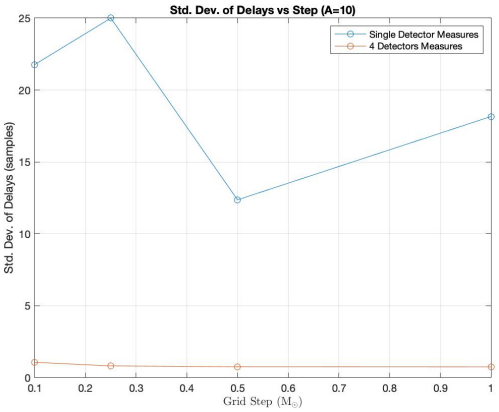

Figure 51: The step of the grid does not influence much time measurements for high noises.

D.5 Newtonian_Detectors.mlx

```
%N DETECTORS OF NEWTONIAN CHIRPS
%This code simulates an experimental setting made of  N detectors
%(different noise on each one) that measure the arrival of a chirp signal
%in the Newtonian approximation. The signal is randomly injected in data
%at the beginning. The aim is to correctly estimate the chirp mass of the
%system that generated the signal (only relevant parameter) and the
%arrival time.
clear, close all

%Number of Detectors (no more than 4)
N_det=4;

%Noise rms
%(with respect to signal mean absolute amplitude)
A=5;

%GRID PARAMETERS
%start1, step1, end1, start2, step2, end2
grid_par=[10, 2, 40, 10, 2, 40]; %solar masses

%Ramdomly generate signal in correct range
```

```
fprintf("Signal Parameters:\n")
m1=grid_par(1)+rand*(grid_par(3)-grid_par(1))
m2=grid_par(4)+rand*(grid_par(6)-grid_par(4))
Chirp_Mass=chirpMass(m1, m2)
dt=1/4096 % sampling time, max freq = 2048 Hz
T_MAX=1 %seconds
signal_parameters={dt,T_MAX}; %inputs of signal function

%SIGNAL GENERATION
signal=Newt_Chirp(m1,m2, signal_parameters{:}); %creation of the signal
signal=signal./max(signal); %signal normalization

%WHITE NOISE GENERATION in every detector
T_data=T_MAX*4;  % Duration of background noise
A=A*mean(abs(signal)); %noise rms
data=randn(round(T_data/dt), N_det); %this is the noise, T_tot/dt samples.
data=A*data; %use this line to work also with A=0

%INJECTION at random time
%time of signal injection, no extremal points
TSTART=dt+rand*(T_data-T_MAX-2*dt);
nSTART=ceil(TSTART/dt); % sample at which signal injection begins
%addition of signal to background noise
data(nSTART:nSTART+length(signal)-1,:)=...
data(nSTART:nSTART+length(signal)-1, :)+signal;

%Plot of Situation in detector 1
signal_noise_plot(data(:,1), signal, TSTART, dt);
title("Signal and Noise in One Detector")
ylabel("Normalized Amplitude")

%Initializing Variables
%number of points in the grid
grid_points=length(grid_par(1):grid_par(2):grid_par(3))*length(...
grid_par(4):grid_par(5):grid_par(6));
SNR=zeros(3, grid_points, N_det); %whole SNR structure
M_list=zeros(N_det, 3); %results in different detectors

tic;

```

```
62 %DETECTION IN EVERY DETECTOR
63 parfor det=1:N_det
64
65     %useful temporary variable (due to parfor)
66     tmp=zeros(1, 3);
67
68     %applying initial grid
69     SNR(:,:, det)=apply_conv_grid(data(:,det), grid_par, 0, ...
70     signal_parameters); %Filtering
71
72     %storing best masses for every detector
73     [tmp(1), tmp(2), tmp(3)] = SNR_max(SNR(:,:, det));
74     M_list(det,:)=tmp;
75 end
76
77 %mean of SNR over different sheets
78 SNR_mean=mean(SNR, 3);
79
80 %best combination over detectors
81 [max_SNR, M1, M2] = SNR_max(SNR_mean);
82 Meas_Chirp_Mass=chirpMass(M1, M2);
83
84 %plotting grid
85 grid_plot(SNR_mean), title("SNR over Grid of Masses"), ...
86 xlabel("Mass 1 (\(\textup{M}_\odot\))",'Interpreter','latex'), ...
87 ylabel("Mass 2 (\(\textup{M}_\odot\))",'Interpreter','latex')
88
89 %storing results for every detector
90 M_list(:, 4)=chirpMass(M_list(:,2), M_list(:,3));
91 M_list(:, 5)=abs(M_list(:, 4)-Chirp_Mass)./Chirp_Mass;
92
93 %TIME MEASUREMENTS
94 Det_time=zeros(N_det, 2); %storage variable
95 masses=M_list(:,2:3); %tmp variable for parfor
96
97 %1) best combination over detectors
98 ch=Newt_Chirp(M1, M2, signal_parameters{:});
99
100 %cycle over detectors
101 parfor det=1:N_det
```

```
102
103     %Applying optimal template to data for every detector
104     [out,time]=apply_MF_conv(ch,data(:,det),dt); %Filtering
105
106     %getting detection sample as max of SNR
107     [~,S_det]=max(abs(out./std(data(:,det))));
108
109     %storing detection time and sample
110     Det_time(det, :)=[time(S_det),S_det];
111 end
112
113 %mean delay over all detectors
114 mean_del=mean(Det_time-[TSTART, nSTART], 1);
115
116 %2) every detector
117 %cycle over detectors
118 parfor det=1:N_det
119     %tmp variable for parfor
120     tmp_sig=signal_parameters;
121     tmp_m=masses;
122
123     %optimal template found
124     ch=Newt_Chirp(tmp_m(det, 1), tmp_m(det, 2), tmp_sig{:});
125
126     %Applying optimal template to data for every detector
127     [out,time]=apply_MF_conv(ch,data(:,det),dt); %Filtering
128
129     %getting detection sample as max of SNR
130     [~,S_det]=max(abs(out./std(data(:,det))));
131
132     %storing detection time and sample
133     Det_time(det, :)=[time(S_det),S_det];
134 end
135
136 %storing results
137 M_list(:,6:7)=Det_time-[TSTART, nSTART]; %units of dt
138
139 if(N_det>1)
140 M_list(N_det+1,:)=[max_SNR, M1, M2, Meas_Chirp_Mass, ...
141 abs(Meas_Chirp_Mass-Chirp_Mass)./Chirp_Mass, mean_del(1), mean_del(2)];
```

```
142 end
143
144 %printing results as a table
145 fprintf("Measurements in Every Detector:")
146 Res_Table = array2table(M_list,'VariableNames',{'SNR','Mass 1','Mass 2',...
147 'Chirp Mass', 'Rel. Error', 'Delay (s)', 'Delay (smpl)'});
148 Detectors={'Virgo', 'LIGO 1', 'LIGO 2', 'Kagra'};
149 Detectors=Detectors(1:N_det);
150 if (N_det>1)
151 Detectors=[Detectors, "Best Comb."];
152 end
153 Res_Table.Properties.RowNames=Detectors
154
155 %Execution Time
156 ex_time=toc;
157 fprintf("Execution Time: " + datestr(seconds(toc),'HH:MM:SS:FFF') + "\n");
```

E Post-Newtonian Corrections

The purpose of this section is to present some relevant formulae in the Post-Newtonian approximation, reported from [1].

E.1 Useful Formulae

First, the dimensionless variable x is defined as a function of the *source orbital frequency* ω_s:

$$x \equiv \left(\frac{G(m_1 + m_2)\omega_s}{c^3} \right)^{2/3} . \tag{17}$$

However, x can be written also making its dependence on the *symmetric mass ratio* ν explicit:

$$\begin{aligned} x =& \frac{1}{4}\Theta^{-1/4} \left\{ 1 + \left(\frac{743}{4032} + \frac{11}{48}\nu \right) \Theta^{-1/4} - \frac{1}{5}\pi\Theta^{-3/8} \right. \\ &+ \left(\frac{19583}{254016} + \frac{24401}{193536}\nu + \frac{31}{288}\nu^2 \right) \Theta^{-1/2} \\ &+ \left(-\frac{11891}{53760} + \frac{109}{1920}\nu \right) \pi\Theta^{-5/8} \\ &+ \left[-\frac{10052469856691}{6008596070400} + \frac{1}{6}\pi^2 + \frac{107}{420}C - \frac{107}{3360}\log\left(\frac{\Theta}{256}\right) \right. \\ &+ \left(\frac{3147553127}{780337152} - \frac{451}{3072}\pi^2 \right)\nu - \frac{15211}{442368}\nu^2 + \frac{25565}{331776}\nu^3 \Big] \Theta^{-3/4} \\ &+ \left(-\frac{113868647}{433520640} - \frac{31821}{143360}\nu + \frac{294941}{3870720}\nu^2 \right) \pi\Theta^{-7/8} \\ &\left. + \mathcal{O}\left(\frac{1}{c^8}\right) \right\} . \end{aligned} \tag{18}$$

The *orbital phase* can be expressed in a similar way:

$$\begin{aligned}\phi(t) = &-\frac{1}{\nu}\Theta^{5/8}\left\{1+\left(\frac{3715}{8064}+\frac{55}{96}\nu\right)\Theta^{-1/4}-\frac{3}{4}\pi\Theta^{-3/8}\right.\\
&+\left(\frac{9275495}{14450688}+\frac{284875}{258048}\nu+\frac{1855}{2048}\nu^2\right)\Theta^{-1/2}\\
&+\left(-\frac{38645}{172032}+\frac{65}{2048}\nu\right)\pi\Theta^{-5/8}\log\left(\frac{\Theta}{\Theta_0}\right)\\
&+\left[\frac{831032450749357}{57682522275840}-\frac{53}{40}\pi^2-\frac{107}{56}C+\frac{107}{448}\log\left(\frac{\Theta}{256}\right)\right.\\
&+\left(-\frac{126510089885}{4161798144}+\frac{2255}{2048}\pi^2\right)\nu\\
&\left.+\frac{154565}{1835008}\nu^2-\frac{1179625}{1769472}\nu^3\right]\Theta^{-3/4}\\
&+\left(\frac{188516689}{173408256}+\frac{488825}{516096}\nu-\frac{141769}{516096}\nu^2\right)\pi\Theta^{-7/8}+\\
&\left.+\mathcal{O}\left(\frac{1}{c^8}\right)\right\}.\end{aligned} \tag{19}$$

It can be shown that the dimensionless time variable Θ

$$\Theta \equiv \frac{\nu c^3}{5G(m_1+m_2)}(t_c - t), \tag{20}$$

where t_c is the time at which the coalescence takes place and m_1 and m_2 represent the two masses of the binary system.

In Formulae and , $C \simeq 0.577$ stands for the Euler-Mascheroni constant.

E.2 The Inverse Change of Coordinates

In this paragraph, the inverse change of coordinates from the new variables chirp mass $\mathcal{M}$ and symmetric mass ratio ν to from the two masses m_1 and m_2 is made explicit. Since the ultimate aim is to estimate the masses of the two astronomical objects generating the signal, it is necessary to use this change to recover the two masses, once $\mathcal{M}$ and ν have been evaluated. It is useful to use the Newtonian variables total mass $M = m_1 + m_2$ and reduced mass $\mu = \frac{m_1 m_2}{M}$. So, from the definitions of $\mathcal{M}$ and ν, on can write:

$$\mathcal{M} = \mu^{\frac{3}{5}} M^{\frac{2}{5}} \qquad\qquad \nu = \frac{\mu}{M}. \tag{21}$$

This relations can be easily inverted, in order to get:

$$M = \mathcal{M}\nu^{-\frac{3}{5}} \qquad\qquad \mu = \mathcal{M}\nu^{\frac{2}{5}}. \tag{22}$$

Now, one should invert the definitions of M and μ in order to get m_1 and m_2. By substituting $m_2 = M - m_1$ into the definition of μ, on gets the equation for m_1:

$$\mu = \frac{m_1(M - m_1)}{M} \qquad\qquad \longrightarrow \qquad\qquad m_1^2 - m_1 M + \mu M = 0. \tag{23}$$

So, one gets two solutions for m_1. This happens because of the symmetry between m_1 and m_2, which can be exchanged without affect the physics of the system. So, it is possible to write simply:

$$m_{1,2} = \frac{M}{2}\left(1 \pm \sqrt{1 - \frac{4\mu}{M}}\right). \tag{24}$$

In the end, the change can be written as:

$$m_{1,2} = \frac{\mathcal{M}}{2\nu^{\frac{3}{5}}}\left(1 \pm \sqrt{1 - 4\nu}\right). \tag{25}$$

It can be seen that a limit to the value of ν is set: it cannot exceed the value of 0.25.

F Post-Newtonian Chirp

All the results obtained till now have been derived analyzing binary systems according to the Newtonian approximation, whose crucial parameter is represented by the *chirp mass* $\mathcal{M}$. According to this picture, if different pairs of astronomical objects had exactly the same *chirp mass*, they would produce an identical gravitational waveform, being then indistinguishable. Based on the hypothesis of slowly moving and weakly self-gravitating sources (see [1] for further developments), the Post-Newtonian approximation, in a certain way, "breaks" this degeneracy, furnishing a valid attempt at the estimate of the two separate masses. The Post-Newtonian terms, however, should be understood as a slight correction to the underlying Newtonian treatment. Thus, as for the grid based algorithm (Section C), the new approach's main aim is to find the couple of masses that reproduces both the *chirp mass* of the gravitating system and the values of descriptive variables depending on the masses of the bodies. Combining the measures of these variables, one should, in principle, be able to conclude the experiment, giving an estimation of the parameters (i.e. their masses) of the two objects separately.
Actually, as a matter of fact, the uncertainty on the masses does not seem to experience a steady reduction when scaling the grid step. While it may appear indicative of an error, it should be recalled that, in the first place, the Post-Newtonian approximation seeks the combination of grid points that best approaches the *chirp mass*, and not the one that perfectly estimates the two separate masses. Therefore, thickening the grid, "good" pairs can be obtained for values of the source masses which could be even considerably distant from the expected values, as long as the *chirp mass* is the same. The ensuing discussion refers to several of the most important tasks that need to be accomplished when dealing with Post-Newtonian chirps, and it almost follows the same outline sketched in Section D.

F.1 Discretisation Limit

As similarly done in D.1 in the Newtonian landscape, it is useful to examine the ideal case also in the Post-Newtonian approximation, assessing the intrinsic limit of the procedure. Indeed, when analyzing a chirp signal, not only do errors arise from the presence of noise, but they also can be partly attributed to the discrete nature of the grid. Therefore, the purpose of this argument is to quantify the error associated to the grid at fixed values of the step. The script written to produce the following results is based on the one discussed in detail in paragraph D.3, but it has been revisited in light of the Post-Newtonian approach, as will be clearly exposed in paragraph F.4. Furthermore, after inspecting several results (see paragraph F.4.1), it has been decided to fix the Post Newtonian Order at 2.5, which accounts for the best precision. Let's now look at some plots, obtained averaging the results

of 120 random simulations. Moreover, it must be said that the *symmetric mass ratio* $\nu = \frac{m_1 m_2}{(m_1+m_2)^2}$ will constitute an important parameter in further analysis.

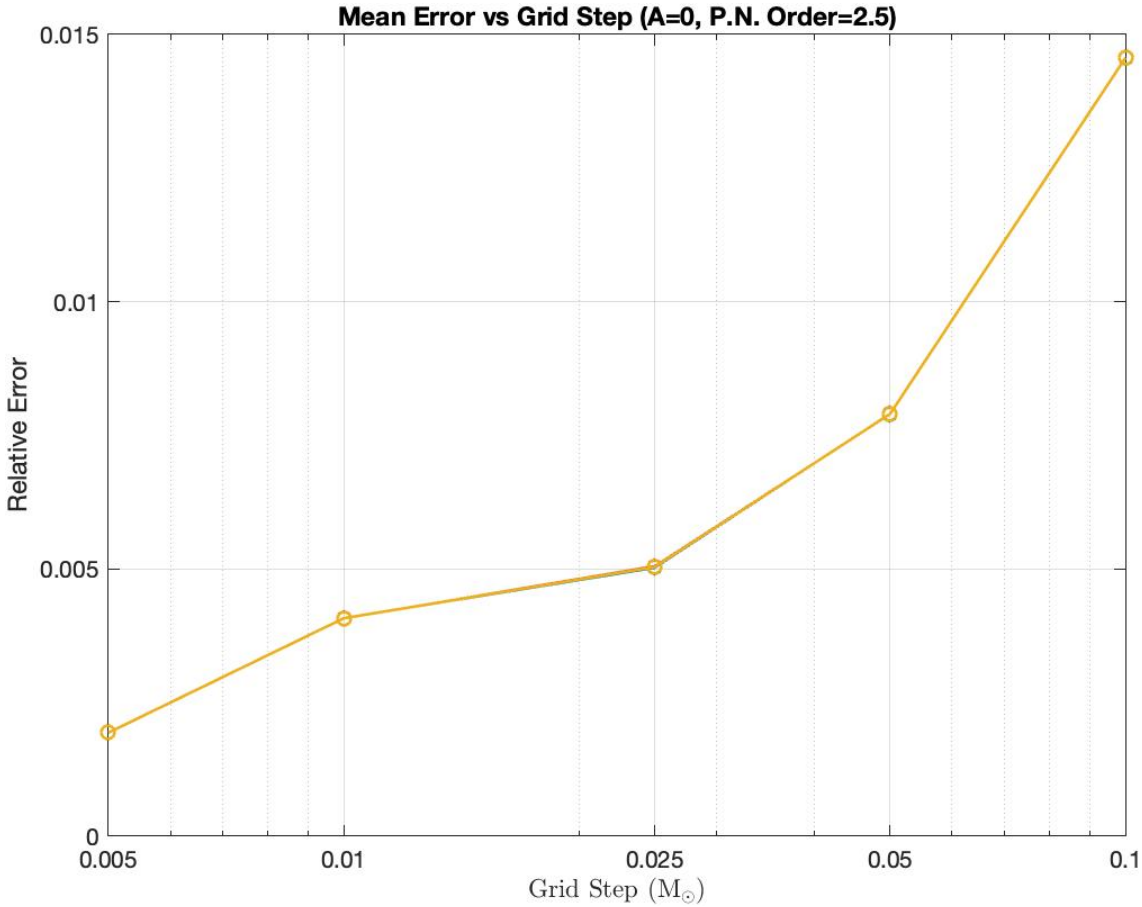

Figure 52: Mean relative error on the two masses and on their average as a function of the grid step (the three curves are exactly overlapped, as expected). The range of analysis spans $3\,\mathrm{M}_\odot$.

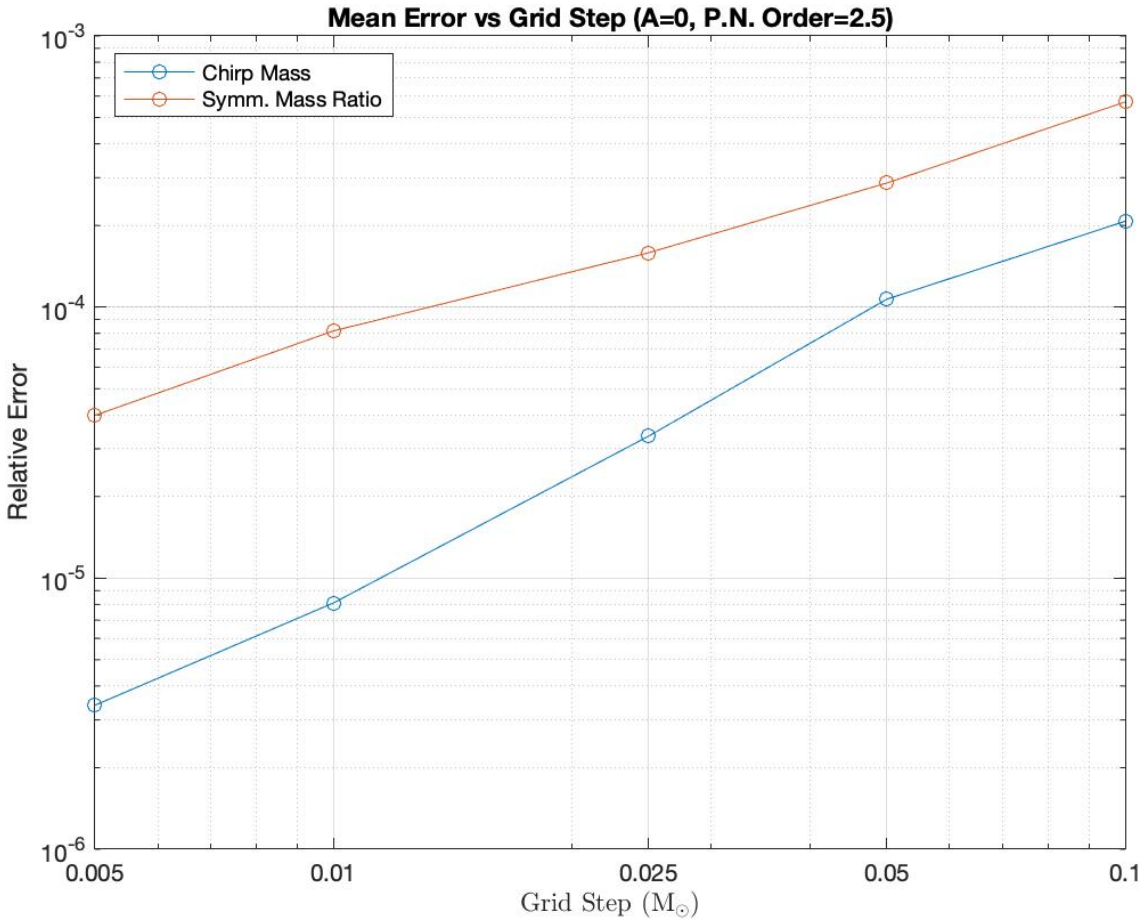

Figure 53: Mean relative error on the chirp mass and on the symmetric mass ratio as a function of the grid step. The range of analysis spans $3\,M_\odot$.

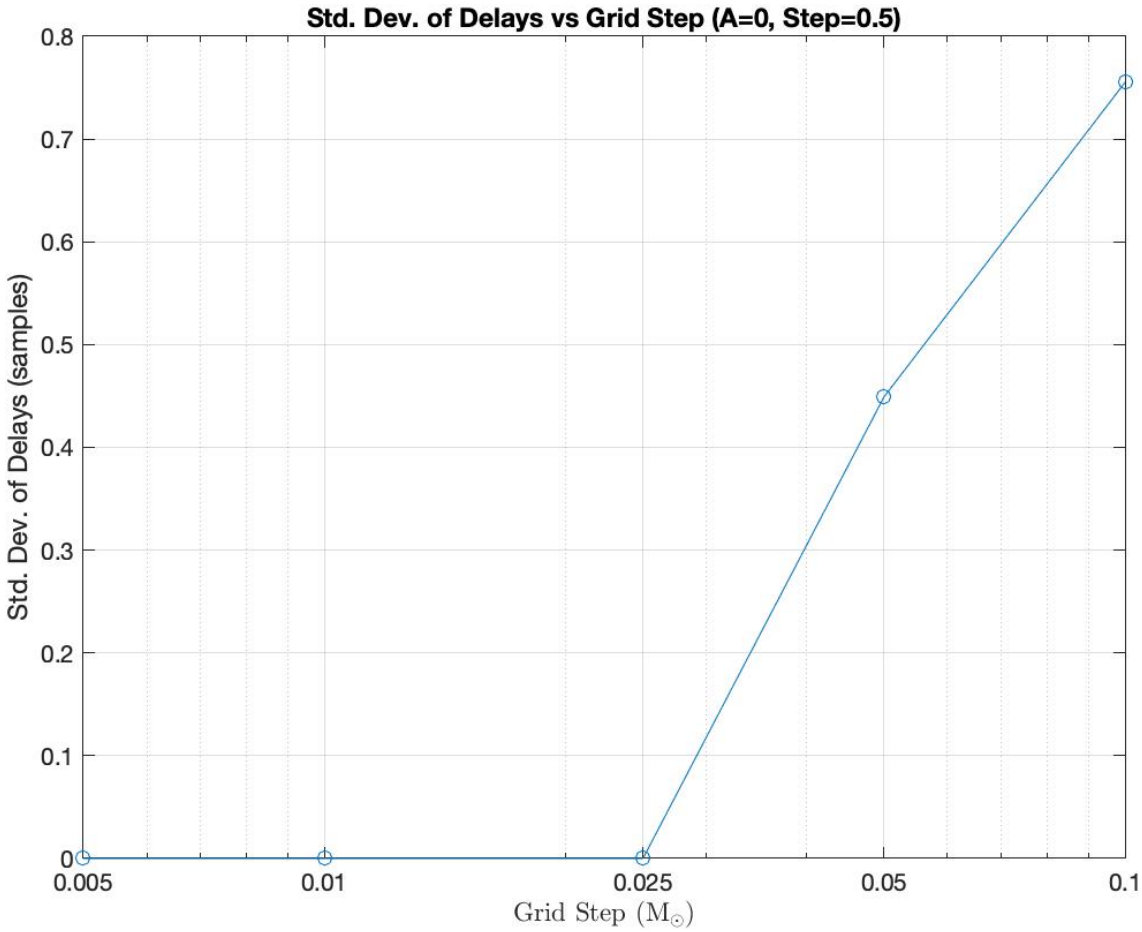

Figure 54: Standard deviation of the distribution of delays as a function of the grid step. The range of analysis spans $3\,M_\odot$.

As it is possible to observe comparing the first two graphs, while the relative error on the masses does not seem to experience a significant reduction (though it always becomes smaller), the errors on the *chirp mass* $\mathcal{M}$ and the *symmetric mass ratio* vary on different order of magnitude diminishing the grid step. This behavior confirms what guessed in the introduction to Section F: in terms of priority, the Post-Newtonian algorithm, being an approximation of the Newtonian method, firstly seeks the couple of masses which gives the best estimate of the *chirp mass*, then maximizes also the *symmetric mass ratio*, and only at the end provides the masses of the two gravitating bodies by combining the previous results. Thus, if grid pairs have a different *chirp mass* from the expected one, they will not generate a sufficiently high SNR, no matter how "near" they are to the true couple.
The last figure is not surprising: in the absence of noise, the *matched filtering* technique, combined with a sufficiently dense grid of masses, reveals perfectly

the time of arrival of the signal. For this reason, even in the Post-Newtonian approximation, the major concern will always be the estimate of the source masses. These considerations will lead to a new approach, extensively described in Section 2, where the grid axis no longer stand for the two masses, but they represent the *chirp mass* $\mathcal{M}$ and the *symmetric mass ratio* ν, those being the "right" variables to analyze the problem.

F.2 Dependence of Error on Masses Values

In an independent analysis[28], it has been observed that the average relative error on the masses is not uniform on the whole grid, as it can be easily understood from the following graph reporting an evaluation of the percentage a a function of the two masses. The obtained results are evaluated from 30 independent measures for every couple of masses. The masses where singularly analyzed with a grid step $0.25\,M_\odot$ in absence of noise:

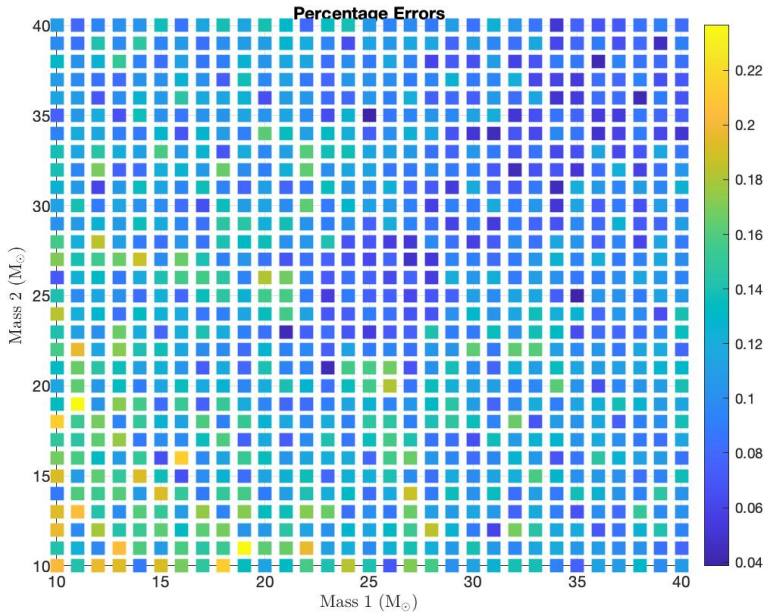

Figure 55: Similar masses are much better estimated than `off-diagonal` ones.

The reader can immediately notice that smaller masses have higher errors: this happens because signals are longer and weaker, so, it is easier for the parameters not to be correctly evaluated. However, if one restricts the analysis to a range between $20\,M_\odot$ to $40\,M_\odot$ for both masses, an interesting trend can be noticed: the error increases when moving away from the diagonal. This means that masses

[28] refer to code `Error_Test.mlx`

with similar values are estimated much better than "unbalanced" ones. Thus, to perform precise error evaluations (as the ones carried out F.4.3), it is important to select masses with similar ratio.
Furthermore, this dependence hints that the analysis would be more meaningful in different variables, as explained in the section 2. One of the main goals will be to reduce the error on masses with different values, since symmetrical couples are already pretty well evaluated.

F.3 Time of Detection

Analogously to what previously examined in Section D, the estimate of the time of arrival of a signal remains one of the main issues, even in the Post-Newtonian picture. Thus, the next pages attempt to describe some important accomplishments, relying on the basis already established before. Firstly, the optimal filter configuration will be studied, resulting in a distribution of delays centered around the origin. Afterwards, an interesting comparison between the Newtonian and the Post-Newtonian approaches will be performed, as far as the time of detection of a signal is concerned

F.3.1 Optimal Filter

As explained in great detail in paragraph D.2, when a given waveform is filtered with its time reversed version (i.e., the *optimal filter*), the SNR peaks at its maximum value, shrinking the difference between the arrival of the signal and its revelation to zero. Needless to say, this behavior is due to the fact that, under those circumstances, the algorithm looks for a chirp identical to the incoming one. Obviously, the associated MATLAB script[29] executes exactly the same operations as the one outlined in D.2, once having carefully substituted all the Newtonian-based chirps with the corresponding Post-Newtonian signals. Therefore, there will be no further discussion of the code itself, and the focus shall be shifted to the outcomes. Relevant plots are thus displayed below, setting `N_exp = 1000` as the default number of experiments. In contrast D.2, `A` must be understood as a factor that, once multiplied by the chirp mean absolute value, gives back the real noise root mean square amplitude.

[29] Refer to `CMF_Delay_PN.mlx`.

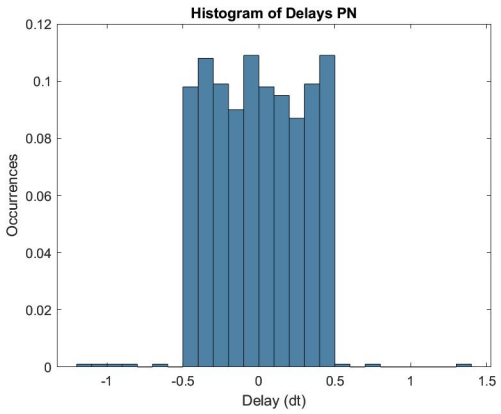

Figure 56: Normalised histogram of delays, expressed in sampling time units. Noise $r.m.s$ `A= 0.5`, bin width 0.1`dt`.

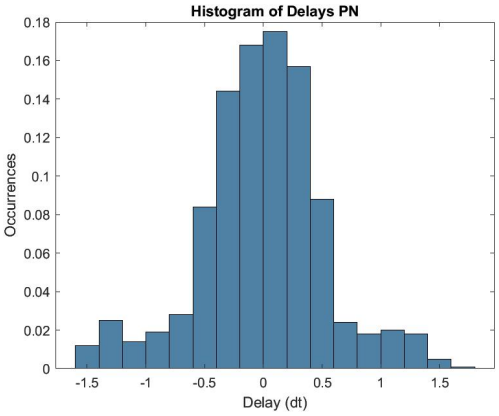

Figure 57: Normalised histogram of delays, expressed in sampling time units. Noise $r.m.s$ `A = 1`, bin width 0.2`dt`.

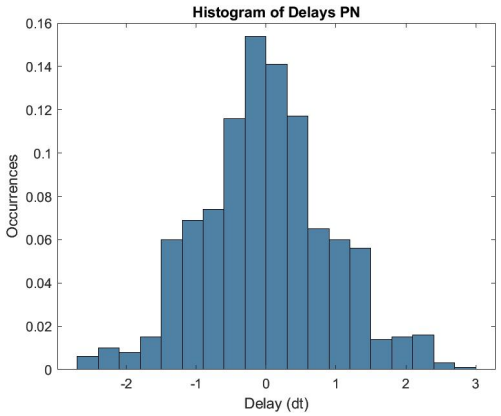

Figure 58: Normalised histogram of delays, expressed in sampling time units. Noise $r.m.s$ `A = 2`, bin width 0.3`dt`.

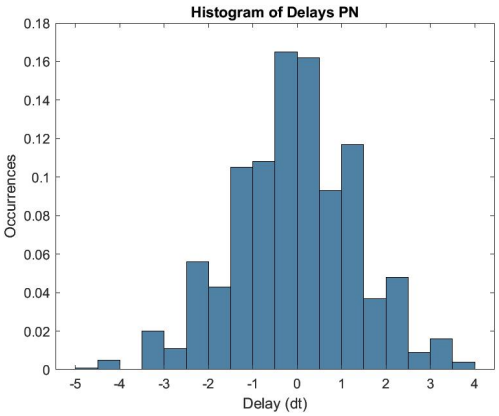

Figure 59: Normalised histogram of delays, expressed in sampling time units. Noise $r.m.s$ `A = 3`, bin width 0.5`dt`.

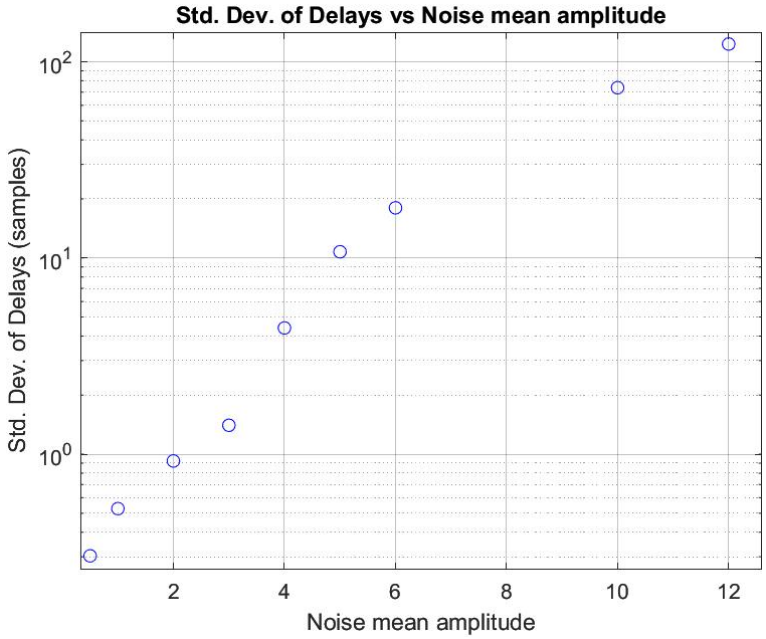

Figure 60: Standard deviation of correct detections, expressed in sampling time units, as a function of the noise r.m.s.

The relative script shows that, for `A` = 10, the *false detection rate* (i.e. rate of measures that are much farther from the real value than the presented ones) oscillates around 7%, which increases to 20% circa for `A` = 12. For the sake of completeness, it must be said that Figure 60 has been plotted showing only the *correct detections*.

F.3.2 Grid of Masses

The aim of this section is to illustrate how well the time of arrival of an injected Post-Newtonian chirp is computed using both Newtonian and Post-Newtonian filters. In fact, since the Post-Newtonian approximation gives rise to signals which better match the revealed gravitational waves, it is necessary to take into account the errors made when filtering the observed waveforms with Newtonian chirps. Let's take a close look at the relative MATLAB code[30], in order to provide both qualitative and quantitative results.
Firstly, various Post-Newtonian chirps are generated and embedded in a white noise background, with fixed mean amplitude `A` = 2. The range of masses explored and the grid step are gathered in the variable `grid_parameters`.

...

[30]Refer to `compare.mlx`.

```
grid_parameters=[20, 1, 25, 20, 1, 25];
%accounts for further enlargements
N_enl=1;
%number of signals
N_dim = 100;
Masses = rand(N_dim, 2)*5 + 20;
...
%Post-Newtonian order
PN_order=2.5;
T_MAX = 0.5;

signal = zeros(N_dim, round(2*T_MAX/dt));
for row = 1:N_dim
  %creation of the signal
  signal_test = chirp_signal(Masses(row,1), Masses(row,2), signal_parameters{:});
  b = length(signal_test)
  signal(row,1:b) = signal(row, 1:b) + signal_test;
  signal(row, :) = signal(row,:)/mean(abs(signal(row,:)));
end

...
%outer loop
for iter = 1:row
A = 2;
% Duration of background noise
T_data=T_MAX*(10+rand);
data=randn(1, round(T_data/dt));
data=A*data'
...
%addition of signal to background noise
a = signal(:,iter);
l = length(a)
data(nSTART:nSTART+l-1-off)=data(nSTART:nSTART+l-1-off)+signal(1:l-off, iter);

%inner loop
    for
        ...
        ...
    end
```

```
...
end
```

The core of the program is represented by the inner loop, which exploits the grid of masses technique for Newtonian (`f_model` = 1) and PostNewtonian (`f_model` = 2) filters in order to compute the delays between the detection and the entrance of the incoming waveforms. Here it is almost fully reported:

```
for f_model= 1:2
    %APPLYING GRID OF FILTERS: get SNR for every filter
    if(f_model == 1)
      SNR=apply_conv_grid(data, grid_parameters, f_model-1, signal_parametersN);
    else
      SNR=apply_conv_grid(data, grid_parameters, f_model-1, signal_parameters);
    end

    %getting best values of SNR
    [M1, M2, max_SNR] = best_points(SNR);

    ...

   %precision measurement are different basing on model:
     if(f_model==1)
       ...
       chN = CHIRP_fromparameters(M1, M2, T_MAX, dt);
       [outN, timeN] = apply_MF_conv(chN, data, dt);
       [~, S_detN] = max(abs(outN));
       Det_timeN = timeN(S_detN);
       DelayN(iter, N_enl) = (Det_timeN - TSTART)/dt;
     elseif(f_model==2)
        ...
       chPN = chirp_signal(M1,M2, signal_parameters{:});
       [outPN,timePN]=apply_MF_conv(chPN,data,dt);
       [~,S_detPN]=max(abs(outPN));
       Det_timePN=timePN(S_detPN);
       DelayPN(iter, N_enl)=(Det_timePN-TSTART)./dt;
     end

end
```

The values of `DelayN` and `DelayPN` are then put in a histogram format:

```
TotalN=histogram(DelayN(:, N_enl), 'Normalization', 'probability');
...
TotalPN=histogram(DelayPN(:, N_enl), 'Normalization', 'probability');
```

The final output is summarized in the two bar charts below. As it can immediately be seen, the Newtonian grid of masses approach misses the true arrival of the signal of several hundreds of `dt`s, which amount to one fifth of the signal time extent circa. In contrast, Post-Newtonian filters turn out to be much more accurate, leading to a virtually null average delay, with deviations of the order of some tens of `dt`s. The plots show 100 simulations, repeated for different values of the grid step.

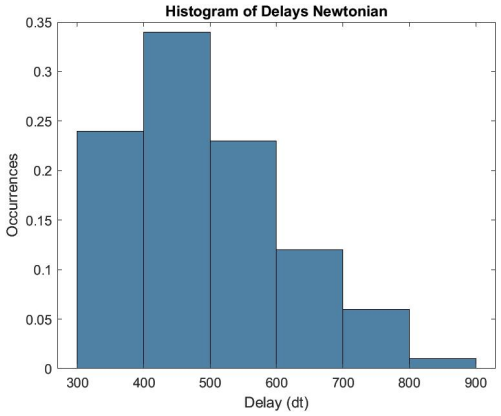

Figure 61: Normalised histogram of delays (Newtonian case), expressed in sampling time units. Grid step: $1\,M_\odot$.

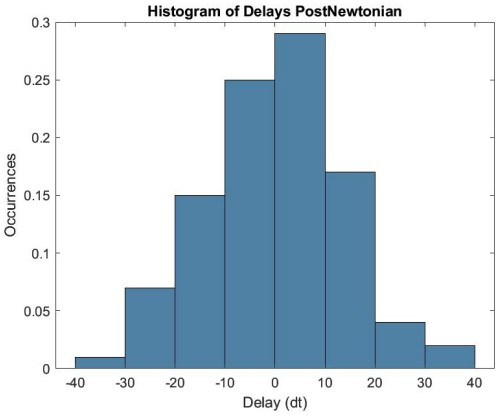

Figure 62: Normalised histogram of delays (Post-Newtonian case), expressed in sampling time units. Grid step: $1\,M_\odot$.

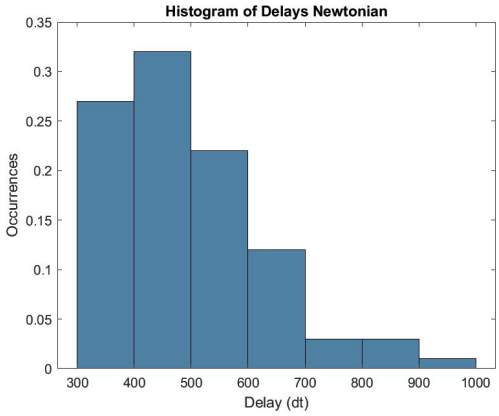

Figure 63: Normalised histogram of delays (Newtonian case), expressed in sampling time units. Grid step: $0.5\,M_\odot$.

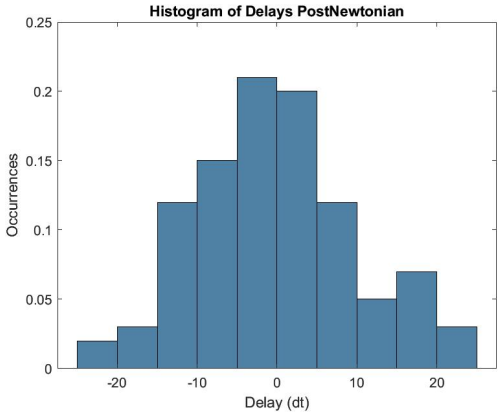

Figure 64: Normalised histogram of delays (Post-Newtonian case), expressed in sampling time units. Grid step: $0.5\,M_\odot$.

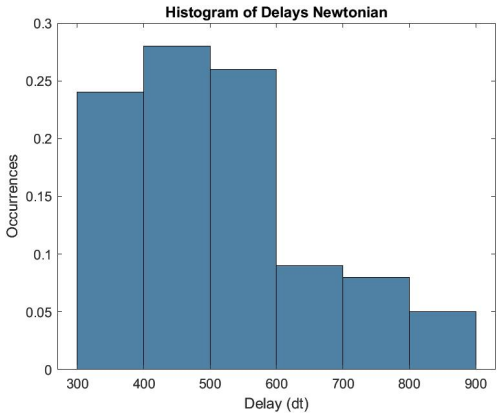

Figure 65: Normalised histogram of delays (Newtonian case), expressed in sampling time units. Grid step: $0.25\,M_\odot$.

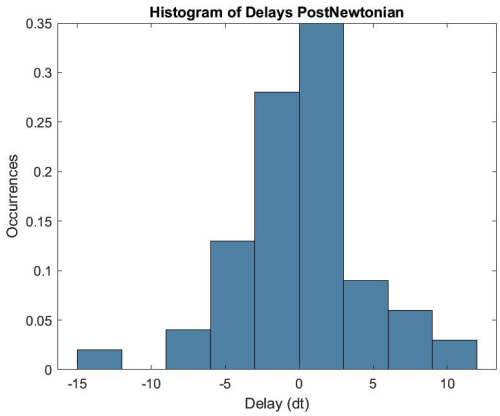

Figure 66: Normalised histogram of delays (Post-Newtonian case), expressed in sampling time units. Grid step: $0.25\,M_\odot$.

F.4 Post-Newtonian Chirp Detection

The purpose of this paragraph is to present in detail the results obtained running many simulations of detections. Since the code[31] used works exactly as the already presented `Newtonian _Detectors .mlx` (see paragraph D), it has been decided not

[31] refer to code `PN_Simple_Detectors.mlx`

to fully explain it. As the reader will notice, the workflow is exactly the same: a randomly chosen signal is revealed by a network of detectors. The important difference with the Newtonian case is in parameters estimation: as discussed in paragraph A.2.2, in the previous case, the only relevant parameter was the chirp mass $\mathcal{M}$. The introduction of post-Newtonian correction splits the degeneracy: even if the curves $\mathcal{M}$=*const* will present very similar values of SNR, the refined signals provide a separate estimate of the two masses.
It is important to underline that these correction are small if compared to the main contribute, that is given by the newtonian approximation. So, the most relevant parameter in estimation will always be the chirp mass, but the addiction of corrections allows to get also a measure of the two masses.
The analysis of the precision of the measures in the post-Newtonian case is rather more interesting and detailed than the one carried out in the Newtonian case (section D.4). It is important to remind that, using these refined signals, it is possible to obtain measures of more parameters than in the Newtonian case, such as the two masses separately and the symmetric mass ratio (which depends on them). All results reported in this section are obtained from averages over 60 runs of the explained code (which means that single detector error estimations are averaged over 200 measures, since 4 detectors were simulated in every run).

F.4.1 Post-Newtonian Order and `A`.

The first important thing to do was to fix some parameters in order to carry out comparable analysis in different situation. It was chosen to fix the step of the used grid to $0.25\,\mathrm{M}_\odot$, to determine some "good" values for the noise $r.m.s$ `A` (defined with respect to signal mean absolute amplitude) and to decide the optimal order for post-Newtonian corrections. Obtained results of the relative error on the two masses, on chirp mass and on symmetric mass ratio are reported in the following graphs, together with time measurements.

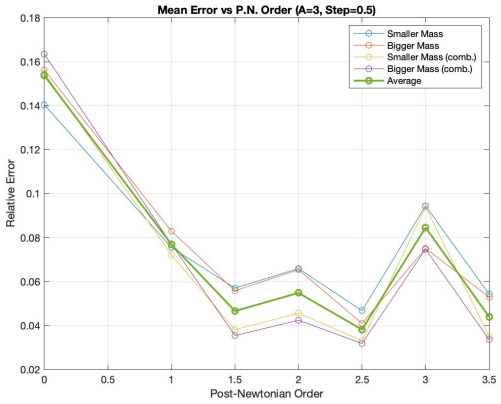

Figure 67: The introduction of Post-Newtonian Correction allows masses identification. The most accurate order is 2.5.

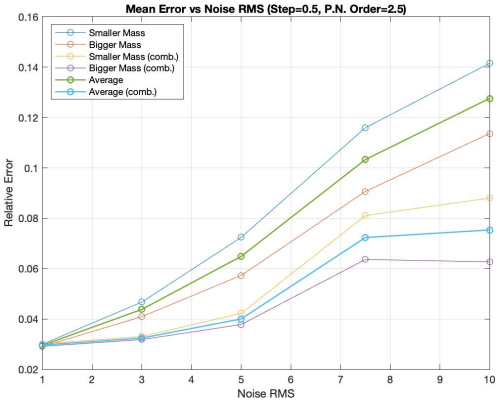

Figure 68: As in the Newtonian case, errors increase almost linearly with noise $r.m.s$ A.

Also in this case, it is important to see that combined measures are always better than single measures, since the noise is "averaged". Especially in the case of high noises, errors on single detector measures become very high, while those on combined measures are moderate. Similar results are obtained for time measures:

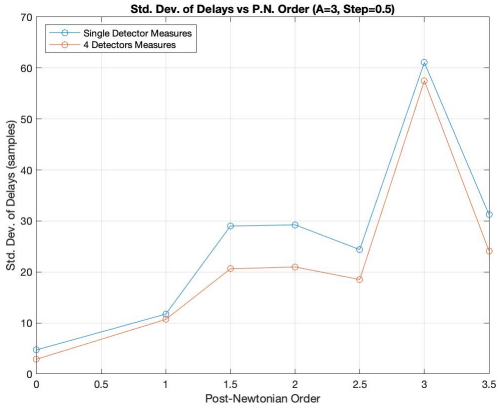

Figure 69: Normalised histogram of delays (Newtonian case), expressed in sampling time units. Grid step: $0.25\,\mathrm{M}_\odot$.

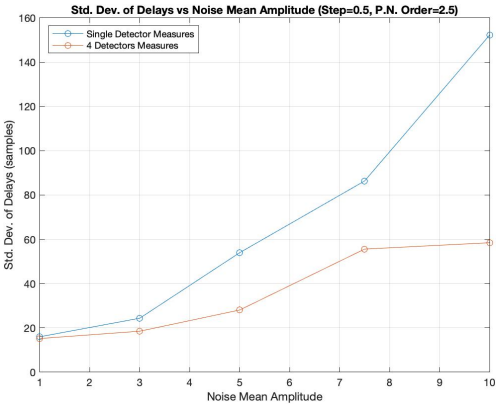

Figure 70: Normalised histogram of delays (Post-Newtonian case), expressed in sampling time units. Grid step: $0.25\,\mathrm{M}_\odot$.

The reader may notice that time measures were more precise with post-Newtonian corrections of order 0 (that do not allow masses identification) or 1.5. Nonetheless, it was evaluated that the best compromise to measure both masses and time was

to select the order 2.5. even if orders 1.5 or 3.5 would still provide a fair estimation of all relevant parameters. Measurements of chirp mass and symmetric mass ratio, that are the real parameters that determine the shape of the signal reflect above-discussed results. This is an expected behavior, since they are highly correlated to measures of masses.

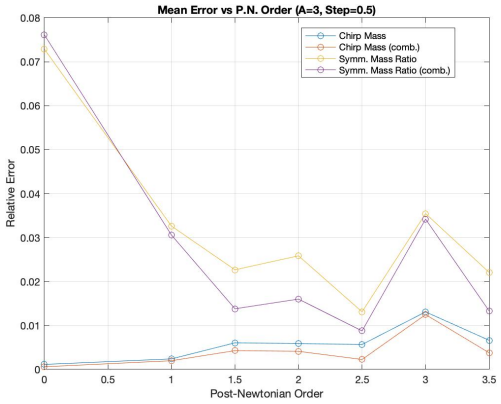

Figure 71: Normalised histogram of delays (Newtonian case), expressed in sampling time units. Grid step: $0.25\,\mathrm{M}_\odot$.

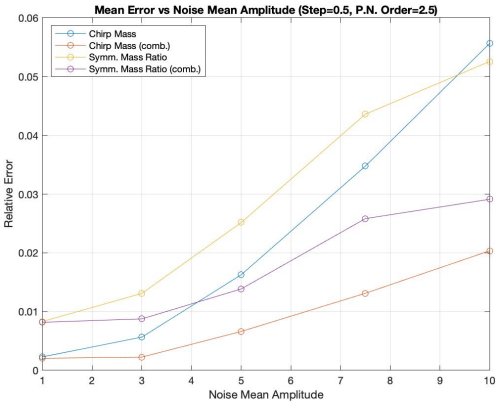

Figure 72: Normalised histogram of delays (Post-Newtonian case), expressed in sampling time units. Grid step: $0.25\,\mathrm{M}_\odot$.

F.4.2 Dependence on Grid Steps

To investigate the dependance of the error on the step of the grid, it was decided to fix `A=3`. In order to work with intense noise, but still in the region where errors are moderate. It can be seen from the following graphs that relative errors decrease almost linearly with the grid step. The cautious reader will notice that combined measures do not increase in precision going from a step of $0.25\,\mathrm{M}_\odot$ to one of $0.1\,\mathrm{M}_\odot$: this shows the beginning of a peculiar behavior discussed in the following chapter.

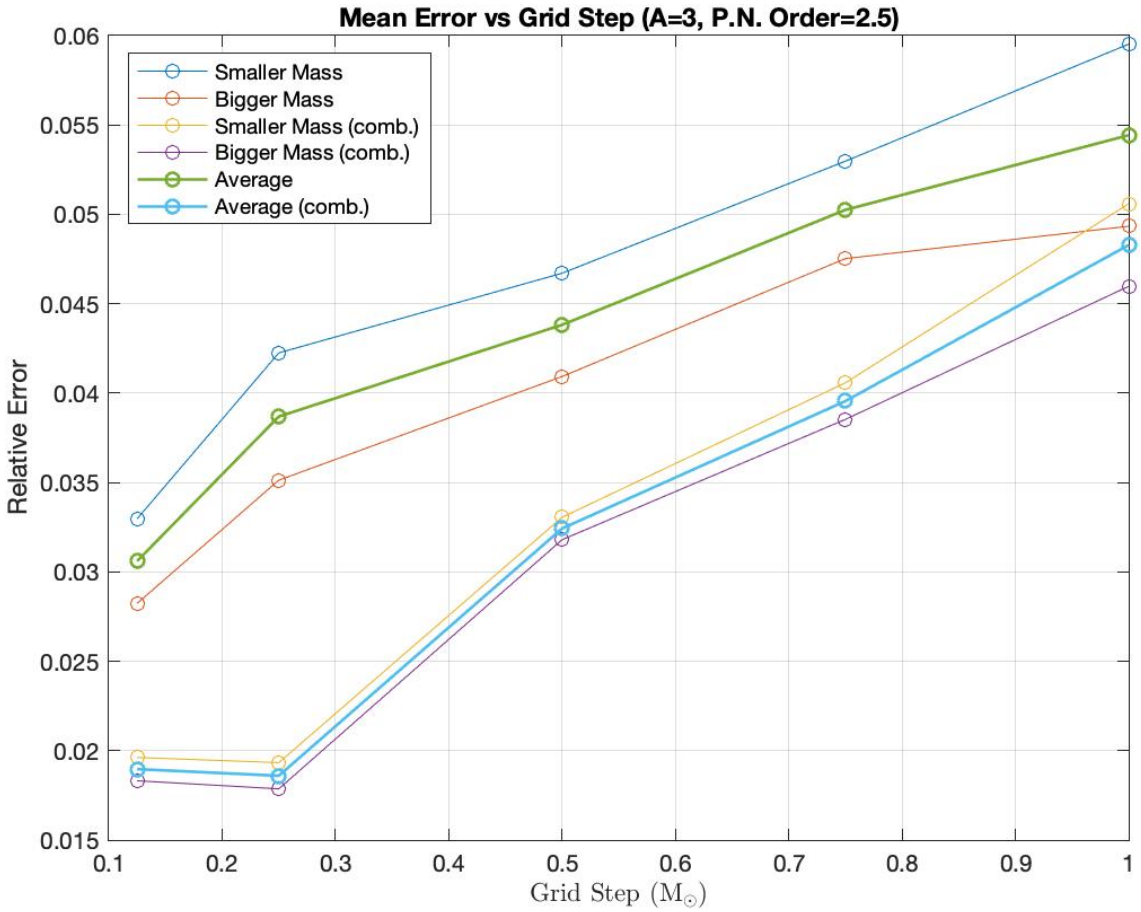

Figure 73: Errors decrease almost linearly with the step. Combined measures give a much more precise evaluation.

A similar behaviour is found for time measures and for chirp mass and symmetric mass ratio measures:

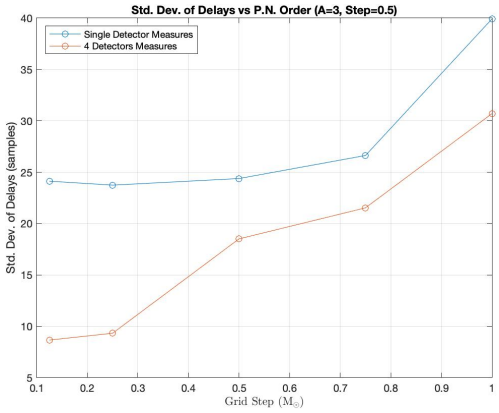

Figure 74: Time measures highly depend on the noise: combined measures are much more accurate.

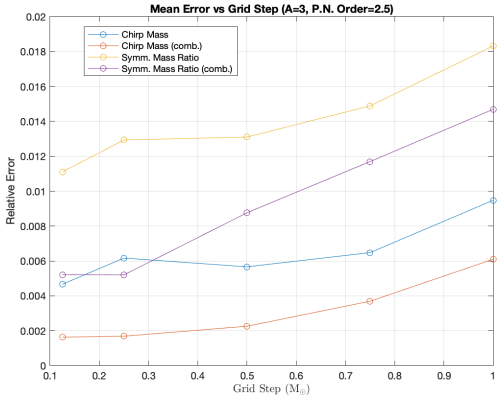

Figure 75: Chirp mass and symmetric mass ratio behave similarly to the two masses, since measures are highly correlated.

F.4.3 Smaller Steps

Since masses identification is the main goal of these detections, it is fundamental to give an estimation as accurate as possible. In order to do so, it was decided to study what happens when one performs analogous analysis with smaller step than the ones used in the previous paragraph. The results obtained are reported in the following graphs. Due to computational limitations, these results have been obtained only in a range going from $30\,M_\odot$ to $33\,M_\odot$ (the choice of this range is explained in section F.2). This is meaningful as far as the trend is concerned, but it should be remarked that, in this way, the resulting errors are underestimated by a factor slightly higher than 2.

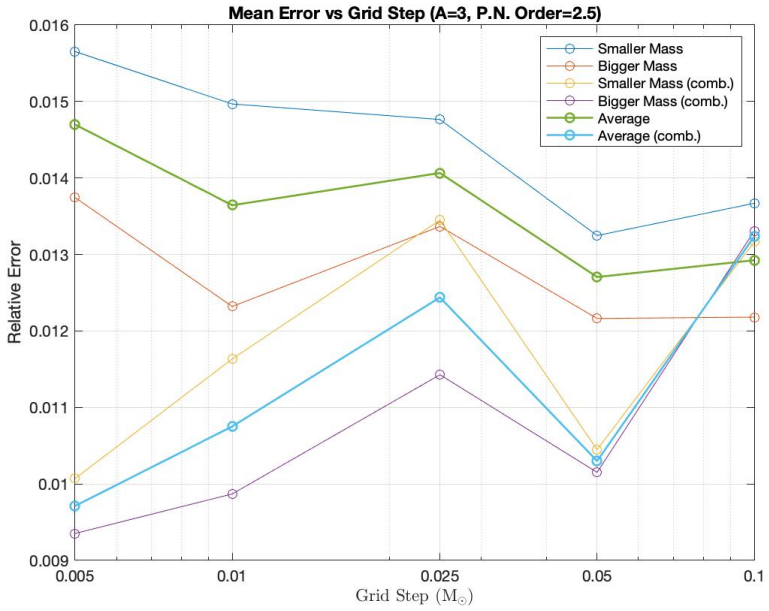

Figure 76: Precision does not significantly increase using smaller steps.

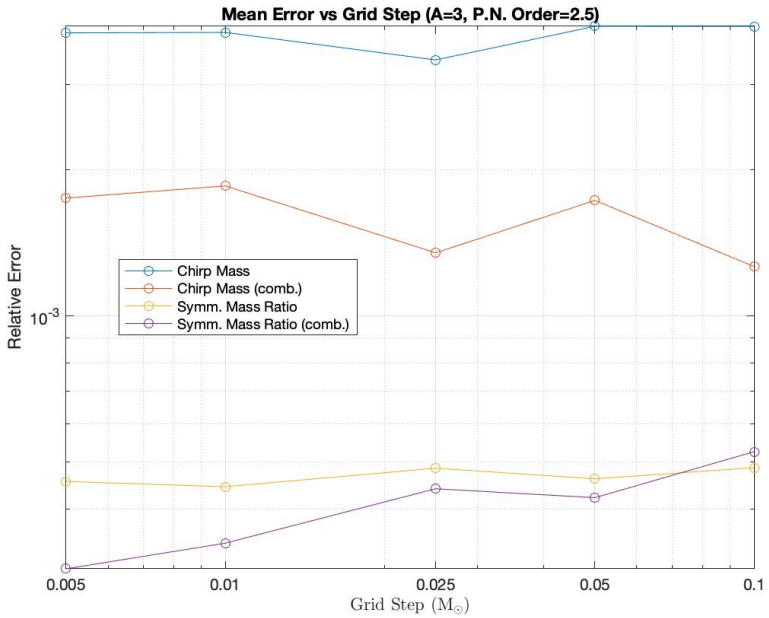

Figure 77: Precision does not significantly increase using smaller steps.

It is important to notice that precision on the two masses varies very much, while errors on chirp mass and symmetric mass are rather independent of the step: this behavior can be explained by keeping in mind that the true measured

parameters are the latter two. Their independence from the grid step is probably due to signal modeling. This means that it should be more meaningful to use methods that evaluate the chirp mass and the symmetric mass ratio from data and then to get the two masses from those measures. These considerations are the key idea behind the method developed in section 2.

F.4.4 Chunks Technique

The dependence of the error on the step of the grid has been investigated more in detail also using the *chunks technique* which has been already introduced in paragraph C.1. The results have been obtained using the same parameters chosen for Figure 76. The following graphs show the resulting estimate of the error and the improvement with respect to the standard technique:

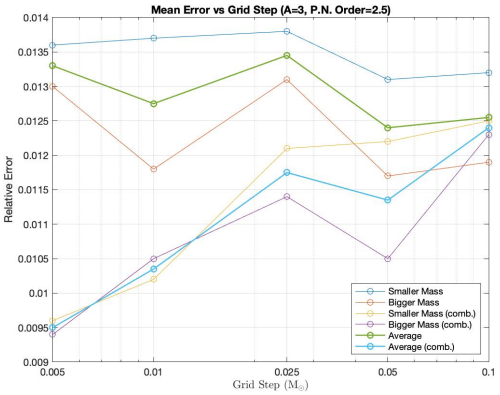

Figure 78: Time measures highly depend on the noise: combined measures are much more accurate.

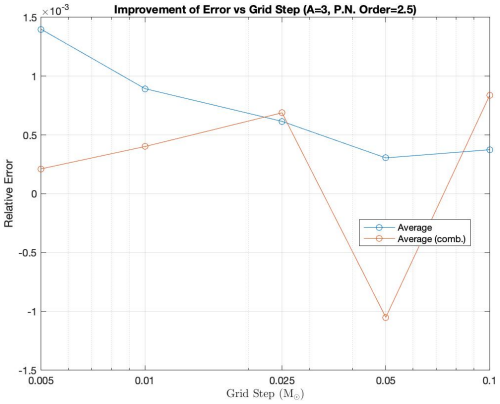

Figure 79: Chirp mass and symmetric mass ratio behave similarly to the two masses, since measures are highly correlated.

A positive improvement value means that the error was reduced from the previous case using this technique. However, it has to be said that the computational cost of this method is very high, thus, it is not always cost-effective advantageous to use it.

G MATLAB Implementation of the ($\mathcal{M}$-ν) Approach

This section deals with the MATLAB implementation of the new ($\mathcal{M}$-ν) approach[32]. First, various signals are generated choosing randomly the *chirp mass* and the *symmetric mass ratio* in a fixed range.

```
...
grid_parameters=[20, 0.5, 23, 0.24, 0.001, 0.25];
%number of injections
N_dim = 10;

%Generation of masses
MV = rand(N_dim,2);
MV(:,1) = MV(:,1)*(grid_parameters(3)-grid_parameters(1))...
 + grid_parameters(1);
MV(:,2) = MV(:,2)*(grid_parameters(6)-grid_parameters(4))...
 + grid_parameters(4);

%need conversion to generate chirps
Masses = convert(MV);

signal_parameters={fin, Dist,dt, 0, PN_order};

%creation of signals
signal = zeros(N_dim, round(2*T_MAX/dt));
for row = 1:N_dim
  signal_test = chirp_signal(Masses(row,1), Masses(row,2),...
 signal_parameters{:});
  signal(row,1:length(signal_test)) = signal(row, 1:length(signal_test))...
 + signal_test;
  signal(row, :) = signal(row,:)/mean(signal(row,:));
end
signal = signal';
```

The function `convert` takes the matrix containing random values of $\mathcal{M}$ and ν and calculates the corresponding masses (through 15 and 1), storing them in the

[32]Refer to `new_grid.mlx`.

matrix `Masses`. Then, various signal are generated: having them different time extensions, a higher-than-the-maximum time interval should be declared, in order to put them in the same matrix. However, only the part effectively corresponding to the signal will contain non zero values.
At this point, the core of the code is put inside a `parfor` loop (see Section I), which finds the SNR of the best grid pair, establishes the precision on the estimate of the couple of masses and extracts the delay between the time of detection and of arrival of the chirp signal. This procedure is repeated `N_dim` times, one for each injected signal. It must be noticed that signals are normalized to their mean absolute value, so that the ensuing results can be compared with Section F. Let's now take a direct look at the code:

```
parfor iter = 1:row
    %mean noise amplitude
    A = 10;
    % Duration of background noise
    T_data=T_MAX*(15+rand);
    data=randn(1, round(T_data/dt));
    data=A*data';

    %Injection
    TSTART=dt+rand*(T_data-5*T_MAX-5*dt);
    %sample at which signal injection begins
    nSTART=ceil(TSTART/dt);
    %addition of signal to background noise
    data(nSTART:nSTART+length(signal(:, iter))-1-off)=data(nSTART:...
nSTART+length(signal(:, iter))-1-off)+signal(1:length(signal(:, iter))-...
off, iter);
    %calculus of SNR
    SNR = apply_conv_grid_new(data, grid_parameters, 1, signal_parameters);
    [M, V, max_SNR] =best_points(SNR);
    [m1, m2] = Mq2mm_new(M1, M2);
    %precision on M and v
    precisionMuNu(iter, :) = [abs((max([M, V])-(max([MV(iter,1),...
 MV(iter,2)])))/(max([MV(iter,1), MV(iter,2)]))),...
 abs((min([M, V])-(min([MV(iter,1), MV(iter,2)])))/...
(min([MV(iter,1), MV(iter,2)])))];
    %precision on masses
    precisionPN(iter, :) = [abs((max([m1, m2])-(max([Masses(iter,1),...
 Masses(iter,2)])))/(max([Masses(iter,1), Masses(iter,2)]))), ...
abs((min([m1, m2])-(min([Masses(iter,1), Masses(iter,2)])))/...
```

```
(min([Masses(iter,1), Masses(iter,2)])))];
    SNR_sample(:,:, iter) = SNR;

    %Time of detection
    chPN = chirp_signal(m1,m2, signal_parameters{:});
    [outPN, timePN]=apply_MF_conv(chPN,data,dt);
    [~,S_detPN]=max(abs(outPN));
    Det_timePN=timePN(S_detPN);
    DelayPN(iter,1)=(Det_timePN-TSTART)./dt;

end
```

As it is possible to notice, the injection of the signal is such that it can never lay outside the noise pattern. Going back to the lines of code, the function `Mq2mm_new` maps the ($\mathcal{M}$-ν) space to the (M_1-M_2) plane, allowing `precisionPN` to associate an error on the estimate of the two masses for each iteration. Finally, some plots and histograms may be produced, showing the SNR in the two system of coordinates and delays between the arrival of a signal and its detection. At the end, an averaged relative error on the estimate of the two masses may be furnished.

H Comparison of Distributions for the "rand_CMR" Technique

In this appendix, a detailed comparison in the three cases presented in Section 3 is reported. The relative errors on $\mathcal{M}$, ν, on the two masses, and on their average is reported for different numbers of iterations (i.e. selected points):

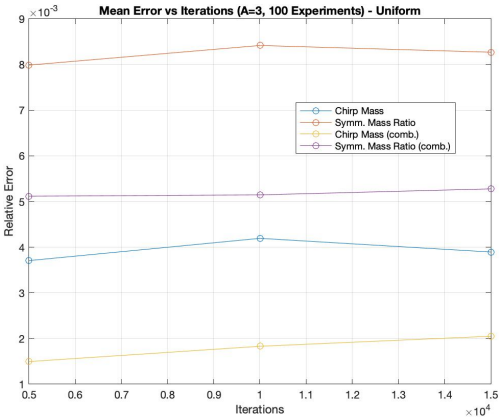

Figure 80: Relative error on chirp mass and on symmetric mass ratio using the uniform distribution.

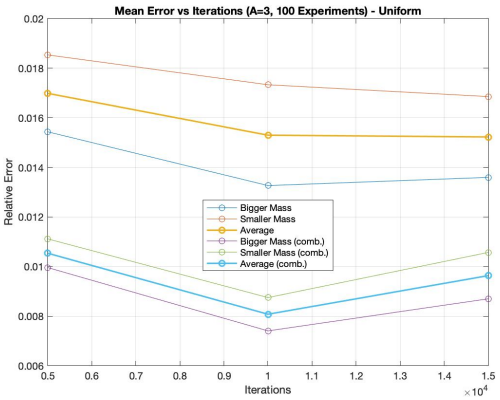

Figure 81: Relative error on masses using the uniform distribution.

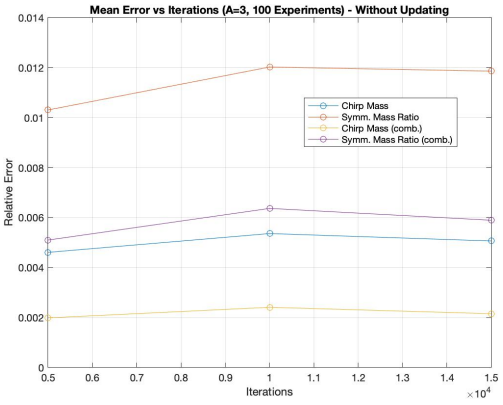

Figure 82: Relative error on chirp mass and on symmetric mass ratio after trying 10^4 points using the normal distribution.

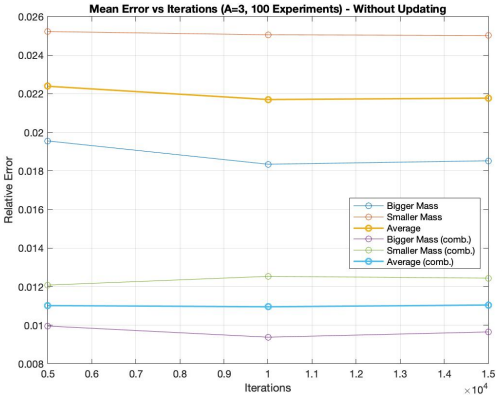

Figure 83: Relative error on masses after trying 10^4 points using the normal distribution.

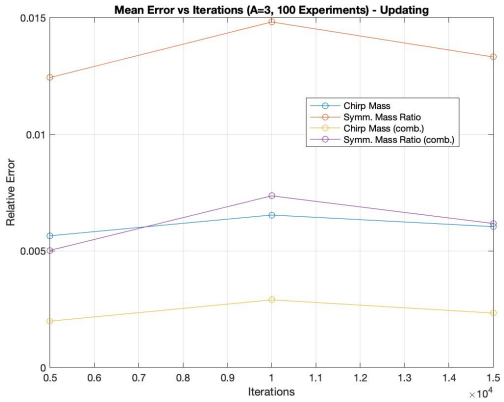

Figure 84: Relative error on chirp mass and on symmetric mass ratio after trying 10^4 points updating the central value of the normal distribution.

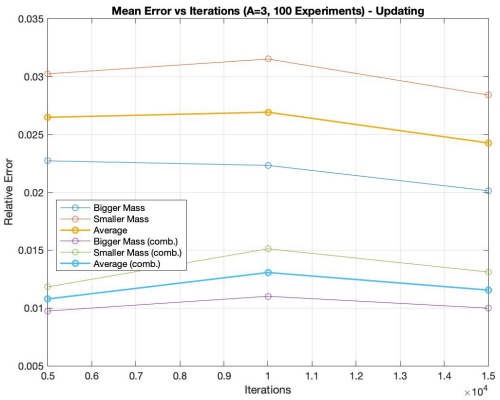

Figure 85: Relative error on masses after trying 10^4 points updating the central value of the normal distribution.

The discussion of the results deduced from these graphs is carried out in Section 3

I Parallel Computing

A conspicuous fraction of presented analysis has been performed using parallel-optimized computation. In particular, programs have been planned and developed in order to take advantage of the MATLAB `parfor` function. Using this function, it has been possible to run iterative cycles not sequentially, but in parallel. In the following paragraphs, the role of parallel computation, its implementation and used computational resources will be presented. As the reader will soon understand, a fundamental requirement to perform parallel computations is to have access to multi-core machines.

I.1 The MATLAB Function `parfor`

The function `parfor` is included in MATLAB Parallel Tool package. Its use is exactly analogous to a standard `for` cycle, but the way it works is conceptually different: while `for` cycles perform sequential iterations, `parfor` cycles do not have a predefined order to run iterations. This happens because, when the function is called, a "Parallel Pool" is created over different available CPUs on the machine being used: MATLAB automatically manages workload in order to perform different iterations on different CPUs.
The use of this function is not automatic (i.e. it is not sufficient to convert `for` cycles in `parfor` cycles): the code has to be designed in order to make all iterations independent and to use storage variables that collect all the results of different iterations. This idea can be better explained using the following example: suppose that the purpose of the code is to calculate the average the measured chirp mass over different experiments with similar parameters. In order to perform experiments in parallel, it is not possible to use a variable where the found value is summed on at every iteration (i.e. C-Style: `sum += new_value`) and divide it at the end by the number of iterations in order to get the mean. One should instead save the results for every iterations in a storage vector and take the average of this vector at the end. It should be also kept in mind that the vector is not filled in order from the first to the last position. In order to reduce executions time, it is also important to preallocate storage variables, even if MATLAB is an high level programming language and would not require it.
It is important to remark that properly code design is key to take advantage of the power of multi-CPU machines: parallelism can be implemented only once (nested parallel loops are not allowed simply because conceptually wrong) and variables that change value during iterations cannot be used. In presented works, parallelism has been implemented at three different levels (never simultaneously, as before mentioned) depending on the aim of the code and on the computational resources available at the moment it was needed to run the code:

1. **Number of Experiments:** During analysis of results (for example in paragraphs D.4 and F.4), it has been necessary to simulate many detections. In this cases, the best choice was to perform different experiments in parallel.

2. **Number of Detectors:** For codes consisting of a single detection, usually it was not necessary to use machines with a high number of cores. In this cases, parallelism was implemented on different detectors that analyzed the same injected chirp signal. This is the option explained in codes `Newtonian_Detectors.mlx` (Section D, code D.5) and in the similar `PN_Simple_Detectors.mlx` (Section F.4).

3. **Grid Application:** The best option for codes simulating a single detection, having a number of available CPUs larger than 4 (number of detectors) is to apply the grid in parallel, i. e. every filter of the grid is applied from a different iteration of the `parfor` loop. This option has been implement with some efforts (especially for the square grid case) due to some indexing problems. When successfully done, it provided the most efficient way to simulate detections.

As it should be clear, the general followed guideline was to implement parallelism at the highest level that had at least as many iterations as available CPUs. This is also the use protocol suggested by MATLAB online documentation (see [8]).

I.2 Computational Resources

It can be easily understood that, once parallelism has been successfully implemented, the speed-up factor is given by the number of available CPUs. Unfortunately[33], it was never possible to have direct access to machines with a number of cores higher than two.[34] In order to run codes using an high degree of parallelism, the possibility to run remote computations has been explored using the resources presented in the next paragraphs. At this point, it should be clear that the success of parallel optimization does not depend strongly on the power of the single CPUs one uses, but mainly on the number of cores used at the same time.

I.2.1 INFN - Virgo Group Resources

Thanks to joint efforts from the Virgo Group, it was possible to remotely access computational resources provided by "Istituto Nazionale di Fisica Nucleare". Five

[33] Mainly due to the COVID-19 pandemic.

[34] Actually, a quad-cored machine was available for a little amount of time. This possibility lead to the idea of simulate 4 different detectors (one on every core) in order to resemble the real network of detectors.

machines, each one having 18 2.1-GHz cores, were made available. The use of these machines has been a fundamental feature in order perform a significant analysis. Such an high degree of parallelism made it possible to scale to some hours the execution time of computations which would require many days on directly-accessible machines. Once more, it is important to stress that these machines were extremely suitable to perform parallel computation: despite not having extremely powerful cores, many computations could be carried out at the same time due to the high number of available CPUs.

I.2.2 AWS Resources

Some computations has been performed using the package MATLAB Parallel Server, which allows to access remote instances provided by Amazon Web Services. The main advantage of this option is flexibility: it is possible to rent hourly instances specifically selected for the calculations to be done.

References

[1] Maggiore, M. (2008). *Gravitational Waves, Volume 1: Theory and Experiments*. Oxford, Oxford University Press

[2] "The Sensitivity of the Advanced LIGO Detectors at the Beginning of Gravitational Wave Astronomy", *The LIGO Scientific Collaboration and The Virgo Collaboration*, `https://www.ligo.org/science/Publication-O1Noise/index.php` (5 June 2020).

[3] The LIGO Scientific Collaboration and The Virgo Collaboration, *Characterization of transient noise in Advanced LIGO relevant to gravitational wave signal GW150914*

[4] The LIGO Scientific Collaboration and The Virgo Collaboration, *Properties of the Binary Black Hole Merger GW150914*, 14 June 2016

[5] "Filtro Adattato", *Wikipedia, L'enciclopedia libera*, `https://it.wikipedia.org/wiki/Filtro_adattato` (3/05/2020).

[6] "Window Function", *Wikipedia*, `https://en.wikipedia.org/wiki/Window_function` (29/05/2020).

[7] The LIGO Scientific Collaboration and The Virgo Collaboration, *GWTC-1: A Gravitational-Wave Transient Catalog of Compact Binary Mergers Observed by LIGO and Virgo during the First and Second Observing Runs*, 30 November 2018

[8] "Parfor", *Mathworks*, `https://it.mathworks.com/help/parallel-computing/parfor.html` (18/05/2020).